Development and Implementation of Ice Recrystallization Inhibitors for the Preservation of Biological Material

Sophia Mangan

A thesis submitted
in partial fulfilment of the requirements for the
M.Sc. degree in Chemistry

Department of Chemistry and Biomolecular Sciences
Faculty of Science
University of Ottawa

Candidate	Supervisor
Sophia Mangan	Professor Robert N. Ben

Acknowledgements

There are so many people who have helped me along this journey, and I am appreciative to everyone. Without all of you none of this work would have been possible, and I wish to extend my heartfelt thanks. Despite there not being enough words to describe my gratitude to all the individuals without whom the completion of this thesis would not be possible, I would still like to try to thank those who have helped me through this invaluable experience.

To start my supervisor Robert Ben, I deeply appreciate all his patience in teaching me to be a better researcher and critical thinker. I am also grateful for the support and guidance he has given me even during the most difficult of times. Despite COVID making the masters process more difficult his mentorship got me through it. I cannot thank him enough for welcoming me into his laboratory and for pushing me out of my comfort zone. Dr. Tony Durst, it has been a pleasure to work in the same lab as you and your team. I appreciate your help and support throughout the years with chemistry and I will value the time you spent talking with me in the office.

I wish to thank everyone who assisted in the development of this research project. Kayla Newell, for laying the groundwork of my project for me to follow, for setting me up in an organized lab bench, and for teaching me the procedures of the lab. Some of my favourite memories include the training period we spent together. To Anna Ampaw and Salma Alasmar, for being amazing group members when COVID limited capacity, for spending a few weeks with me teaching me circling, cell work, and synthesis. Thank you for showing me some tips and tricks along the way and for encouraging me to persevere. I am grateful to you three for your endless patience and support. I want to extend many thanks to Romeo El Issa. I would not have made it through my master's if not for the support he provided for me. I am so grateful for all the memories and laughs we shared in the lab. Thank you for helping me with everything, no matter how big or small. I wholeheartedly wish to thank Dan Celestin not only for being a model undergraduate student, but for helping me to begin wrapping up my project. Thanks to him I learned the importance of mentorship and the positive outcomes of patience when teaching through my time with him.

I have been fortunate enough to have been surrounded by some truly intelligent and funny lab mates and coworkers. Elly Walsh, Gabriela Saab, Jatinder Singh, Julia Meyer, Leah McMunn, Marcus Diamante, Odile Pressoir, Stephanie Bogdan, Stephanie Sibbald, and Tomonori Waku - thank you for all the fun memories and for making 3-hour long lab meetings entertaining. As well, a special thanks go out to Elly Walsh and Jason Dagher for their help in editing this thesis. Thank you to both Emil Zaripov and Jason Dagher, for all your hard work and help during our collaborations. Thank you to all the departmental staff and students who were always willing to help or give advice when needed.

I am so grateful to have been surrounded by wonderful friends without whose support I would not be here today, to the many people who have been in my life for many years, thank you for always believing in me and telling me I can when I thought I couldn't. I really could not have made it to this point without the space each one of you has provided me, whether it be by listening to me speaking on my experience or having fun with me. I would not have made it through the difficult periods without all of you. So, no matter how big or small you

believe your impact on my life over the past few years has been, every single friend I have seen throughout my master's experience: I am so deeply appreciative to you.

Finally, I would like to thank my entire family for their constant love and belief in whatever I set out to do. Thank you to my grandparents for always supporting me and encouraging me to go as far as I can. To my siblings for always providing me with support and entertainment. To Qassim for being my rock, the person I could always go to and who helped me on a daily basis to work towards this goal. Qass, I will cherish forever everything you did to help me accomplish it and have so much love for you. Special thanks go out to my parents, who have instilled in me the value of hard work, determination, and a good education. My thesis would not have been possible without their love and support. I have grown so much throughout this master's, and I will carry the lessons I've learned with me for the rest of my life. Thank you all for having been a part of it and for providing the support I needed.

Statement of Contribution

Experimental Design

My project supervisor, Dr. Robert Ben, conceived the presented ideas. Previous students performed preliminary research and experimental designs. Dr. Jennie Briard investigated N-Aryl-β-D-aldonamides and N-Benzyl-β-D-gluconamide in her doctoral thesis providing preliminary results. Kayla Newell, Emil Zaripov, Dr Robert Ben, and Dr. Maxim Berezovski designed the experimental protocol for the RT-qPCR protein work presented in chapter 3. Dr. Véronique Moulin, Dr. Robert Ben, Jason Dagher, and I consulted and designed the tissue work experimental protocol presented in chapter 4, based on previous protocol from Université Laval's Research Centre: The Tissue Engineering Laboratory (LOEX). I performed literature research of published information to select the available and most effective benzylic compounds. I optimized the experiments through research to make informed decisions about calculations and execution. Both Dr. Robert Ben and I provided the remaining experimental design.

Experiments

Dose-response curve of N-Octyl-β-D-gluconamide was created by Kayla Newell (figure 2.2). Cytotoxicity graphs of N-Aryl-β-D-aldonamides were created in collaboration with Dan Celestine (figure 2.11). Previous existing compound property data included in this thesis was performed by Dr. Jennie Briard, Dr. Chantelle Capicciotti, and Dr. Jessica Poisson (table 2.3). Initial preliminary qPCR experiments were prepared and performed by Kayla Newell and Emil Zaripov (figure 3.6). Remaining qPCR experiments were prepared by me and run by Emil Zaripov or myself in CAREG building. All tissue experiments presented in chapter 4 were prepared and performed by Jason Dagher and Raphaël Giroux at LOEX. All figures throughout this thesis were created by me with permissions. All remaining experiments for this project were performed by me in D'lorio building in Dr. Robert Ben's laboratory.

Written Report

The thesis report was written by me, edited by Elly Walsh, Jason Dagher, and Dr. Robert Ben, and reviewed by Dr. Robert Ben.

Abstract

Cryopreservation of biological materials has many useful applications and is currently the most effective long term storage method used across a variety of fields. The success of freezing products or biological materials, however, varies because of the process' complexity and related cryo-injuries. One of the primary issues is the ice recrystallization induced development of extracellular and intracellular ice throughout the freezing and thawing process. Ice recrystallization is a significant contributor to freezing damage, ultimately reducing post-thaw viability and function. To address this issue, the Ben laboratory has developed and synthesized a variety of classes of small molecule carbohydrate-based ice recrystallization inhibitors (IRIs). These compounds act as supplements or alternatives to current cryoprotectants, such as trehalose, DMSO, or glycerol, which do not address ice recrystallization and can be cytotoxic. This thesis focuses on the comprehensive chemical property assessment of N-Aryl-β-D-aldonamides and N-Benzyl-β-D-gluconamides, as well as optimization of biopreservation protocols for tissue products and freeze-dried proteins.

Utilizing a 5-minute modified splat cooling assay, dose-response curves of five N-Benzyl-β-D-gluconamides were generated. All compounds produced ice recrystallization inhibition active IC_{50} values comparable to previously investigated active compounds such as, N-Octyl-β-D-gluconamide and N-4-Bromophenyl-β-D-glucopyranoside. Furthermore, validation that the dose-response curves follow a 4-parameter logistic (4PL) or 5PL sigmodal trend depending on symmetry was obtained. In addition, all tested compounds had lower cytotoxicity than N-4-Bromophenyl-β-D-glucopyranoside and higher solubility than

N-Octyl-β-D-gluconamide. Overall, N-Benzyl-β-D-gluconamides proved to be a promising class of compounds with the *para* derivatives being the most IRI active.

The second part of this work involved the examination of IRIs' ability to cryopreserve two different biological materials using different biopreservation protocols. The first being proteins and master mix (enzymes and oligonucleotides) during RT-qPCR after the freeze-drying process. The data showed that the IRIs did not interfere and were effective during both the lyophilization and qPCR processes. When compared to most effective concentration of the current industry standard, N-4-Bromophenyl-β-D-glucopyranoside increased the protein activity by ~30%, reducing the number of cycles to reach threshold value. The most significant contribution of this work was the discovery that carbohydrate-based small molecules may be working in more than one mechanism, as both cryoprotectants and lyoprotectants. In addition to proteins, the ability of IRIs to cryopreserve tissue products was investigated. Cell media supplemented with IRIs indicated that they can increase viability and reduce mortality in both cell suspension and single dermal sheets. With N-4-Methylbenzyl-β-D-gluconamide and N-Octyl-β-D-gluconamide being the most effective at reducing the damage associated with freezing and increasing recovery of the cells within the system of a simple one cell type thin tissue matrix.

Table of Contents

List of Figures

Chapter 1

Chapter 2

List of Tables

Chapter 2

Chapter 3

Chapter 4

List of Schemes

Chapter 2

Chapter 6

List of Abbreviations

β	Beta
δ	Delta
^{1}H	Proton
^{13}C	Carbon
2,6-DFB	N-2,6-Difluorobenzyl-β-D-gluconamide
2FA	N-2-Fluorophenyl-β-D-gluconamide
3D	Three-dimensional
3FA	N-3-Fluorophenyl-β-D-gluconamide
4-CBA	N-4-Chlorobenzyl-β-D-gluconamide
4-MBA	N-4-Methylbenzyl-β-D-gluconamide
4-MOBA	N-4-Methoxybenzyl-β-D-gluconamide
4PL	Four-parameter logistic equation
5PL	Five-parameter logistic equation
AFGP(s)	Antifreeze glycoprotein(s)
AFP(s)	Antifreeze protein(s)
AMU	Atomic mass unit
BA	N-Benzyl-β-D-gluconamide
BA(s)	Biological antifreeze(s)
$BF_3 \bullet OEt_2$	Boron trifluoride diethyl etherate
br	Broad
BSA	Bovine serum albumin
BSE	Bovine spongiform encephalopathy
C-AFGP	Carbon-linked antifreeze glycoprotein
C-linked	Carbon-linked
CB	Cord Blood
CDC	Centers for Disease Control and Prevention
cDNA	Complementary DNA

CH_2Cl_2	Dichloromethane
CO_2	Carbon dioxide
COVID	Coronavirus disease
CPA(s)	Cryoprotective agent(s)
Ct	Cycle threshold fluorescence
CTRL	Control
Cq	Threshold cycle number
d	Doublet
dd	Doublet of doublets
dH_2O	Distilled water
DIS	Dynamic ice shaping
DNA	Deoxyribonucleic acid
dNTPs	Deoxyribonucleotide triphosphate
DME	Dulbecco's Modified Eagle's Medium
DMEc	Phenol-free medium without added glutamine
DMSO	Dimethyl sulfoxide
DMSO-d_6	Dimethyl sulphoxide-d6 ($(CD_3)_2SO$)
DPBS	Dulbecco's phosphate buffered saline
ED	Electron donating
ESI	Electrospray ionization
EW	Electron withdrawing
EtOH	Ethanol
E gene	Envelope gene
FBS	Fetal bovine serum
HBS	Hank's balanced salt solution
HepG2	Human liver hepatocellular carcinoma cells
HI	Hydration index
HRMS	High resolution mass spectrometry
HSV-1	Herpes simplex virus type 1
Hz	Hertz
IC_{50}	Half maximal inhibitory concentration

IIF	Intracellular ice formation
Ih	Hexagonal ice
iPSCs	Induced pluripotent stem cells
IRI	Ice recrystallization inhibition
IRI(s)	Ice recrystallization inhibitor(s)
LD_{50}	Median lethal dose
LOEX	Université Laval's Research Centre: The Tissue Engineering Laboratory
m	Multiplet
m/z	Mass-to-charge ratio
M^+	Parent molecular ion
MEM	Eagle's minimum essential media
MeOH	Methanol
MGS	Mean grain size
MHz	Mega hertz
mM	Millimolar
mmol	Millimole
mRNA	Messenger ribonucleic acid
MS	Mass spectrometry
M gene	Membrane gene
NaOMe	Sodium methoxide
NMR	Nuclear magnetic resonance
NOGlc	N-Octyl-β-D-gluconamide
N gene	Nucleocapsid gene
ns	Not significant
OCH_3	Methoxy
pBrPhGlc	N-4-Bromophenyl-β-D-glucopyranoside
PBS	Phosphate buffered saline
q	Quintet
QLL	Quasi-liquid layer
R^2	Coefficient of determination
RBC(s)	Red blood cell(s)

RFUs	Relative fluorescence units
RNA	Ribonucleic acid
RT	Room temperature
RT-qPCR	Reverse transcription - quantitative real-time polymerase chain reaction
RdRp gene	RNA dependent RNA polymerase gene
s	Singlet
SARS-CoV-2	Severe acute respiratory syndrome coronavirus 2
SD	Standard deviation
SEM	Standard error of the mean
S gene	Spike gene
ssRNA	Single stranded ribonucleic acid
t	Triplet
td	Triplet of doublets
TH	Thermal hysteresis
VFF	Vapour fast freezing
VSV	Vesicular stomatitis virus
VV	Vaccinia virus
wt%	Percentage by weight
w/v	Weight/volume

Chapter 1: Introduction – Cryopreservation, the Types, and Mechanisms to Avoid Cryoinjury

1.1 Cryopreservation

Low-temperature preservation techniques that are frequently used can be broadly categorized into hypothermic (1 °C to 4 °C), high sub-zero (0 °C to -20 °C), or low sub-zero (-80 °C to -196 °C) preservation, allowing for short-term (hours), moderate (days/weeks), or long-term (months/years) storage, respectively.[1,2] Cryopreservation, which is typically in the high sub zero range, is the use of very low temperatures to preserve structurally intact living cells and tissues.[3] Low temperature significantly slows down biological and chemical processes in cells, which could result in the long-term preservation of cells and tissues.[3] However, freezing is lethal to the majority of organisms because it causes the formation of intra- and extracellular ice crystals as well as changes to the chemical makeup of cells which results in mechanical stress and harm to the cells.[3] For example, it is customary for large, complex tissues like organs to be preserved at hypothermic temperatures since they have a hard time withstanding some of the basic stressors connected with sub-zero storage.[1]

In 1948, a mix up in the lab led to the freezing of fowl spermatozoa at -70 °C in a mixture of glycerol, albumen, and water rather than the intended solution of levulose, this led to the discovery that glycerol was highly effective at increasing cell recovery post-freezing.[4,5] The method would now be termed the “classical freezing” approach deeming glycerol a successful cryoprotective compound.[4,5] This discovery was the start of a very complex field of study to ensure the viability of biological materials after freezing. Cryopreservation can be summarized into four main steps; (1) combining cryoprotectant agents (CPAs) with cells or tissues before

cooling; (2) lowering the temperature of the cells or tissues and storing them; (3) thawing the cells or tissues; and (4) removing CPAs from the cells or tissues after thawing.[3]

Although there are many applications for the cryopreservation technology in both basic and applied research, there are still certain restrictions.[3] The difficulty in success of cryopreservation is due to the number of variables that have been shown experimentally to affect survival; such as, the reduction of metabolism at low temperature, which has unavoidable side effects like a genetic drift toward biological variations of cell-associated alterations in lipids and proteins that could compromise cellular activity and structure.[3,4] Cells would be perfectly preserved if the amount of CPA that could be employed had no limit.[3] CPAs themselves, however, can harm cells in typical circumstances, especially when applied in high quantities, which is typically the case, necessitating a CPA removal step.[3] As well, when freezing, damage can be caused by thermal shock, dehydration, increased salt concentration after the water has frozen, osmotic shock, and most notably formation of ice crystals.[6]

1.2 Kinetic Effects of Cryopreservation

To address the many possibilities for damage a variety of freezing techniques have been used based on principles of freezing. Some of the first principles discovered as important determinants of survival were cooling rate, followed by warming rate.[5] These kinetic effects were investigated by Mazur who determined that the chance of intracellular freezing was indirectly controlled by the rate of temperature change because it influenced the movement of water across cell membranes.[5,7] As a theory to why intracellular freezing is generally fatal, Mazur suggests that the rate of temperature change affects the rate at which water is transported out of the cells during cooling and into the cells during warming, by regulating the osmolarity of the surrounding fluid.[5] The rate of cooling controls the rate at which water is converted to ice,

thus controlling the rate at which the concentration of the solution surrounding the cells changes.[5] If water can rapidly leave cells, the ice will all be outside of the cells, the cytoplasm won't fall below its freezing point, and thermodynamic equilibrium will be maintained across the cell membrane.[5] The protoplasm, on the other hand, will cool below its freezing point (supercooled) if the cooling rate is too quick for the cell's membrane to move enough water out of the cell.[5] The higher the extent of supercooling, the greater the likelihood that the cell would internally freeze.[5] Each cell exhibits maximum survival due to the interaction of these two factors—solution effects and intracellular freezing; as the cooling rate rises from very low rates, survival increases because the harmful effects of exposure to high salt concentrations are diminished; however, survival eventually declines because intracellular freezing supervenes.[5] Absolute survival is typically very low unless a cryoprotectant is present to lessen the damage at low cooling rates, therefore each cell has its own optimal cooling rate.[5]

1.3 Types of Biopreservation

Biopreservation, a hypernym which includes cryopreservation, is defined as preserving the integrity and functionality of cells, tissues, and organs held outside the native environment for extended storage times.[8] The most common approaches to biopreservation are vapour freezing, fast programmable freezing, slow programmable freezing, and vitrification.[9,10] Since samples are initially immersed into liquid nitrogen vapours before being submerged in liquid nitrogen (−196 °C), quick freezing is also known as vapour fast freezing (VFF).[9,10] Slow/fast programmable freezing occurs by samples being placed into the chamber of a programmable biological freezer and cooled in accordance with a predetermined program.[10] These program's freezing rates are established by experimentation and can go through a multitude of different temperature variations in the process. Lastly, vitrification involves submerging the sample in

liquid nitrogen to solidify the liquid into an amorphous, glassy condition.[9] It has been asserted that since vitrification minimizes the production of intra- and extracellular ice, it is less harmful than traditional freezing.[9] It is important to note that smaller ice crystals are produced generally by a faster freezing rate.[11] The small crystals are produced as a result of the water being super-cooled and crystallization into ice occurring rapidly.[11] On the other hand, larger ice crystals are produced by a slower cooling rate.[11]

There are many other freezing techniques outside of the previously mentioned ones. The following categories can be used to categorize different biopreservation techniques: (1) slow freezing; (2) vitrification; (3) sub-zero non-freezing storage; and (4) preservation in the dry state.[3] The focus in this thesis will be on slow freezing (rate-controlled freezing) and preservation in the dry state (freeze-drying).

1.3.1 Rate Controlled Freezing

The rate of cooling, which Mazur has referred to metaphorically as the inverted "U" of cryoinjury, is the fundamental concept that governs cell survival in this kind of procedure.[12] The concept dictates that as cooling rate rises from very low rates, survival increases due to a reduction in the harmful effects of exposure to high salt concentrations, but eventually survival declines due to intracellular freezing, creating a distinctive inverted U-shaped curve (figure 1.1).[5,13] Achieving success requires finding a balance between cryoinjuries since cells cannot survive if the rate is either too rapid or too slow.[12] The formation of extracellular ice, the creation of a differential water gradient across the cell membrane, and the exocytosis of intracellular water all occur when cells are cooled at a controlled, steady rate.[12] Since less water is available to produce ice, this has a significant cryoprotective impact.[12] Any water that does remain is so little that it prevents ice from forming and most likely causes the cytoplasm to vitrify.[12]

Generally, the sample is precultured or acclimated, followed by cryoprotection, as part of a sequence of manipulations used in controlled rate cooling techniques.[12] Specifically for slow cooling techniques, slow freezing initially replaces the water in the cytoplasm with CPAs in order to reduce cell damage and modify the cooling rate in accordance with the permeability of the cell membrane.[3] When using slow-cooling procedures, a costly controlled-rate freezer or a portable benchtop freezer are utilized, with a typical cooling rate of about 1 °C/min when there is less than 1.0 M of CPA present.[3] Low manipulation skill requirements and less risk of contamination throughout procedures are two advantages of slow freezing.[3] However, there is a sizable risk of freeze damage because extracellular ice develops during progressive freezing.[3]

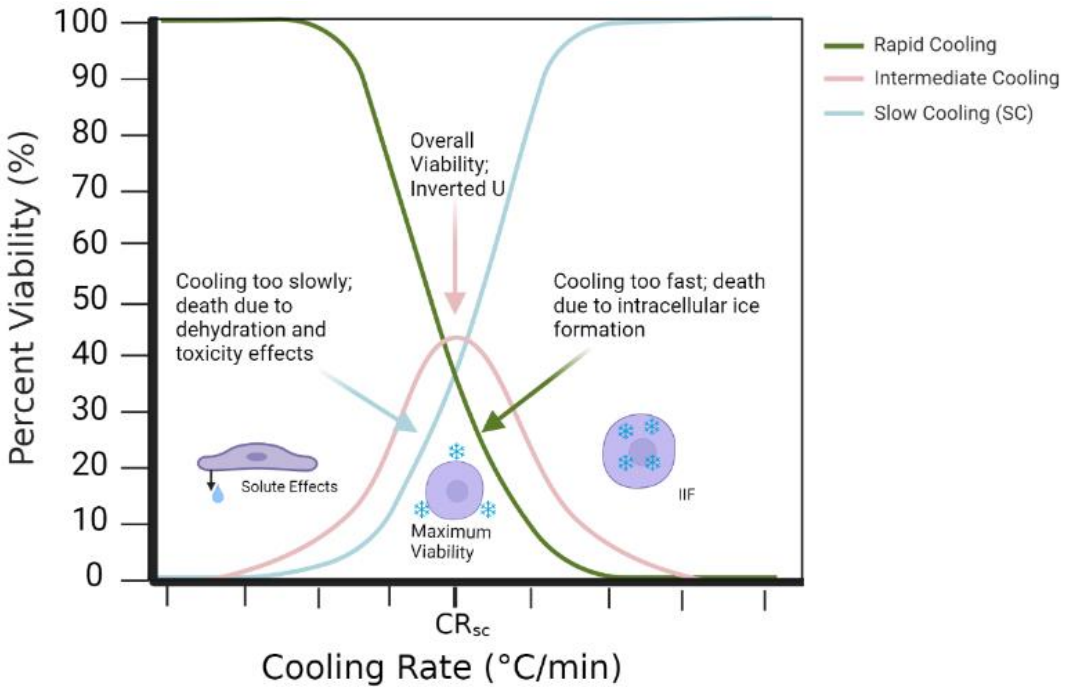

Figure 1.1. Graphic Representation of Mazur's Inverted "U" Two-factor Hypothesis of Freezing Injury. *Image describing the injury associated to rapid cooling and slow cooling. Figure adapted using BioRender ©.*[14]

1.3.2 Freeze-Drying

In the process of freeze-drying, ice is eliminated through sublimation, or a transition from a solid to a vapour without going through the liquid state.[15] This requires a freeze dryer, which is

made up of three fundamental parts; a drying chamber, a condenser chamber, and a vacuum system.[16] The main goal of the freezing process is to separate the solvent from the solutes.[16] In an aqueous environment, water will freeze into ice crystals, and solutes will be confined to the interstitial regions between the crystals.[16] The type of the solvent and other formulation components will determine the temperature required to accomplish complete freezing of the formulation.[16] The pressure inside the freeze-dryer is then decreased until it is below the vapour pressure of the ice.[15] Two main phases make up this procedure: freezing the solution and vacuum-drying the frozen solid (figure 1.2).[11] The drying phase can then be further divided into primary and secondary drying.[11] The frozen water is removed by primary drying, while the non-frozen "bound" water is removed by secondary drying.[11]

The cooling rate is one crucial characteristic that must be defined during freezing.[11] As previously mentioned, the size of the ice crystal is determined by the freezing rate. The size of the crystals play an important role as they dictates the size of the pores that will be produced during ensuing drying.[11] Large ice crystals have large pores, which causes water to sublimate quickly during primary drying, while secondary drying may be slower due to reduced surface areas, which restricts water absorption.[11] A moderate level of supercooling (10–15 °C) has been suggested to maintain balance.[11] The primary drying process sublimates ice to release frozen water, and the secondary drying process releases 'bound' water that is not frozen (desorption of water).[11] For sublimation to occur, the energy must be supplied in an amount equivalent to the heat required to sublimate ice.[15] This is done by raising the temperature of the transfer fluid and the shelves to a level that causes sublimation but not one that melts the frozen material in contact with the vial's bottom or collapses the partially dry product.[15] Water vapour is principally eliminated from the product by a process of bulk flow from a region of relatively high pressure

(the sublimation front) to low pressure.[15] The condenser keeps the partial pressure of water vapour in the chamber at a low level.[15] The major drying stage of the process is distinguished by a boundary that can be seen regressing from the top of the frozen layer.[15] The heat of sublimation is no longer required once the ice has sublimed, and the product temperature typically rises quickly toward the shelf temperature.[15] When all of the frozen water has been removed and the rate of water sublimation has been greatly decreased, the primary drying process is complete.[15] In general, not all of the water that was originally present in the product freezes into ice.[15] The formulation's composition and, to a lesser extent, the freezing process's thermal history determine how much unfrozen water is present.[15] Secondary drying is the process of removing this unfrozen water, which may make up 20% or more of the weight of the dry solids.[15] The removal of water vapour during secondary drying is mostly accomplished through the process of diffusion, or flow by molecular motion from a region of high concentration to a region of lower concentration, as opposed to primary drying, where water vapour is removed by bulk flow.[15] Even though less water is removed, secondary drying frequently accounts for a bigger proportion of the overall drying time than primary drying since it is generally slower than primary drying.[15]

Freeze drying is the most typical method for preserving solid proteins and is often referred to as lyophilization.[11] Mammalian cells are typically difficult to store in the dry condition due to challenges of delivering CPAs into the intracellular area.[3] Unfortunately, this technique has some adverse effects as the drying and freezing pressures produced by the lyophilization process can denature proteins to varying degrees.[11] Proteins in the solid state may still only have a limited ability to withstand long-term storage even after successful lyophilization with a protein stabilizer(s).[11]

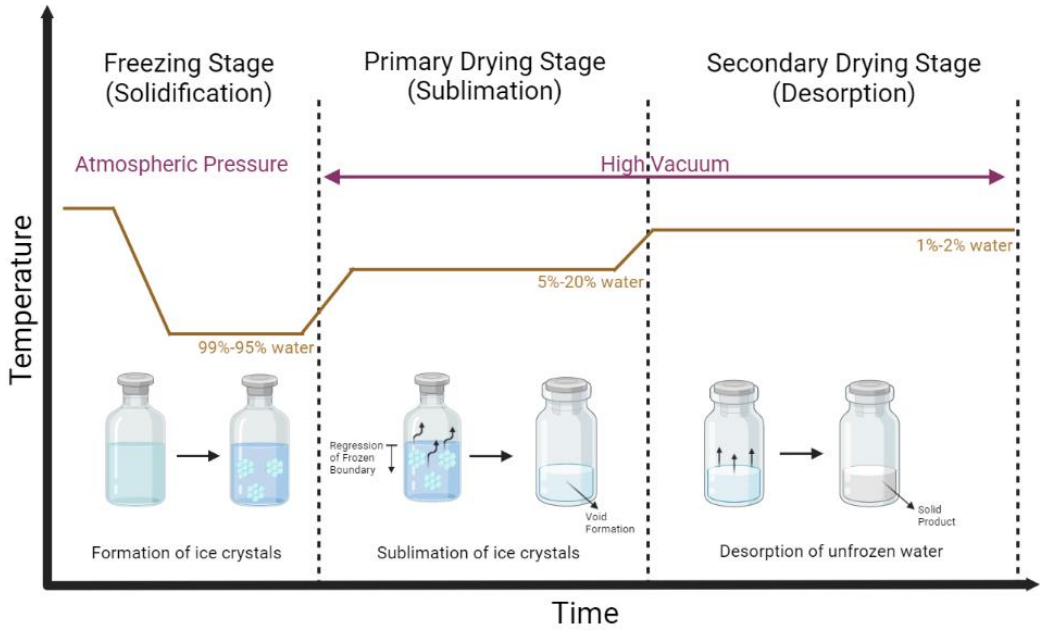

Figure 1.2. Graphic Illustration of Lyophilization Process. *The process of lyophilization, involving three stages to remove water from a sample through freezing, specific vacuum pressures, and temperatures. Figure adapted using BioRender ©.*[17]

1.4 Cryoinjury

All the previously mentioned approaches to cryopreservation come with shared and specific detrimental cryoinjuries (figure 1.3). Cryoinjuries are the physical and biological processes that cause harm to cells when temperatures are low, particularly those connected to the water's ability to change phases both extra- and intracellularly.[13] The lethality of an intermediate zone of temperature (-15 to -60 °C), which cells must pass through twice—once during cooling and once during warming—is the biggest challenge that cells face during cryopreservation.[13] In some cases, when cells are returned to isosmotic circumstances, they swell beyond their typical isotonic volume and lyse.[13] The swelling is because the hyperosmotic stress may produce a net leak/influx of nonpermeating solutes (mostly electrolytes).[13] Additionally, the water flux across the cell membrane during freezing and thawing can cause harm by producing intracellular ice formation (IIF).[13] IIF typically results in the death of cells.[5,13] As a result of the experimental finding that IIF phenomena depends on cooling rate, temperature, and CPA concentration, the

best cooling procedures have been developed to reduce IIF (section 1.3).[13] As previously mentioned, cells can be killed by cooling rates that are either too high or too low, however the mechanisms causing cell damage vary.[13] These two mechanisms of damage are the solution effect and IIF, which can be summarized by the following two points: (1) At slow cooling rates, the cryoinjury occurs due to the solution effects (i.e., the solute/electrolyte concentration, severe cell dehydration, and the reduction of unfrozen fraction in the extracellular space); and (2) at high cooling rates, cryoinjury occurs due to the lethal IIF.[13] Therefore, the cooling rate should be high enough to minimize the solution effects but low enough to avoid IIF.[13] Each cell exhibits maximum survival due to the interaction of solution effects and intracellular freezing at a characteristic cooling rate.[5,13] Proteins experience a comparable stress when a protein solution is frozen because ice formation quickly raises the concentration of all solutes.[11] As a result of selective crystallization, all concentration-related physical parameters, such as ionic strength and the relative composition of solutes, may be altered.[11] These alterations might cause a protein to become unstable.[11] In general, chemical reactions proceed more slowly as the temperature is lowered.[11] However, because of the higher solute concentration in a partially frozen aqueous solution, chemical reactions might even accelerate.[11]

Since no thermally induced reactions may take place at -196 °C, the duration of storage while frozen has so far not shown a significant level of damage to cells or proteins.[13] The reactions that might take place are the gradual accumulation of ionizing radiation direct harm, but this accumulation would probably not become substantial for hundreds of years of storage.[13] Another important mechanism that harms biological material is the process of warming and thawing [13]. One reason the warming rate has a significant impact is that relatively modest levels of intracellular ice are compatible with recovery.[11] As a result, these effects are dependent on

whether intracellular freezing or cell dehydration was brought on by the previous rate of cooling.[11,13] Rapid thawing can save many cells in the first scenario because extremely small intracellular ice crystals behave differently under slow and rapid warming.[11,13] Under gradual warming, the crystals can recrystallize, coalesce, and proliferate.[11,13] It has been shown to damage the cells in which it occurs; however, during rapid warming there is insufficient time for this to happen and the ice merely melts.[11,13]

In addition to the cryoinjuries obtained from the thawing and warming process a variety of other damages can occur to cells. Factors like cold shock, which have nothing to do with ice production, can harm cells.[13] Another factor is that the plasma membrane is assumed to be intact and to still have some of its typical semipermeable qualities.[13] Critical organelles inside cells might not be able to "survive" under the same circumstances that allow the plasma membrane to during the freezing process.[13] Lastly for cells, the "Cell Packing Effect" [5], which describes when cells are particularly densely packed in some systems that must be conserved, also results in cryoinjury. The traditional cryoinjury mechanisms—solution effects and intracellular freezing—cannot explain this observation.[5] The most likely explanation is that when the channels in which they are sequestered change form, densely packed cells are more prone to be harmed by mechanical pressures.[5] The ice that forms at their boundaries has undergone recrystallization, which is the cause of this phenomena.[5] Therefore, few multicellular systems have been investigated leaving a gap of knowledge in the research.

Freeze-drying provides its own distinct mechanisms of cryoinjuries, as the procedure not only contains the mechanism of injury from freezing but may also add additional stress due to the drying process. An unprotected protein may become destabilized, unfolded, or denatured under the many pressures that lyophilization may produce, which results in a loss of activity.[11]

Different proteins respond differently to stressors from freezing and/or drying.[11] Some proteins can continue to function both when they are dried and frozen.[11] Many proteins, however, cannot withstand drying or freezing conditions.[11] The first of these stresses is low temperature; the second is freezing stress, which causes dendritic ice crystals to form as well as increased ionic strength, altered pH, and phase separation; and the third is drying stress (removal of the protein hydration shell).[11]

Similar to cells, proteins have a maximum stability temperature, and both high and low temperatures can cause a protein to become unstable.[11] Low temperature stress is related to cold denaturation of proteins.[11] Oligomeric proteins often exhibit cold denaturation, which causes the dissociation of subunit oligomers.[11] Extracellular ice during the freezing process can also be problematic for proteins because it creates an ice-water interface when a protein solution is frozen.[11] Proteins that are adsorbed to surfaces can loosen their native folds, which causes surface-induced denaturation.[11] Additionally, the previously discussed solution effect has an impact on proteins in that freezing a buffered protein solution may cause pH shifts by selectively crystallizing one buffering species.[11] The storage stability of lyophilized proteins may be impacted by the pH reduction that occurs after freezing.[11] Increased electrostatic attraction between like charges in proteins brought on by this pH change can tend to trigger protein unfolding or denaturation.[11] Thus, pH has a significant impact on the rate of protein aggregation.[11] Finally, proteins might be impacted by the drying process. In an aqueous solution, proteins are completely hydrated.[11] The term "hydration shell" refers to the monolayer of water that covers the surface of a fully hydrated protein.[11] A lyophilized protein product typically has less than 10% water content.[11] The hydration shell is thus partially removed during lyophilization.[11] A protein's natural state may be disturbed, and denaturation may result from the

removal of the hydration shell.[11] When a protein is dehydrated, it tends to transfer protons to ionized carboxyl groups.[11] This eliminates as many charges as possible from the protein.[11] Protein aggregation could be facilitated by the reduced charge density via protein-protein hydrophobic interaction.[11] Another essential component of a protein's active site or sites are water molecules.[11] Proteins are quickly rendered inactive when these functional water molecules are removed during dehydration.[11]

The identification of these cryobiological characteristics and a deeper comprehension of cryoinjury mechanisms are essential for protein function and cell survival. It is necessary to keep in mind that survival is typically characterized in terms of the viability (e.g., the cell membrane's integrity) and/or capacity for continued growth and development of the cells.[13] The most effective technique to mitigate the cryoinjuries described above, in addition to prediction and protocols, has been with CPAs and lyoprotectants, which will be further detailed in section 1.6.

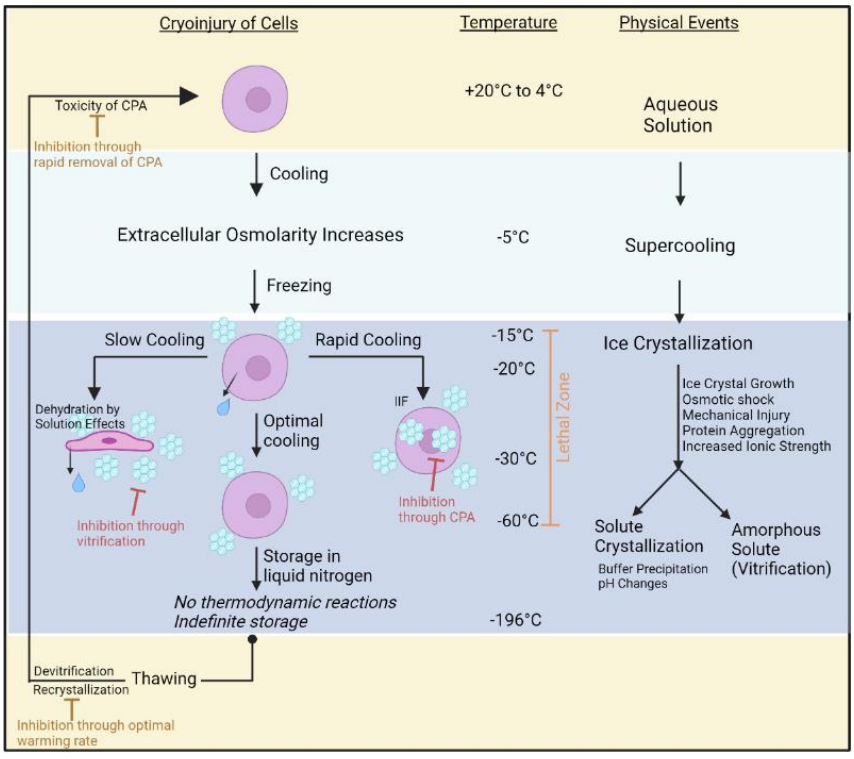

Figure 1.3. Schematic of Physical Events and Cryoinjury of Cells and Proteins During Freezing and Thawing. *Figure adapted using BioRender ©.*[13,15]

1.5 Ice Recrystallization

For successful cryopreservation the least amount of intracellular ice possible is essential.[18] This is due to the negative consequences brought on by intracellular ice accumulation. Although there is a link between intracellular ice accumulation and cell death, there is evidence to show that this relationship is not causal.[19] Cell death linked with IIF is not induced by the initial nucleation of ice, but rather by an alternative process during warming.[19] As previously mentioned, cell survival post-cryopreservation is reliant upon the rate at which the cells are warmed during thawing.[19] It has been determined that ice recrystallization is the main mechanism of damage that results in cell death after IIF.[19,20] Cell death during cryopreservation has been linked in large part to ice recrystallization[19] The literature on metallurgy and material science has thoroughly examined the mechanism of recrystallization.[19] According to a generally accepted theory, intracellular ice damage develops as a consequence of mechanical trauma as a result of a net increase in intracellular ice crystal size during warming (recrystallization), however, it has been hypothesized that intracellular ice may play a crucial role depending on its quantity, size, or location.[21]

When biological materials are cryopreserved, this behaviour of ice can negatively impact them.[22] The rates of ice recrystallization are highest when the frozen sample is being thawed, though they can happen during the freezing, storage, and thawing cycles of cryopreservation.[22] Ice recrystallization is a thermodynamically driven process, this process is known as Ostwald ripening in which large ice crystals develop at the expense of small ones, resulting in an increase in the mean ice crystal size and a decrease in the number of ice crystals at a constant total ice volume.[22,23] Ostwald ripening is the result of a decrease in the system's overall ice

crystal/solution interface energy, which is the driving force underlying this process.[23] Overall, less free energy is generated as a result of this process.[22]

The loss of cell viability during cryopreservation is linked to the formation of ice inside of cells and the net increase in crystal size due to recrystallization during thawing.[21] The main cause of damage in the cryopreservation of single-cell and multicellular systems is ice recrystallization.[20] It is crucial to reduce intracellular ice recrystallization in order to encourage the recovery of cells that undergo IIF.[20] More particularly, it has been shown how preventing ice from recrystallizing is essential for boosting post-freeze-thaw cell survival.[19] Despite the fact that the mechanisms causing cellular damage during cryopreservation are numerous and intricate, the relationship between cell viability after freeze-thaw and a substance's capacity to prevent ice recrystallization has significant ramifications for the creation of better cryopreservation protocols.[19]

1.5.1 The Structure and Growth of Ice

It is crucial to describe the structure of ice in order to better comprehend the mechanism of ice recrystallization[22] The hexagonal ice (Ih) lattice unit is the most prevalent type of ice at atmospheric pressure.[22] A single oxygen atom is hydrogen-bonded to two hydrogen atoms in a regular crystalline structure, which has an organized arrangement of intermolecular hydrogen connections between water molecules (figure 1.4).[22] The inability of the water molecules inside an ice crystal to make the ideal amount of hydrogen bonds causes them to have a larger free energy than the water molecules at the bulk-water/ice crystal contact.[22] Large ice crystals with a lower surface area to volume ratio are thermodynamically more stable than smaller ice crystals.[22] Water molecules move from an ice crystal through a semi-ordered quasi-liquid layer (QLL), which is the layer between ice crystals and the bulk water, as the system tries to minimize its free

energy.[22] The water molecules then go to bulk water and are then transferred to an ice crystal that is actively growing, resulting in a general decrease in the surface area to volume ratio and, ultimately, a reduction in the system's free energy.[22] The total amount of ice and liquid water in the sample doesn't change during this procedure, but the quantity of ice crystals and the average size of the crystals do.[22]

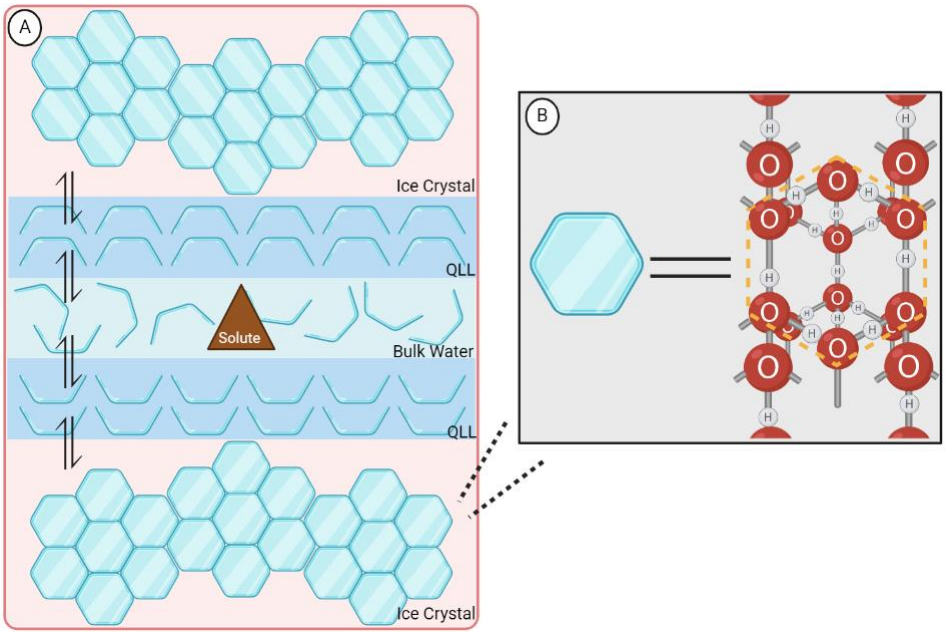

Figure 1.4. Illustration of Ice Growth and Structure of Ice. *A) Water moves from a crystal layer through a QLL to bulk water. If a solute is added, it will reside at the QLL–bulk water interface between two adjacent ice crystals. B) Structure of Ih lattice unit. Each oxygen ion is linked to its four nearest neighbours by hydrogen bonds, protons are nearer to one end than the other in such a way that each oxygen ion has two 'near' hydrogen ions. The hexagonal shape of a single ice unit is outlined in a dashed yellow line. Figure adapted using BioRender ©.*[22,24]

1.5.2 The Mechanism of Ice Recrystallization

Recrystallization proceeds as a result of the total crystal phase's surface free energy being minimized and the chemical potential being balanced between all phases.[23,25] Recrystallization is most likely to happen by the following three mechanisms: migration (also known as diffusional growth), isomass, and accretion.[23,25] Most of the time, migration and accretion are how polycrystalline ice in a liquid solution undergoes Ostwald ripening.[23,26]

The process of migration is best simplified as the melting of smaller crystals, and the melted liquid is then transported to the surface of larger crystals.[26] In a polycrystal system, there is a propensity for larger crystals to develop at the expense of smaller crystals during migratory recrystallization.[25] Because of the increased curvature and hence greater surface free energy, smaller crystals cannot bond their surface water molecules as tightly as bigger crystals.[25] As a result, through the freeze concentrated matrix, the water molecules on the surface of small crystals have a tendency to migrate to the surface of larger ones, leading to the formation of larger crystals and the disappearance of smaller ones.[25] At smaller ice volume fractions, this diffusion of water molecules through the intermediary liquid from smaller to larger ice crystals often predominates.[23] Therefore, the internal product temperature has an impact on this mechanism.[26] When the temperature is dropped again after the smaller ice crystals partially or totally melt, the liquid re-freezes on the larger crystals.[26] The pace at which the water molecules diffuse to the bigger ice crystal surface, or diffusion kinetics, has a significant impact on migration.[26] The viscosity of the serum phase has a significant impact on how the crystals diffuse or migrate, therefore the rate of diffusion is sluggish when the viscosity is high.[26]

In a single crystal, a similar process known as isomass recrystallization can take place.[25] Take a single crystal that has been separated and has a rough surface.[25] High curvature portions of surfaces cannot bind surface water molecules as tightly as smoother portions of surfaces.[25] The rougher surface consequently becomes smoother.[25]

Accretion can be described as a single, bigger crystal formed by the merging of two or more nearby ice crystals.[25,26] Since ice crystals are stationary during this operation, they must be placed close together and have a point of contact.[25,26] The ice crystals coalescing occurs preferentially at large ice volume fractions because the contact point has an apparent high

curvature and is not as stable as the remainder, leading to the creation of a neck by transportation of water molecules to this area.[23]

Lastly, it is interesting to note that the mobility of water molecules in a matrix that has undergone freeze-concentration may be one of the variables determining the pace of recrystallization given the mechanisms of recrystallization mentioned above.[25] Ice crystal growth is accompanied by water molecule movement.[25] As a result, boosting water mobility may boost the rate of recrystallization.[25]

1.6 Cryoprotective Agents

IIF should be prevented by using a gradual cooling method, as discussed in section 1.4. Slow cooling can increase cell viability, as it avoids numerous and large intracellular ice crystals, although it is insufficient.[13] CPAs are necessary for the majority of cells for optimal survival.[13] These cryoprotectants have a variety of mechanisms, including those that enable freeze-tolerance (the capacity to be frozen and then thawed), freeze avoidance (the ability to stop ice from forming), and even freeze promotion (as a predatory strategy).[27] A cryoprotectant's capacity to prevent ice from recrystallizing is a crucial quality for boosting cell viability after a freeze-thaw.[19] This is due to the fact that CPAs can alter the cells' freezing behavior by affecting the rates of water transport, crystal nucleation, and growth.[13] The ability of cells to survive cryopreservation is dependent not only on the presence of CPAs but also on their concentration.[13] To address the many potential damage scenarios, an ideal CPA must have two crucial properties: (1) they must be highly soluble in water and maintain this solubility at low temperatures in order to produce a significant decrease in the freezing point; and (2) they must be biologically acceptable by having a low enough toxicity so that they can be used at concentrations high enough to produce these effects.[3,4,12,13]

Treatment of the cells or tissues with cryoprotectant solutes, frequently in high concentrations, is the typical method of cryoprotection.[4] This creates a driving force for the passage of water via osmosis and of solutes by diffusion.[4] Aqueous solutions undergo concentration and composition changes during freezing, which also creates forces that cause water and solutes to migrate.[4] Numerous obstacles to solute free diffusion exist in biological systems (membranes), and these barriers can cause momentary, and occasionally equilibrium, changes in compartment volumes.[4] If these changes are too great, these changes may be detrimental.[4] Therefore, it is crucial to revisit Mazur's inverted "U" theory of cryoinjury and take into account cooperative cryoprotection in relation to the dynamics of the freezing process.[12] Controlling cooling rate is to achieve the ideal level of cell dehydration between too little (which leads to ice damage) and too much (resulting in colligative damage).[12] Colligative agents control the degree to which excessive and inadequate dehydration take place.[12] In conclusion, gradual freezing used in cryopreservation of cells causes the cell to become dehydrated in response to rising osmotic pressure because electrolytes are drawn outside the cell during extracellular ice formation.[19] Dehydration of the cells is harmful to cell viability even if it aids in preventing intracellular ice development.[19]

Cryoprotectants can help stop excessive dehydration. Non-permeating and permeating CPAs are the two cryoprotectant classes employed.[19] Non-permeating cryoprotectants, which are most frequently used during fast cooling, do not cross the cell membrane and thus remain outside the cell, increasing the osmolarity of the extracellular solution, allowing the cell to dehydrate more easily before freezing and preventing the formation of intracellular ice.[19] In contrast, permeating CPAs raise the cell's total osmolarity.[12] These cryoprotectants easily penetrate cell membranes and lower intracellular electrolyte concentrations while maintaining higher cell

volumes.[19] Osmotic dehydration occurs when cells are exposed to a high concentration of cryoprotectant.[4] The cells first expand in volume as the cryoprotective chemical penetrates, bringing water with it, until they reach their final volume.[4] The permeability parameters determine the degree of shrinkage and the pace of change in cell volume.[4] This is because the cryoprotectant takes up space inside the cells; as a result, if the total volume is to be normal, the volume of water must be smaller than the physiological water content.[4] This leads us to the two crucial steps involved in using penetrating CPAs to preserve cells: (1) Pre-freezing addition of a CPA to the cells, and (2) post-thaw removal of the CPA from the cells.[13] When a CPA is introduced, cells temporarily shrink before gradually expanding back to their almost normal size as the CPA permeates.[13] When the CPA is removed, they temporarily expand in volume; how much this happens depends on how the CPA is removed as well as how permeable the cell naturally is to water and CPA.[13] The osmotic uptake of water leads the cells to enlarge over their initial volume when a penetrating cryoprotectant is eliminated by exposing the cells to a reduced concentration of the substance.[4] They subsequently begin to contract as the cryoprotectant leaves, accompanied by enough water to keep the osmotic balance; they only reach their physiological volume if the nonpermeating solute has not been lost or gained throughout the process.[4] Cryoprotectants are typically more dangerous to remove than to introduce because cells are typically more sensitive to swelling than to shrinkage.[4] Another major problem with penetrating cryoprotectants is cytotoxicity, which can lead to the disruption of intracellular signaling.[19]

1.6.1 Common Cryoprotective Agents

Cryoprotectants lessen the amount of ice generated at any given temperature by merely increasing the total concentration of all solutes in the system.[4] Depending on the cell type,

cooling rate, and warming rate, different CPAs have been created and are utilized to decrease the amount of ice formed at any given temperature.[3] All factors should be calibrated to achieve the highest survival rate of cells and tissues.[3] Based on the two categories indicated in the paragraph above, many compounds share these characteristics. Examples of cell membrane-permeating cryoprotectants, include dimethyl sulfoxide (DMSO), glycerol, ethanediol, and 1,2-propanediol [3,4,19]; and nonmembrane-permeating cryoprotectants, such as 2-methyl-2,4-pentanediol and polymers such as polyvinyl pyrrolidone, hydroxyethyl starch, and various sugars.[3]

Glycerol was the first of the cryoprotectants to be discovered. Due to the fact that glycerol is a nonelectrolyte, it has the potential to act by lowering the electrolyte concentration in the remaining liquid solution in and surrounding a cell at any given temperature.[3] A colligative addition, like glycerol, raises the cell's initial osmolarity before the freezing process begins.[12] This lessens the solution effects, lowering the optimal cooling rate and raising the maximum survival attained as a result.[4] However, one impact of freezing an aqueous solution was to raise the concentration of solutes in the decreasing volume of the remaining solution, and this could be the primary cause of harm.[4] James Lovelock provided strong evidence in a series of papers published in the 1950s that freezing injury to cells is caused by salt concentration rather than ice, and that glycerol only offers protection from this damage to the extent that it regulates the rise in salt concentration during freezing.[4] As a result, glycerol's effectiveness—or that of any other similar cryoprotectant—depends on a number of factors.[4] With that being said, glycerol is frequently employed for the storage of animal sperm and microorganisms.[3]

In 1959 the protective effect of DMSO was demonstrated, this polyol compound remains the most effective additive [3]. Currently, DMSO is the most often utilized cryoprotectant.[22] Because it is inexpensive, DMSO has been widely employed to cryopreserve cultured

mammalian cells.[3] Similar to glycerol, DMSO works by lowering the concentration of electrolytes in the remaining, unfrozen solution in and around a cell at any given temperature.[3] However, the survival rate of some cell types is still quite low and cryopreservation of biological material with DMSO does not guarantee 100% recovery.[22] The fact that DMSO is cytotoxic is a significant problem.[22] While DMSO generally becomes more effective as a cryoprotectant as concentration increases, its harmful effects on cells are temperature- and time-dependent and have been well-documented.[19] Additionally, DNA methylation and histone modification have been observed to decrease survival rates and induce cell differentiation.[3] The use of DMSO in typical therapeutic applications is made more challenging by these detrimental consequences of cryopreservation.[3] Unfortunately, considerable cellular damage happens in the absence of a CPA.[28] However, because of their toxicity, CPAs like DMSO and glycerol (figure 1.5) must be removed after thawing, which may have a negative impact on the functionality and integrity of the retrieved cells, tissues, or material.[28] In order to avoid DMSO's toxic effects, it may be possible to replace it with non-cytotoxic cryoprotectants that prevent ice from recrystallizing or at least minimize the amount of DMSO needed for cryopreservation.[22]

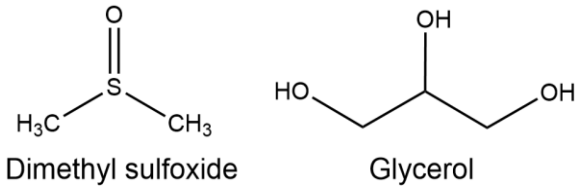

Figure 1.5. Structures of Dimethyl Sulfoxide (DMSO) and Glycerol.

1.6.2 Lyoprotectants

Many efficient cryoprotectants or protein stabilizers in solution do not stabilize proteins during dehydration because the dehydration (drying) stress is distinct from the freezing stress.[11] Some cryoprotectants even cause protein destabilization.[11] Therefore, compounds referred to as lyoprotectants (lyophilization stabilizers), are used to prevent proteins from becoming

denaturized during lyophilization.[11] In cases where when a single stabilizer is unable to act as both a cryoprotectant and a lyoprotectant, two (or more) stabilizers may need to be utilized.[11] Sugars, polymers, proteins themselves, non-aqueous solvents, surfactants, amino acids, and various excipients are only a few of the many groups of lyoprotectants.[11] According to Dr. Wang, each class has its own hypothesized mechanism of action.[11] The water replacement concept is, nonetheless, one of the most important.[11] In order to meet the hydrogen bonding needs of the polar groups on the protein surface, this mechanism involves the formation of hydrogen bonds between a protein and a lyoprotectant at the conclusion of the drying process.[11] These lyoprotectants act as water substitutes to protect the proteins' natural structure.[11] In this method, during dehydration, intra- or interprotein hydrogen bonding may be avoided.[11] Protein binding, which may prevent protein-protein interactions, and other processes of protein stabilization such as, forming a monomolecular layer on the protein surface to accomplish the maximal stabilization also appear to be operational mechanisms.[11]

1.6.3 Biological Antifreezes (Antifreeze Glycoproteins)

Biological antifreezes (BAs) are another powerful ice recrystallization inhibitor (IRI), that can provide an alternative for CPAs besides synthetic compounds.[28] In order to prevent cryo-injury in species living in sub-zero settings, nature has evolved BAs as naturally occurring "antifreezes".[28] BAs regulate the development of ice and protect organisms from the cellular harm caused by freezing.[28] These peptide-based substances are present in a variety of plants, insects, and fish.[28] These peptide can be broadly categorized into antifreeze proteins (AFPs) and antifreeze glycoproteins (AFGPs).[27]

There are two different antifreeze actions that biological antifreezes display.[29] The first being IRI activity, AF(G)Ps were the initial substances found to possess this desired trait.[22]

Thermal hysteresis (TH) is the other and most researched. TH refers to a solution's freezing point being selectively lowered in relation to its melting point.[29] The binding of a BA to the surface of a seeded ice crystal results in TH activity.[29] A localized freezing point depression is made possible by the BA's binding to the ice's surface, and this results in a change in the ice crystal habit.[29] Dynamic ice shaping (DIS) is the name for this shift in ice crystal behavior.[29] AF(G)Ps are currently the most effective IRIs.[22,27] However, because they are not always suited for cryopreservation, these biological molecules have not been developed as cryoprotectants.[22,27] This is due to potential immunogenicity and toxicity concerns, expense of production, and their TH activity and ice binding capabilities, as this unique ability to bind to ice alters the habits of ice crystals leading to the formation of needle like ice crystals seen with DIS.[22,27] As well, cryopreservation temperatures typically drop below the TH gap (the temperatures between the freezing and melting point), where AF(G)Ps can exacerbate cellular damage.[22,27] This has resulted in a combination of successes and failures as cryoprotectants.[22,27]

Compounds that possess the very desirable feature of maintaining small ice crystal size within a frozen solution have several medical, commercial, and industrial applications.[29] Therefore, it makes sense to create synthetic mimics that can be customized and have configurable function.[27] It is unknown why some substances are better inhibitors of ice recrystallization than others.[19] Additionally, the fundamental structural elements required for efficient ice recrystallization inhibition have not been identified.[19] This is due to the fact that BAs are a complicated family of substances with radically varied structural characteristics, making it challenging to understand how they prevent ice from recrystallizing.[29] Nevertheless, all "rationally constructed" novel IRIs are based on this significant class of chemicals.[29]

Our lab's early research resulted in the creation of carbon-linked antifreeze glycoprotein (C-AFGP) analogues with "tailored" antifreeze action.[22,28] These C-linked AFGP analogues show strong IRI activity but no ice binding and hence no TH activity or DIS. Subsequently, it was reported that simple mono- and disaccharides exhibit moderate IRI activity.[22,29] This led to the discovery of several small carbohydrate-based IRIs with ice recrystallization inhibition activity, that are more amenable to large-scale preparation for the medical and commercial applications of IRIs.[22,29]

1.7 Small Molecule Carbohydrate-based Ice Recrystallization Inhibitors

The larger significance of these findings is that novel cryoprotectants which inhibit ice recrystallization may be able to overcome the current drawbacks of existing cryoprotectants, making it possible to preserve tissues and possibly even organs effectively in addition to cells.[19] Numerous carbohydrates have IRI action, making them appealing for reducing the amount of DMSO needed or potential future substitutes as they have minimal to no cytotoxicity.[19] In addition, polyhydric alcohols like glycerol, which we know to affect the structure of nearby water and ice formation, are comparable to carbohydrates.[19] It has been demonstrated that carbohydrates, when combined with DMSO, glycerol, or 1,2-propanediol, increase cell viability post-thaw.[19] The outcomes of the trials where carbohydrates appeared to be helpful seemed to rely on the structure of the carbohydrate that were utilized.[19] Although, these investigations use various cell types, cooling rates, and carbohydrate concentrations, which leads to further challenges as it is difficult to evaluate the true efficiency of carbohydrates as cryoprotectants in light of these findings.[19] In contrast to naturally occurring AF(G)Ps, which have been shown to be harmful when used at low temperatures or high concentrations, novel small molecule carbohydrate derivatives discovered by our lab have proven to exhibit the IRI activity of

AF(G)Ps, while lacking DIS characteristics.[20] These small carbohydrate-based compounds, with molecular weights under 300 AMU, are active IRIs at millimolar to sub-millimolar concentrations, which is why their less complex synthesis makes them of special interest.[21,28]

1.7.1 Properties of Carbohydrates and Mechanism of Action

Previous findings in the lab led to the conclusion that the level of activity and carbohydrate hydration are correlated.[19] The quantity of tightly linked water molecules that surround a carbohydrate in aqueous solution is known as the hydration layer or hydration shell of the carbohydrate.[29] The relationship between IRI activity and the carbohydrate's hydration index (HI) was discovered as a result of this finding.[22] The HI, which measures the degree of hydration per molar volume of carbohydrate, is defined as the hydration number divided by the partial molar volume of the carbohydrate.[22,29] It gave a hint as to the substrate's level of hydration in relation to its size or volume.[22,29] Using this metric, it was found that IRI activity and HI were linearly correlated for all of the mono- and disaccharides evaluated in the study.[22]

Furthermore, solid-state NMR studies and TH measurements suggested that ice binding was not a requirement for IRI activity because none of the non-ionic carbohydrate-based compounds evaluated in this study exhibited TH activity or DIS abilities, indicating that the activity exhibited by these compounds was not brought on by an interaction with the ice lattice.[22,29] This led to the development of a different, based on the compatibility of a solute with bulk water, hypothesized mechanism for the suppression of ice recrystallization[22,29] The highly ordered ice lattice and bulk water are separated by a QLL, which is covered in detail in section 1.5.1 of this chapter.[22,29] Bulk water molecules transfer to the QLL, then from there to the expanding ice lattice, causing the ice to recrystallize.[22,29] Carbohydrates may be concentrated in the bulk-water-QLL interface, according to Tam et al.[29] A carbohydrate that fit poorly into bulk

water will disrupt its three-dimensional hydrogen-bonded network more severely, which raises the energy required to move bulk water to the QLL.[29] It was believed that this ability was connected to the extent to which carbohydrate residues were hydrated.[22] Thusly, it was proposed that the inhibition of ice recrystallization caused by carbohydrates occurred at the bulk-water-QLL interface because more highly hydrated carbohydrates, such as D-galactose, disrupted the pre-ordering of bulk-water and made it less energetically advantageous for water molecules to transfer to the QLL.[22,29] Whereas, the suppression of ice recrystallization was not noticed with less hydrated carbohydrates, such as D-talose, which fit into bulk water better and disrupted the pre-ordering of bulk water less.[22,29] Therefore, it was assumed that these substances were preventing the recrystallization of ice by modifying the bulk-water and/or QLL structures.[22]

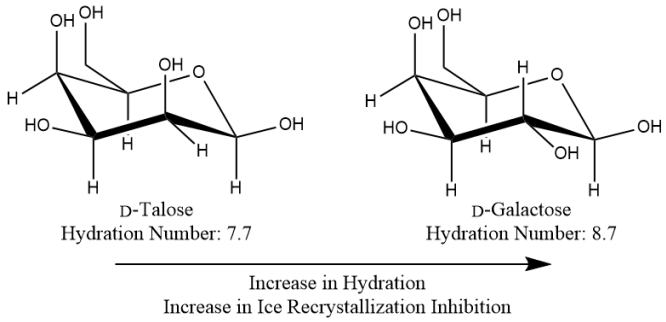

Figure 1.6. Comparison of Hydration and Structure of D-Galactose and D-Talose. *Figure adapted using ChemDraw ©.*[22]

1.7.2 Previous Ice Recrystallization Inhibitor Results and Structures

Following this work, several structurally different carbohydrate derivatives have been synthesized and their IRI activity have been evaluated.[22] Our group has successfully proven that it is possible to rationally design low molecular weight derivatives of carbohydrates over the previous nine years.[21,27] These small-molecule IRIs can avoid cellular harm in some cases by regulating the formation of intracellular and extracellular ice during freezing and thawing.[21] Our group has carried out numerous structure-function experiments to pinpoint the essential structural components of these IRIs throughout the course of our research. Amphipathic

structures with both hydrophilic and hydrophobic portions are one of the fundamental requirements for IRIs.[27] This is a difficult design criterion because hydrophobicity tends to encourage aggregation or self-assembly, which results in only hydrophilic surfaces being exhibited.[27] Additionally, a recent study showed that these small molecule IRIs' size and amphiphilicity can facilitate passive penetration into endothelial cells and regulate intracellular ice recrystallization, one of the main causes of damage that occurs after IIF.[20] The relevance of the amide bond was also discovered for some IRIs since the activity of the IRIs was dramatically reduced when the amide was replaced with an ether linkage.[22]

While we have identified several structurally distinct families of IRIs, the aryl-glycosides in particular have shown to be effective cryoprotectants for the freezing of human red blood cells (RBCs).[21] IRIs based on aryl-glycosides have the ability to enter cells and regulate the recrystallization of intracellular ice in addition to controlling the growth of extracellular ice.[21] During warming to high sub-zero temperatures, the IRI treatment was shown to maintain a significant amount of small ice crystals and to significantly block intracellular ice recrystallization.[21] It was proposed that additional substances, such as surfactants and hydrogelators, which have the ability to modify the structure of bulk water, may also function as effective IRIs (general structures shown in figure 1.7).[22] This investigation of these small molecules that were extremely effective IRIs led to the development of these compounds, which were significantly more active than the prior reducing sugars.[22] The capacity of hydrogelators like N-Octyl-β-D-aldonamides to prevent ice from recrystallizing was also studied.[22] At a low dosage of 0.5 mM, the glucose derivative N-Octyl-β-D-gluconamide (NOGlc) (**1**) was discovered to have powerful IRI action, compared to all other compounds which were tested at 22 mM.[22] This small molecule IRI remains the most effective IRI developed by the Ben lab today.[22]

According to studies on these substances, micelle formation, gelation, or interaction with the ice lattice are not required for these substances to exert their powerful IRI activity.[22]

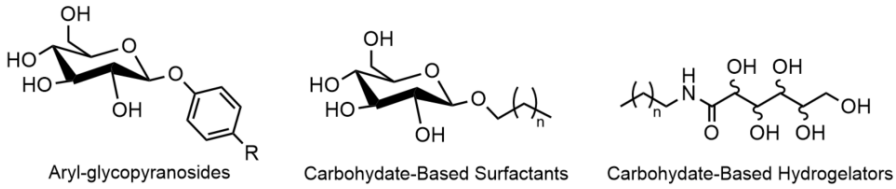

Figure 1.7. General Structures of Aryl-Glycosides, Surfactants, and Hydrogelators.

Our strategy controls ice growth once intracellular ice formation has taken place rather than attempting to prevent it in order to reduce subsequent cellular harm.[21] Some IRIs can internalize into cells, changing how cells react to gradual and rapid freezing as well as regulating intracellular ice recrystallization during freezing.[21] From this, the conclusion that IRIs are excellent candidates for use as cryoprotectants to preserve cells and tissues at extremely low temperatures can be reached.[21] The identification of novel cryoprotectants that can significantly improve upon the currently constrained cryopreservation protocols as well as potentially significantly reduce or eliminate the need for conventional toxic cryoprotectants like DMSO will result from further development of these novel small molecules with a high degree of IRI activity.[22,29]

1.8 Goals and Objectives

As discussed in the previous sections, cryopreservation has many useful applications that can greatly improve the commercial and medical fields.[13] Although, due to the complexities of the process and the associated cryo-injuries, the success of freezing products or biological materials varies. One of the main concerns being the IIF that takes place as a result of ice recrystallization during the freezing and thawing process.[13] As a result, the goal of the Ben laboratory is to design small molecule carbohydrate-based IRIs. This is an intricate undertaking as the specific structural requirements to make an effective IRI are still not known.[22] Despite our

laboratory's large library of active IRIs, there are still many compounds to be investigated and altered based on structure-function analyses in order to improve outcomes. As well, there are many different types of biological materials that can be more effectively cryopreserved that have yet to be investigated. The specific goals of this thesis can be divided into three main experiments as an effort to continue these ongoing studies; investigate and conduct structure-function analyses on surfactant and hydrogelator derivatives; investigate the ability of small molecule carbohydrates to effectively preserve proteins during freeze drying; and assess the ability of IRIs to increase the post-thaw viability of simplified human tissue model suitable as a universal skin graft.

1.8.1 Objective 1 – Assessment of Compound Properties

To date the most effective IRI developed by our laboratory is N-Octyl-β-D-aldonamide (**1**) (IC_{50} 0.09 mM), however due to a low solubility limit (1 mM) the applications of **1** are limited. In 2011, Dr. Briard from our lab performed structure-function analyses to investigate a similarly structured class of compounds.[30] This new class of hydrogelators are known as N-Aryl-β-D-gluconamides (figure 1.8). Due to previous results identifying that a replacement of the alkyl chain with an aromatic ring in the alkyl-glycosides resulted in the discovery of active IRIs, it was hypothesized that the same replacement in the N-Alkyl-β-D-gluconamides could also result in the discovery of active IRIs.[30] As well, these studies revealed that the identity of the aromatic substituent had a dramatic effect on the IRI activity of the molecule.[30] The location of the aromatic substituent also impacted IRI activity.[30] Therefore, N-Aryl-β-D-gluconamides with various aryl substituents at different positions on the aromatic ring were investigated.

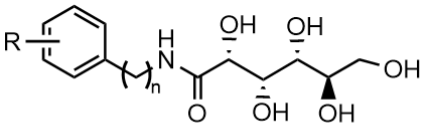

N-Aryl-ß-D-gluconamides

Figure 1.8. General Structure of N-Aryl-β-D-gluconamides.

Dr. Briard's research led to the discovery of new potential IRIs, including N-3-Fluorophenyl-β-D-gluconamide (3FA) (**2**) (figure 1.9) which showed IRI activity while also displaying a higher solubility limit (15 mM) compared to **1**.[30] Although, it must be mentioned that the IRI activity of **2** was not as active as that of **1**. However, in this study the IRI activity of these compounds were reported as a percent mean grain size (% MGS) of ice crystals, which is the average ice crystal sizes relative to a positive phosphate-buffered saline (PBS) solution control for ice recrystallization. Thus, these derivatives were previously assessed at a single concentration (typically 22 mM) and time point (30 minutes), an approach that neglects both the effects of time and concentration on IRI activity.[30] Therefore, an objective of this thesis is to broaden the current library of compounds using the improved splat cooling assay. By assessing the rate of ice crystal growth, dose-response curves can be constructed and IC_{50} values can be calculated. The IC_{50} value represents the concentration at which IRIs have obtained half of their maximum inhibitory capability. Compared to the % MGS formerly used, the IC_{50} value provides a more quantifiable measure of IRI activity.[30] In addition to IRI activity, cytotoxicity can be a major concern for CPAs; therefore, to evaluate compounds further a cytotoxicity assay will be performed on each derivative.

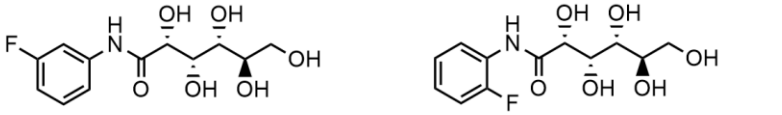

N-3-Fluorophenyl-ß-D-gluconamide (3FA) **2**

N-2-Fluorophenyl-ß-D-gluconamide (2FA) **3**

Figure 1.9. Structure of N-3-Fluorophenyl-β-D-gluconamide (3FA) (2) and N-2-Fluorophenyl-β-D-gluconamide (2FA) (3).

In an effort to find a solution for the low solubility limit of **1** while also maintaining the IRI activity, a new class of compounds with a benzyl group and various substituents will be assessed for IRI activity and cytotoxicity. With this research we will be able to search for trends to further develop our understanding of how the structure of these IRIs effect the IRI activity. As each biological material requires unique conditions and compounds for optimal cryopreservation having a library of compounds with unique structures is an asset. Therefore, the objective of this study is to synthesize and assess a small library of compounds (figure 1.10) for cytotoxicity and IRI activity-based on the modified splat cooling assay to produce the optimal dose-response curves.

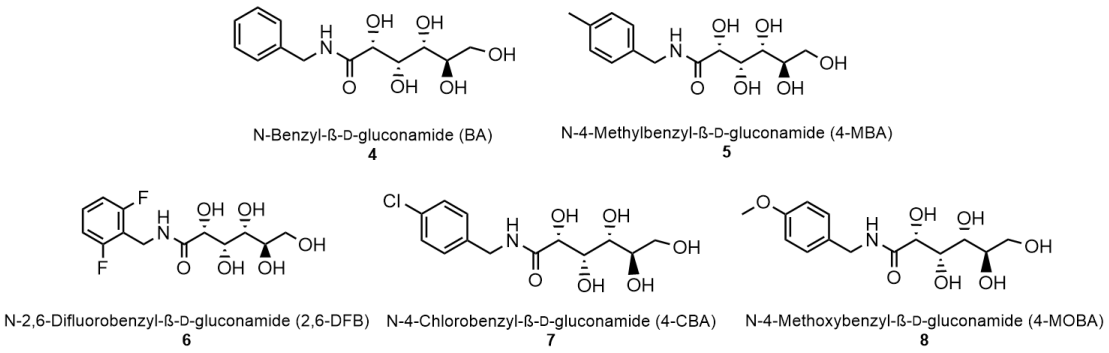

Figure 1.10. Structure of N-Benzyl-ß-D-gluconamides to Assess.

1.8.2 Objective 2 – Increasing Thermostability of Proteins with Ice Recrystallization Inhibitors

In the current climate of the world the preservation and storage of proteins has seen an increase in interests due to SARS-CoV-2. Cryoprotective agents such as trehalose are utilized during cryopreservation due to their important storage properties, such as the recovery of protein function after cryo-storage.[11] While trehalose is able to enhance the recovery of cells, it fails to control the growth of ice.[11] Thus, strategies that control ice growth during cryopreservation to mitigate cellular damage are required, as the inability of vaccines to retain thermostabilization poses a major limitation for vaccination and viral therapy. Our lab has previously shown the

ability of small molecule IRIs successfully applied to cryopreservation of cells and oncolytic viruses. Our lab has conducted a study in attempt to stabilize three live viral vectors from vesicular stomatitis virus (VSV), vaccinia virus (VV) and herpes simplex virus type 1 (HSV-1).[31] Results indicated that **1** was the most active compound resulting in the stabilization of VV and HSV-1 at room temperature and exposure to -20 ºC.[31] Lyophilization (freeze-drying) of VV and VSV with the IRI demonstrated successful preservation of the viruses.[31] It was determined that direct addition of the IRIs to the virus sample increased its infectivity by 20%, suggesting that the compounds disperse virus aggregates and stabilize the individual virus particles in solution during the lyophilization process.[31]

This work leads into the query if these carbohydrate-based IRIs are capable of protein stabilization. Freeze-dried products are usually preferred to increase the shelf life of protein pharmaceuticals.[11] However, proteins can lose their activity during freeze-drying, thus excipients are often added prior to freezing to act as a stabilizer.[11] To address this major limitation, we utilized small molecule-based IRIs to assess if they are capable of protein stabilization using the nucleocapsid gene (N gene) from viruses. The N gene is ssRNA that can act as mRNA. In this work, we examined the activity and thermostability of master mix and RNA during lyophilization and reverse transcription quantitative real-time polymerase chain reaction (RT-qPCR) using a variety of small molecule IRIs to identify promising compounds. The IRIs used for preliminary testing are **1** and N-4-Bromophenyl-β-D-glucopyranoside (pBrPhGlc) (**9**) (figure 1.11), as they have demonstrated the ability to inhibit ice recrystallization and significantly increase thermostability of viruses in past studies. As well as N-4-Methylbenzyl-β-D-gluconamide (4-MBA) (**5**) and N-2,6-Difluorobenzyl-β-D-gluconamide (2,6-DFB) (**6**) as further assessment of cryoprotectant abilities. Thus, the main objective of this study is to assess if IRIs

are capable of protein stabilization after freeze drying and qPCR using the N gene RNA from SARS-CoV-2 (COVID) virus.

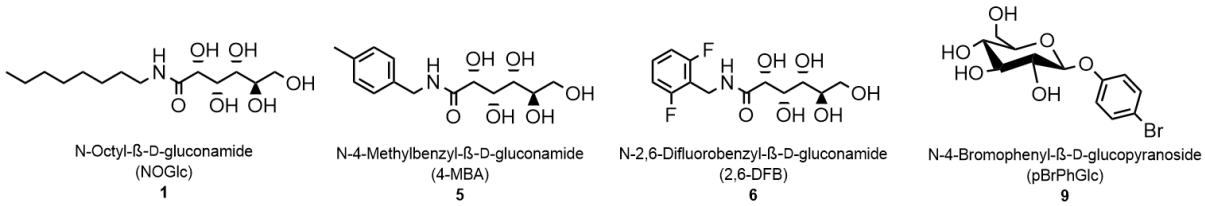

Figure 1.11. Structure of Compounds to Assess in Objective 2.

1.8.3 Objective 3 – Bioengineering and Long-term Storage of Complex Tissue Constructs for Transplantation

Cell/organ replacement therapy remains the only treatment option for many life-threatening diseases and is severely limited by availability of donor organs.[32] While cryopreservation is an attractive option for the long-term storage that would alleviate this limitation, the successful cryopreservation of voluminous and complex tissue constructs is not currently possible.[4] The reason for this is that significant cellular damage occurs to cells and tissues during freezing and thawing.[4] Conventional cryoprotectants fail to mitigate this form of cellular damage resulting in tissues that are unsuitable for transplant.[4] Having a means to successfully store and transport organs for long periods of time is a major unmet need for health care in the twenty-first century.[32] It is our hypothesis that the challenges faced during the cryopreservation can be addressed by small molecule IRIs.

Specifically, skin injuries such as burns remain one of the most common injuries in Canada and worldwide (more than one million patients annually in the USA alone).[32] The survival rates of patients with burns have significantly improved due to the application of tissue engineered reconstituted skin grafts and these grafts are currently being evaluated in a clinical

trial.[32,33] Pluripotent stem cells harbor the potential to provide an inexhaustible supply of donor cells/tissues/organs for transplantation.[33] We propose as an end goal to use human induced pluripotent stem cells (iPSCs) and human skin keratinocytes with a unique bioprinting technology to develop 3D organ constructs such as skin and other essential tissues. Once constructed, these constructs will be cryopreserved and available for transplant immediately after thawing. Successful cryopreservation of these complex tissue architectures will be accomplished using IRIs to prevent cryoinjury from IIF during freezing and thawing thus enabling the successful long-term storage and transport of these constructs prior to transplant.

IRI technology has been shown to improve cryopreservation outcome in a number of cellular systems. From these initial studies 2FA (**3**) has demonstrated the ability to control extra- and intracellular ice recrystallization, improve post-thaw viability/function and have favorable pharmacokinetic profiles (toxicity, bioavailability, etc.) making it an ideal IRI for tissue preservation applications.[34] Furthermore, aldonamide based IRI are unique amongst the different classes of IRIs developed because they have been shown to cross cell membranes.[31] Cytotoxicity is a common problem with all cryoprotectants. While the cytotoxicity of a few simple mono- and disaccharides has been reported, it is unknown whether all saccharides are cytotoxic. Similarly, very little is known about the cytotoxicity of the carbohydrate-based IRIs proposed in this study. Consequently, we will investigate the cytotoxic nature of these substrates over a wide range of concentrations above and below the IC_{50} values. As we continue to build a successful library of IRIs from the initial group of compounds that will be tested (figure 1.12), simplified tissue models of different thicknesses will be investigated. Thus, the main objective of this study is to assess if IRIs are capable of cryopreserving a simplified human tissue model suitable as a universal skin graft.

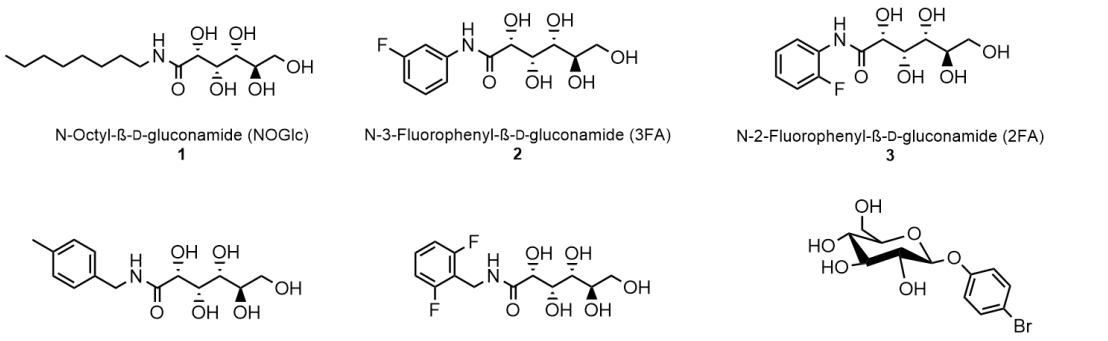

Figure 1.12. Structure of Compounds to Assess in Objective 3.

1.9 References

1 Mahler, S. *et al.* Hypothermic Storage and Cryopreservation of Hepatocytes: The Protective Effect of Alginate Gel against Cell Damages. *Cell Transplantation* **12**, 579-592, doi:10.3727/000000003108747181 (2003).

2 Matsuda, H., Yagi, T., Matsuoka, J., Yamamura, H. & Tanaka, N. SUBZERO NONFREEZING STORAGE OF ISOLATED RAT HEPATOCYTES IN UNIVERSITY OF WISCONSIN SOLUTION. *Transplantation* **67**, 186-191 (1999).

3 Tae Hoon Jang, S. C. P., Ji Hyun Yang, Jung Yoon Kim, Jae Hong Seok, Ui Seo Park, Chang Won Choi, Sung Ryul Lee, and Jin Han. Cryopreservation and its clinical applications. *Integrative Medicine Research* **6**, 12-18, doi:https://doi.org/10.1016%2Fj.imr.2016.12.001 (2017).

4 D.E. Pegg, M. D. The History and Principles of Cryopreservation. *Seminars in Reproductive Medicine* **20(1)**, 005–014, doi:10.1055/s-2002-23515 (2002).

5 Pegg, D. E. 3-19 (Springer New York, 2015).

6 Patrik Stanica, M. T., Zdenko Sonickib, Velimir Simunica, Branko Radakovica, Ernest Suchaneka. Comparison of protective media and freezing techniques for cryopreservation of human semen. *European Journal of Obstetrics & Gynecology and Reproductive Biology* **91**, 65-70, doi:https://doi.org/10.1016/S0301-2115(99)00255-9 (2000).

7 P.Mazur, S. P. L., E.H.Y.Chu. A two-factor hypothesis of freezing injury: Evidence from Chinese hamster tissue-culture cells. *Experimental Cell Research* **71**, 345-355, doi:https://doi.org/10.1016/0014-4827(72)90303-5 (1972).

8 Acker, J. P. 157-187 (Springer Berlin Heidelberg, 2005).

9 Arciero, V. *et al.* Vapour fast freezing with low semen volumes can highly improve motility and viability or DNA quality of cryopreserved human spermatozoa. *Andrology*, doi:10.1111/andr.13208 (2022).

10 Suchanek, P. S. M. T. Z. S. V. S. B. R. E. Comparison of protective media and freezing techniques for cryopreservation of human semen. *European Journal of Obstetrics & Gynecology and Reproductive Biology* **91**, 65-70, doi:10.1016/s0301-2115(99)00255-9 (2000).

11 Wang, W. Lyophilization and development of solid protein pharmaceuticals. *International Journal of Pharmaceutics* **203**, 1-60, doi:10.1016/s0378-5173(00)00423-3 (2000).

12 Benson, E. E. 15-32 (Springer New York, 2008).

13 Gao, D. & Critser, J. K. Mechanisms of Cryoinjury in Living Cells. *ILAR Journal* **41**, 187-196, doi:10.1093/ilar.41.4.187 (2000).

14 Raju, R., Bryant, S. J., Wilkinson, B. L. & Bryant, G. The need for novel cryoprotectants and cryopreservation protocols: Insights into the importance of biophysical investigation and cell permeability. *Biochimica et Biophysica Acta (BBA) - General Subjects* **1865**, 129749, doi:10.1016/j.bbagen.2020.129749 (2021).

15 Nail, S. L., Jiang, S., Chongprasert, S., & Knopp, S. A. . Fundamentals of Freeze-Drying. *Development and Manufacture of Protein Pharmaceuticals*, 281-360, doi:10.1007/978-1-4615-0549-5_6 (2022).

16 Jennings, T. A. *Lyophilization, introduction and basic principles*. 664 (1999).

17 Kawasaki, H., Shimanouchi, T. & Kimura, Y. Recent Development of Optimization of Lyophilization Process. *Journal of Chemistry* **2019**, 1-14, doi:10.1155/2019/9502856 (2019).
18 Seki, S. & Mazur, P. Effect of Warming Rate on the Survival of Vitrified Mouse Oocytes and on the Recrystallization of Intracellular Ice1. *Biology of Reproduction* **79**, 727-737, doi:10.1095/biolreprod.108.069401 (2008).
19 Chaytor, J. L. *et al.* Inhibiting ice recrystallization and optimization of cell viability after cryopreservation. *Glycobiology* **22**, 123-133, doi:10.1093/glycob/cwr115 (2012).
20 Nishaka William, J. P. A. Cryoprotectant-dependent control of intracellular ice recrystallization in hepatocytes using small molecule carbohydrate derivatives. *Cryobiology* **97**, 123-130, doi:https://doi.org/10.1016/j.cryobiol.2020.09.008 (2020).
21 Poisson, J. S., Acker, J. P., Briard, J. G., Meyer, J. E. & Ben, R. N. Modulating Intracellular Ice Growth with Cell-Permeating Small-Molecule Ice Recrystallization Inhibitors. *Langmuir* **35**, 7452-7458, doi:10.1021/acs.langmuir.8b02126 (2019).
22 Balcerzak, A. K., Capicciotti, C. J., Briard, J. G. & Ben, R. N. Designing ice recrystallization inhibitors: from antifreeze (glyco)proteins to small molecules. *RSC Adv.* **4**, 42682-42696, doi:10.1039/c4ra06893a (2014).
23 Budke, C., Heggemann, C., Koch, M., Sewald, N. & Koop, T. Ice Recrystallization Kinetics in the Presence of Synthetic Antifreeze Glycoprotein Analogues Using the Framework of LSW Theory. *The Journal of Physical Chemistry B* **113**, 2865-2873, doi:10.1021/jp805726e (2009).
24 Fletcher, N. H. Surface structure of water and ice. *Philosophical Magazine* **7**, 255-269, doi:10.1080/14786436208211860 (1962).
25 Hagiwara, T., Hartel, R. W. & Matsukawa, S. Relationship between Recrystallization Rate of Ice Crystals in Sugar Solutions and Water Mobility in Freeze-Concentrated Matrix. *Food Biophysics* **1**, 74-82, doi:10.1007/s11483-006-9009-0 (2006).
26 Adapa, S., Schmidt, K. A., Jeon, I. J., Herald, T. J. & Flores, R. A. MECHANISMS OF ICE CRYSTALLIZATION AND RECRYSTALLIZATION IN ICE CREAM: A REVIEW. *Food Reviews International* **16**, 259-271, doi:10.1081/fri-100100289 (2000).
27 Biggs, C. I. *et al.* Polymer mimics of biomacromolecular antifreezes. *Nature Communications* **8**, doi:10.1038/s41467-017-01421-7 (2017).
28 Robert Ben, J. G. B., Jessica S. Poisson, Tracey R. Turner, Jayme D.R. Kurach, Jason P. Acker. Ice recrystallization inhibitors – Mitigating cellular damage during freezing, transient warming and thawing. **71**, 171, doi:https://doi.org/10.1016/j.cryobiol.2015.05.031 (2015).
29 J, C., Doshi, M. & N, R. (InTech, 2013).
30 Briard, J. G. *The Rational Design and Use of Novel Small-Molecule Ice Recrystallization Inhibitors for the Cryopreservation of Hematopoietic Stem Cells and Red Blood Cells* Department of Chemistry and Biomolecular Sciences thesis, University of Ottawa, (2016).
31 Ghobadloo, S. M. *et al.* Carbohydrate-Based Ice Recrystallization Inhibitors Increase Infectivity and Thermostability of Viral Vectors. *Scientific Reports* **4**, doi:10.1038/srep05903 (2015).

32 Madden, M. R. M. L., Anthony A. MD; Hajjar, David P. PhD; Staiano-Coico, Lisa PhD. Transplantation of Cryopreserved Cultured Epidermal Allografts. *The Journal of Trauma and Acute Care Surgery* **40**, 743-750 (1996).

33 Diana Kitala, M. K., Agnieszka Klama-Baryła, Wojciech Łabuś, Małgorzata Kraut, Justyna Glik, Ireneusz Ryszkiel, Marek P. Kawecki, Mariusz Nowak. Allogeneic vs. Autologous Skin Grafts in the Therapy of Patients with Burn Injuries: A Restrospective, Open-label Clinical Study with Pair Matching. *Advances in Clinical and Experimental Medicine* **25**, 923-929, doi:10.17219/acem/61961 (2016).

34 Suria Jahan, M. K. A., Javed K. Manesia, Emily Doxtator, Robert N. Ben, Nicolas Pineault. Inhibition of ice recrystallization during cryopreservation of cord blood grafts improves platelet engraftment. *Transfusion* **60**, 769-778, doi:https://doi.org/10.1111/trf.15759 (2020).

Chapter 2: Assessment of Compound Properties

2.1 Introduction

The Ben laboratory has performed extensive structure-function studies of many different classes of compounds to utilize as IRIs. The purpose of these studies is to elucidate the structural elements required to inhibit ice recrystallization and also be effective cryoprotectants. The latter is even more complex than the former as the work in the Ben laboratory has demonstrated that many different classes of IRI that are effective at controlling ice crystal size can have dramatically different cryopreservation abilities. This highlights the importance of also mitigating any undesired toxic effects or undesired biological interactions.[1,2] Each cell type has its own specific set of conditions (membrane permeability, predisposition to cryo-injury, etc.) to consider when undergoing cryopreservation in order to maximize viability.[1,3] The requirements increase in complexity as we move from single cells to more complicated multicellular systems or changes in environment.[3,4] For example, hepatocytes are more prone to IIF than most mammalian cells, and therefore require an IRI which can permeate and function within them.[5] Therefore, it is essential to have a library of effective compounds in order to further structure-function analyses and address the many situations in which CPAs are required to preserve biological material.

The current hypothesis is that IRIs inhibitory activity is attributed to their ability to disorder the structure of bulk water.[6] As a result, non-ionic carbohydrate-based surfactants and hydrogelators that modify and/or sequester bulk water as well as self-assemble in solution were investigated previously as inhibitors of ice recrystillization.[6] Unique small molecules that display strong IRI activity have been found among these substances.[6] The

three of main focus in this thesis are as follows: N-Octyl-β-D-gluconamide (NOGlc) (**1**), N-4-Bromophenyl-β-D-glucopyranoside (pBrPhGlc) (**9**), and N-2-Fluorophenyl-β-D-gluconamide (2FA) (**3**) (figure 2.1). Each of these IRIs have demonstrated improved post-thaw viability and functional capability when added to cells and tissues before freezing to prevent ice development. Some examples include; **1**, the most active of the IRIs (IC_{50} = 0.09 mM) (figure 2.2) has the ability to permit room temperature storage of viral vectors, **9** increased post-thaw RBC integrity, and **3** demonstrated both an increase in the post-thaw recovery of CB progenitors and reduced rates of intracellular recrystallization in hepatocytes.[5,7-9] One of the current limitations with some of these IRIs is solubility, with **1** having a max solubility of 1 mM. Although **3** and **9** have higher solubility limits, 15 mM and 55 mM respectively, they have lower IRI activity (3 mM and 15 mM respectively) and have shown cytotoxicity (**9** has a LD_{50} of 2 mM).

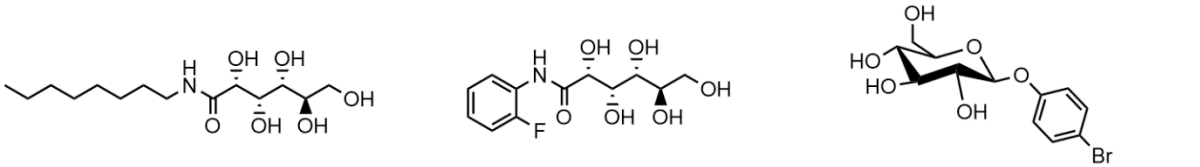

Figure 2.1. Structures of Previously Investigated Ice Recrystallization Inhibitors.

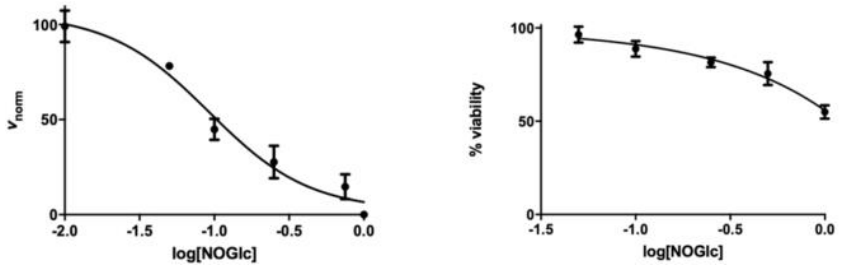

Figure 2.2. Dose-response Curve and % Viability of NOGlc (1). *NOGlc (1) IC_{50} = 0.09 mM, R^2 = 0.96, no LD_{50} value could be determined because the curves could not be completed due to limiting solubility at 1 mM. Adapted from Ben Laboratory.*

Former PhD students of the Ben laboratory, Jennie Briard and Chantelle Capicciotti have previously synthesized a variety of surfactants and hydrogelators derivatives for

comparative purposes to address these issues. Their studies made it clear that activity of these compounds is dependent on specific structural characteristics (figure 2.3). For instance, an alkyl chain of more than 6 carbons is important.[6] This demonstrated the significance of hydrophobic moieties for IRI activity and was consistent with other amphiphilic compounds that our lab has evaluated as IRIs.[6] The idea that amphiphilicity is important was further supported by the structural attributes in **1**, in which IRI activity is modulated by the length of the octyl chain.[6] It was also discovered that the IRI activity of **1** was correlated to the presence of the amide bond between the hydrocarbon chain and carbohydrate head-group.[6] IRI activity was eliminated when the nitrogen was methylated or replaced by an ether-linkage.[10] The decreased activity of the N-methylated derivatives further indicated that **1**'s ability to prevent ice recrystallization depends on the ability of this amide bond to function as a hydrogen bond donor or due to the introduction of the cis conformation after methylation.[10] IRI activity was also increased by prolonging the hydrophobic moiety by including a carbon spacer between the amide bond and aromatic ring.[10] Like previously identified IRIs, micelle formation, gelation, or binding to the ice lattice are not necessary for IRI activity.[1]

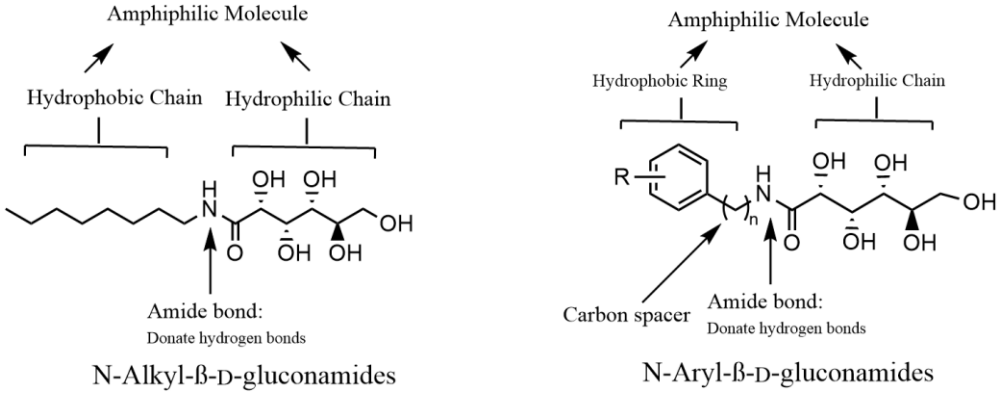

Figure 2.3. Key Structural Features of N-Alkyl-β-D-gluconamide and N-Aryl-β-D-gluconamide Derivatives.

There are a variety of structural changes and substitutions on the benzyl ring that have yet to be investigated. In addition, all of the compounds tested were expressed as a %

MGS of the ice crystals in comparison to a PBS solution.[10] As a result, the effectiveness of these derivatives was previously evaluated at a single concentration and time point, a method that ignores the effects of both time and concentration on IRI activity.[10] The reality that researchers are assessing recrystallization using a variety of assays and that the variance across the assays is unknown is one of the major problems in this field because it prevents direct data comparisons.[11] Currently, our lab uses the modified splat cooling assay, which involves comparing the ice crystal size in the presence and absence of IRIs (figure 2.4).[11] The modified splat cooling assay, which has been extensively described in the experimental section (section 6.1), produces a numerical value that quantifies how effectively a compound can prevent ice from recrystallizing as a function of its concentration (typically referred to as an IC_{50} value).[11] Compared to the % MGS previously used, the IC_{50} number provides a more accurate indication of IRI activity.[10] As % MGS is not an accurate representation of a non-homogeneous system, whereas the sigmoidal curve that the IC_{50} is obtained from approximates the rate of crystal growth.

In addition to IRI activity, an assay to determine the cytotoxicity of a compound which is usually represented as LD_{50} (concentration of a toxic substance lethal to half of the cells), is needed to determine the toxic effect of our compounds. Therefore, all tested compounds were assessed for cytotoxicity using a resazurin assay which is commonly used to monitor cell viability / cytotoxicity.

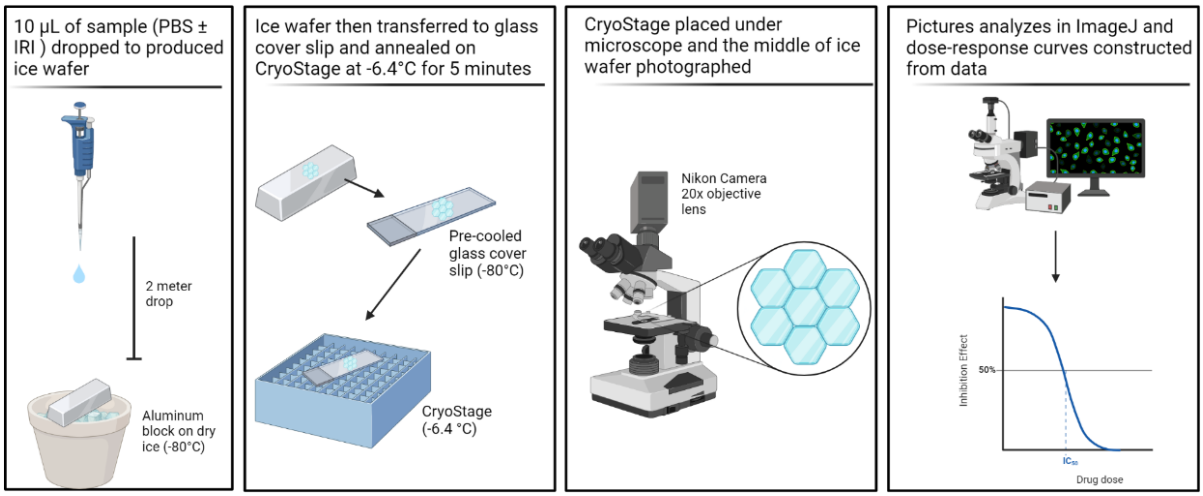

Figure 2.4. Experimental Procedure of Modified Splat Cooling Assay. *Image created in BioRender ©.*

Our lab's previous studies serve as a basis for the rational design of other small molecule IRIs that exhibit IRI activity.[6] During Dr. Briard's research she identified a novel class of compounds which showed higher solubility than **1** and IRI activity. These compounds are N-Benzyl-β-D-gluconamides (figure 2.5). N-Benzyl-β-D-gluconamides are derivatives of N-Aryl-β-D-aldonamides that possess a carbon linker between the amide nitrogen and aromatic ring.[10] Thus, the purpose of the following chapter will be to outline the progress towards designing non-ionic carbohydrate-based surfactants and hydrogelators as well as further characterization of previous compounds that exhibit the ability to inhibit ice recrystallization. This is important for understanding the key structural features that are important for the IRI activity exhibited by these molecules.[2] This will be done through the synthesis of a variety of N-Benzyl-β-D-gluconamides with a variation of substituents added on the aromatic ring to increase the current library of compounds.

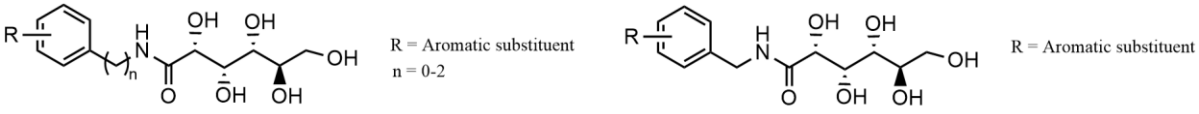

Figure 2.5. General Structures of N-Aryl-β-D-gluconamides and N-Benzyl-β-D-gluconamides to be Assessed in the Following Sections.

2.2 Synthesis and Assessment of Ice Recrystallization Inhibition Activity of N-4-Methylbenzyl-β-D-gluconamide (5) and N-2,6-Difluorobenzyl-β-D-gluconamide (6)

The first of the N-Benzyl-β-D-gluconamides that will be investigated in this thesis are N-4-Methylbenzyl-β-D-gluconamide (4-MBA) (**5**) and N-2,6-Difluoroprbenzyl-β-D-gluconamide (2,6-DFB) (**6**). These two compounds were previously investigated and possess a MGS of <10% and 13% respectively.[10] In order to validate these findings both compounds were synthesized and underwent a modified splat cooling assay to generate dose-response curves to further characterize their ability to inhibit ice recrystallization. The N-Benzyl-β-D-gluconamides are synthesized starting from commercially available δ-gluconolactone and the appropriately substituted aryl amines (Scheme 2.1).

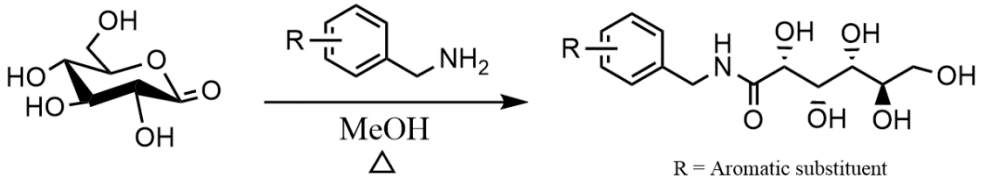

Scheme 2.1. Synthesis of N-Benzyl-β-D-gluconamides.

Compared to **1**, compounds **5** and **6** have a benzyl group connecting to the amide bond instead of a hydrocarbon chain. The hydrocarbon chain connected to the carbohydrate head-group in **1** was found to be crucial for its activity in previous structure function analysis, as the long hydrophobic chain imparts the amphiphilic nature of these alditols.[7,10] Although, solubility decreases as carbon chain length increases. Therefore, increasing the surface area of the structure by replacing the long chain with a benzyl group, despite it being a nonpolar substituent maintains the necessary hydrophobicity while potentially increasing solubility. As well, the addition of the benzyl group increases the stability of the compounds. In another attempt to increase hydrophobicity, an addition of a carbon spacer between the ring and amide bond was maintained in these compounds. This carbon spacer and amide

bond has previously been determined beneficial for increasing IRI activity in compounds.[6,10] In addition, the hydrogen-bond donating ability of this amide bond may be important for IRI activity.[6] Specifically for **5,** addition of the electron donating methyl group at the *para* position increases hydrophobicity of the compound. Whereas for **6**, fluorine is electronegative and maintains the hydrophobicity.

Figure 2.6 shows the dose-response curves for compounds **5** and **6**. The compounds were evaluated at different concentrations by measuring the area of each ice crystal while the IRI was present. The initial rate of ice crystal growth was computed and normalized to that of a PBS control, since the overall area of ice crystals grows with decreasing concentration. Following that, dose-response curves were generated using the normalized rates of ice crystal growth. The IC_{50} value—the concentration at which our IRIs reaches half of their inhibitory power—was derived from these dose-response curves. Both IRIs showed activity with IC_{50} values of 25 mM (±3.63 SEM) and 1.1 mM (±0.02 SEM) for **6** and **5** respectively.

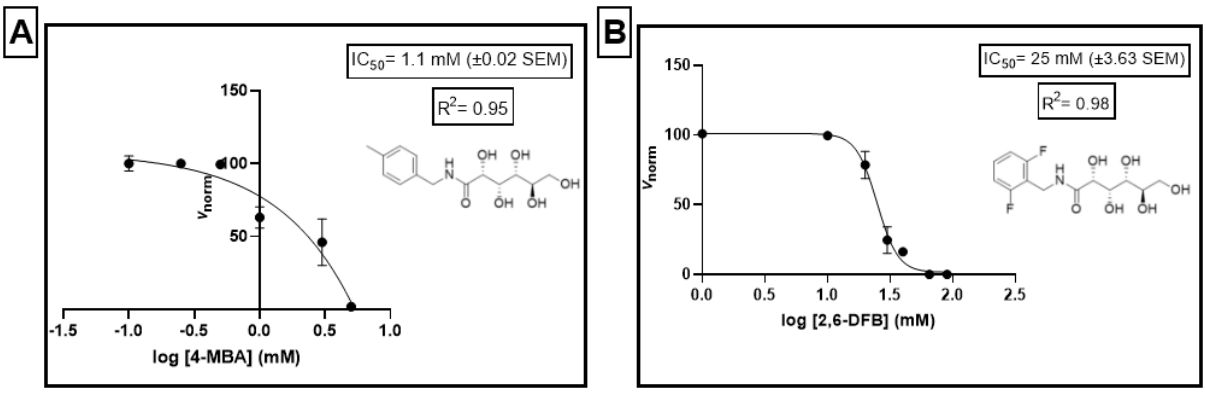

Figure 2.6. Dose-Response Curve of 4-MBA (5) and 2,6-DFB (6) Generated from Modified Splat Cooling Assay. *Dose-response curve for 4-MBA (**5**) and 2,6-DFB (**6**). V_{norm} (%) as a function of log[compound] (mM). Rate constants (k_{norm}) were normalized to a PBS control and measured in triplicate. Error bars represent the standard error of the mean (SEM). A variable four-parameter sigmoidal curve was fit to the data.*

Since **5** and **6** can reach full inhibition at their greatest solubility (i.e., V_{norm} = 0%), figure 2.6 implies that they are effective inhibitors of ice recrystallization. Both compounds

fit a sigmoidal dose-response curve with R^2 values above 0.95, making it possible to determine an IC_{50} value from their inflection points. The 4-MBA derivative **5** is also an effective inhibitor of ice recrystallization since it causes inhibition at low doses, as shown by its corresponding IC_{50} value of 1.1 mM (±0.02 SEM). The IC_{50} value of **5** is closer to **1** (IC_{50} = 0.09 mM) than **3** or **9 (**IC_{50} = 3.1 mM and 15 mM respectively), suggesting that **5** is a promising new IRI. In addition, **5** despite showing IRI activity at concentrations as low as 0.5 mM had a solubility limit of ~50 mM in PBS. This is a compelling discovery as the solubility limit was a major obstacle for the use of **1**. This prompted further investigation into these IRIs such as the importance of the *para* position as well as the cytotoxicity of each compound which will be further described in the following sections.

2.3 Assessing the Influence of the *Para* Position in the Aryl Ring of N-Benzyl-β-D-gluconamides

Dr. Briard previously demonstrated that changing the nature of the substituent on the aromatic ring can influence the IRI activity of N-Benzyl-β-D-gluconamides since a variety of compounds with different substituents produced varying % MGS values. As the only structural difference between **6** and **5** were the substituents located on the benzyl ring, the large variation in IC_{50} values (25 mM ±3.63 SEM and 1.1 mM ±0.02 SEM, respectively) must be a result of the difference in substituents. This led to the inquiry as to what role the *para* position places on the N-Benzyl-β-D-gluconamides. Therefore, three additional compounds were assayed based on different chemical properties: N-Benzyl-β-D-gluconamide (BA) (**4**), N-4-Chlorobenzyl-β-D-gluconamide (4-CBA) (**7**), and N-4-Methoxybenzyl-β-D-gluconamide (4-MOBA) (**8**). These compounds were assessed for the importance of a substituent at the *para* position in the benzyl ring as well as the function of

electron donating (ED) and electron withdrawing (EW) substituents (figure 2.7). As with the previous gluconamides, the three new derivatives were synthesized starting from δ-gluconolactone with various aryl amines as described in Scheme 2.1.

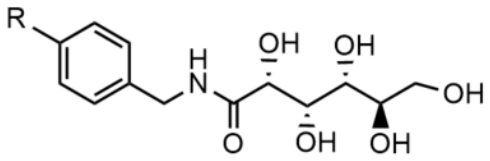

	Structural Component	Electronic Property
4:	R = H	No Aromatic substituent
7:	R = Cl	EW
8:	R = OCH_3	ED

Figure 2.7. Structures of N-Benzyl-β-D- gluconamides Analogues to be Assessed for Influence of the* Para *Position.

Compounds **4**, **7**, and **8** share the same characteristic N-Benzyl-β-D-gluconamide structure with modifications to the *para* position. The removal of the methyl group to give **4** is an attempt to determine the importance of that position and determine the activity of the parent structure to all N-Benzyl-β-D-gluconamides. As previously discussed, the methyl group increases hydrophobicity and stability of the compound which may play an important role in disrupting the bulk water layer.[1] In an attempt to further characterize chemical properties of these structures chlorine was added in the *para* position instead of the methyl group. Halogens are very electronegative; this means that inductively they are electron withdrawing thus removing electron density from the ring, making the ring less reactive. The halogen substituents have two electronic effects on the benzyl ring: 1) *para* directing, and 2) electron withdrawing. The Cl group is also highly soluble in water and hydrophilic giving us a new perspective on the importance of hydrophobicity of the substituents on the benzyl ring. Lastly, methoxy (OCH_3), an electron donating group was added in the *para* position instead of the methyl group. This addition of an oxygen is a minor change which effects the properties of the benzyl group as the oxygen can push electrons into the ring, making the *para* position more reactive. In addition, the oxygen has the possibility to increase solubility

but not enough to completely reduce the hydrophobicity of the ring maintaining the amphiphilicity of the compound. Figure 2.8 shows the dose-response curves for **4**, **7**, and **8**. As with the previous compounds, dose-response curves were created producing a IC_{50} value. All IRIs showed activity with IC_{50} values of 5.8 mM (±0.05 SEM), 0.48 mM (±0.34 SEM) and 1.4 mM (±0.58 SEM) for **4**, **7**, and **8** respectively.

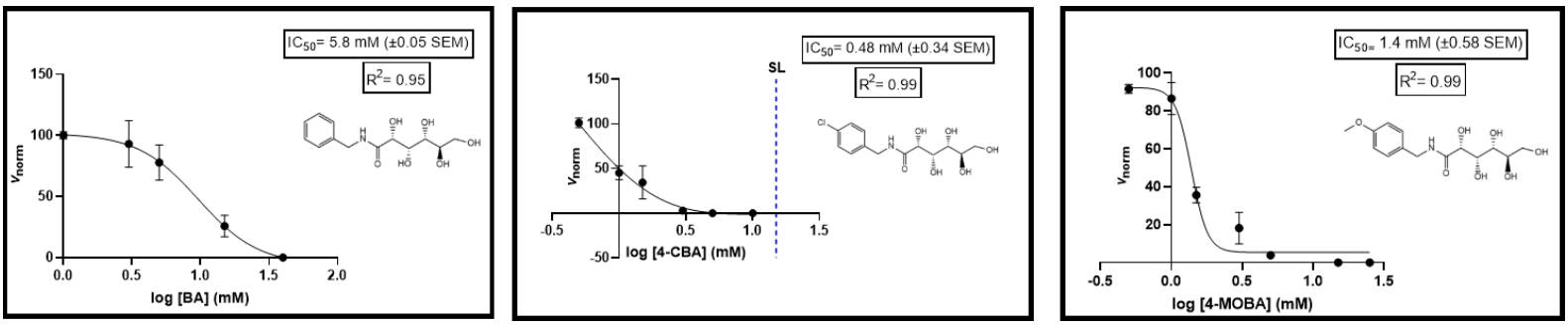

Figure 2.8.* Para *Dose-Response Curves Generated from Modified Splat Cooling Assay. *Dose-response curves for BA (**4**), 4-CBA (**7**), and 4-MOBA (**8**). V_{norm} (%) as a function of log[compound] (mM). Rate constants (k_{norm}) were normalized to a PBS control and measured in triplicate. Error bars represent the standard error of the mean (SEM). A variable four-parameter sigmoidal curve was fit to the data. Blue dashed line labeled SL indicates the solubility limit of the compound.*

As with the previous derivatives, **4**, **7**, and **8** can reach full inhibition at their greatest solubility (i.e., V_{norm} = 0%), figure 2.8 implies that they are effective inhibitors of ice recrystallization. Like **5**, the **7** and **8** derivatives are active inhibitors since they cause inhibition at low doses, as shown by their corresponding IC_{50} values of 0.48 mM (±0.34 SE) and 1.4 mM (±0.58 SEM). These IC_{50} values are similar to **5** (1.1 mM ±0.02 SEM), with **7** being even more active than **5**. In addition, all of these compounds have solubility limits higher than that of **1** with **4**, **7**, and **8** dissolving into PBS at 90 mM, 15 mM and 40 mM respectively. Compound **4** displays a typical sigmoidal dose-response curve, however **7** and **8** both do not fit the typical sigmoidal curve precisely as they have steep slopes and points outside the curve. Despite this, four-parameter sigmoidal curves were applied with R^2 values of 0.98 and IC_{50} values were still obtained from the inflection points of these graphs. This led

to investigate whether other equations fit to the curves may produce better results. In the next section, we assess equations to find the best fit of dose-response curves based on R^2 values.

2.4 Assessing the Best Fit of Dose-Response Curves Based on R^2 Values

Stephanie Abraham (a previous master's student) determined the method of quantifying IRI activity by constructing dose-response curves. This quantification was done by determining the kinetic profile of the Ostwald ripening theory from features in a high ice volume fraction assay.[12] The distribution of ice crystal sizes was fit to a time-dependent equation that results in the acquisition of rate constants.[12] These rate constants were then used to construct dose-response curves. By plotting the rate constants against concentration, it yielded a sigmoidal curve.[12] From these curves IC_{50} values were obtained. To do so, the rate constants (k_{obs}) were normalized by dividing them by the average PBS (0 mM) rate constant, resulting in a set of normalized rate constants (k_{norm}) for each inhibitor.[12] Each data set was fit to a four-parameter sigmoidal equation.[12]

Equation 2.1. Four-Parameter Sigmoidal Dose-Response Curve Used for Quantification of IRI Activity.

$$k_{norm} = \frac{k_0 - k_f}{\left(1 + n \times 10^{\left(logIC_{50} - log[I]\right)} + k_f\right)}$$

Many inhibitory dose-response curves follow the symmetrical sigmoidal shape.[13,14] This model does not assume a standard slope but rather fits the Hill Slope from the data, and so it is called a Variable slope model.[13,14] It may also be called a four-parameter dose-response curve, or four-parameter logistic (4PL) curve.[13,14] In this equation, k_{norm} is the normalized rate constant mentioned above, measured in triplicate using the data from mono-

exponential decay curves; k_0 is the top plateau (blank value); k_f is the bottom plateau (efficacy); n is the Hill slope, where values above 1 indicate some degree of cooperativity; IC_{50} is the concentration at which k_{norm} is 50, essentially giving a k_{obs} value half that of PBS, and thus a measure of the inhibitor's potency; and I is the concentration of inhibitor and must be greater than 0. The four parameters of the equation were thus k_0, k_f, n, and IC_{50}.[12] Derivatives **7** and **8** as seen in section 2.3 both do not precisely fit the 4PL sigmoidal shape. Therefore, to investigate the best fit for these novel IRIs an array of equations of nonlinear regression curves were applied to the data to compare to the 4PL symmetrical sigmoidal shape. Figure 2.9 shows the dose-response curves of **7** and a comparison of R^2 values obtained from each equation is outlined in table 2.1. Similarly, figure 2.10 shows the dose-response curves of **8** and a comparison of R^2 values obtained from each equation is outlined in table 2.2. Lastly, figure 2.11 shows the dose-response curves of **5** and a comparison of R^2 values obtained from each equation is outlined in table 2.3.

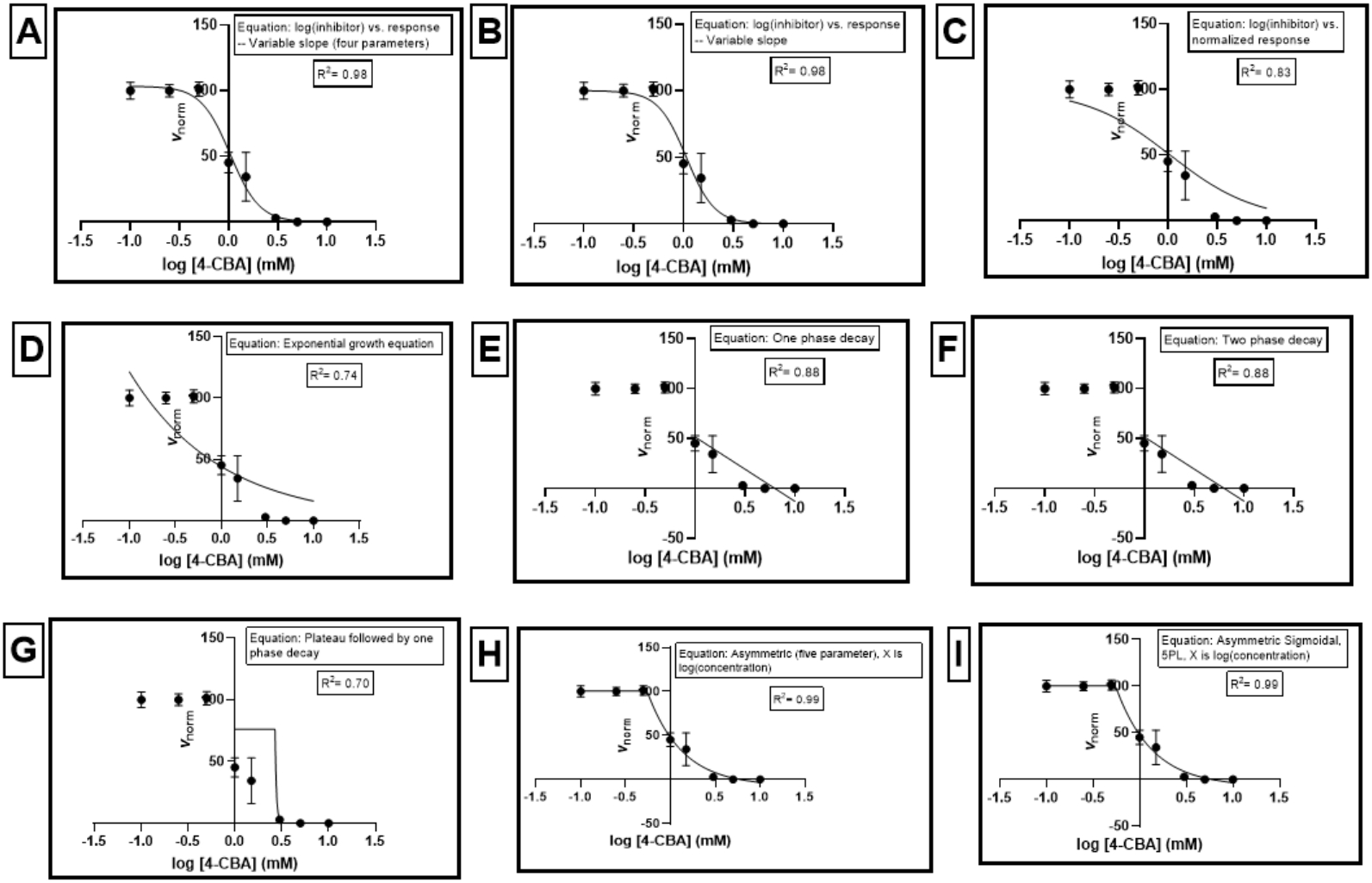

***Figure 2.9. 4-CBA (7) Dose-Response R^2 Comparison**. Dose-response curves for 4-CBA (7) with different nonlinear regression curves fitted comparing fit based on R^2 Value. V_{norm} (%) as a function of log[4-CBA] (mM). Rate constants (knorm) were normalized to a PBS control and measured in triplicate. Error bars represent the standard error of the mean (SEM).*

***Table 2.1. 4-CBA (7) Dose-Response R^2 Values Comparison.** Table comparing the R^2 Value based on dose-response curves for 4-CBA (7) with different nonlinear regression curves fitted.*

Graph	Curve Fit Equation	R-Value
A	log(inhibitor) vs. response -- Variable slope (four parameters)	0.9837
B	log(inhibitor) vs. normalized response -- Variable slope	0.9820
C	log(inhibitor) vs. normalized response	0.8295
D	Exponential growth equation	0.7441
E	One phase decay	0.8760
F	Two phase decay	0.8760
G	Plateau followed by one phase decay	0.7040
H	Asymmetric (five parameter), X is log(concentration)	0.9934
I	Asymmetric Sigmoidal, 5PL, X is log(concentration)	0.9934

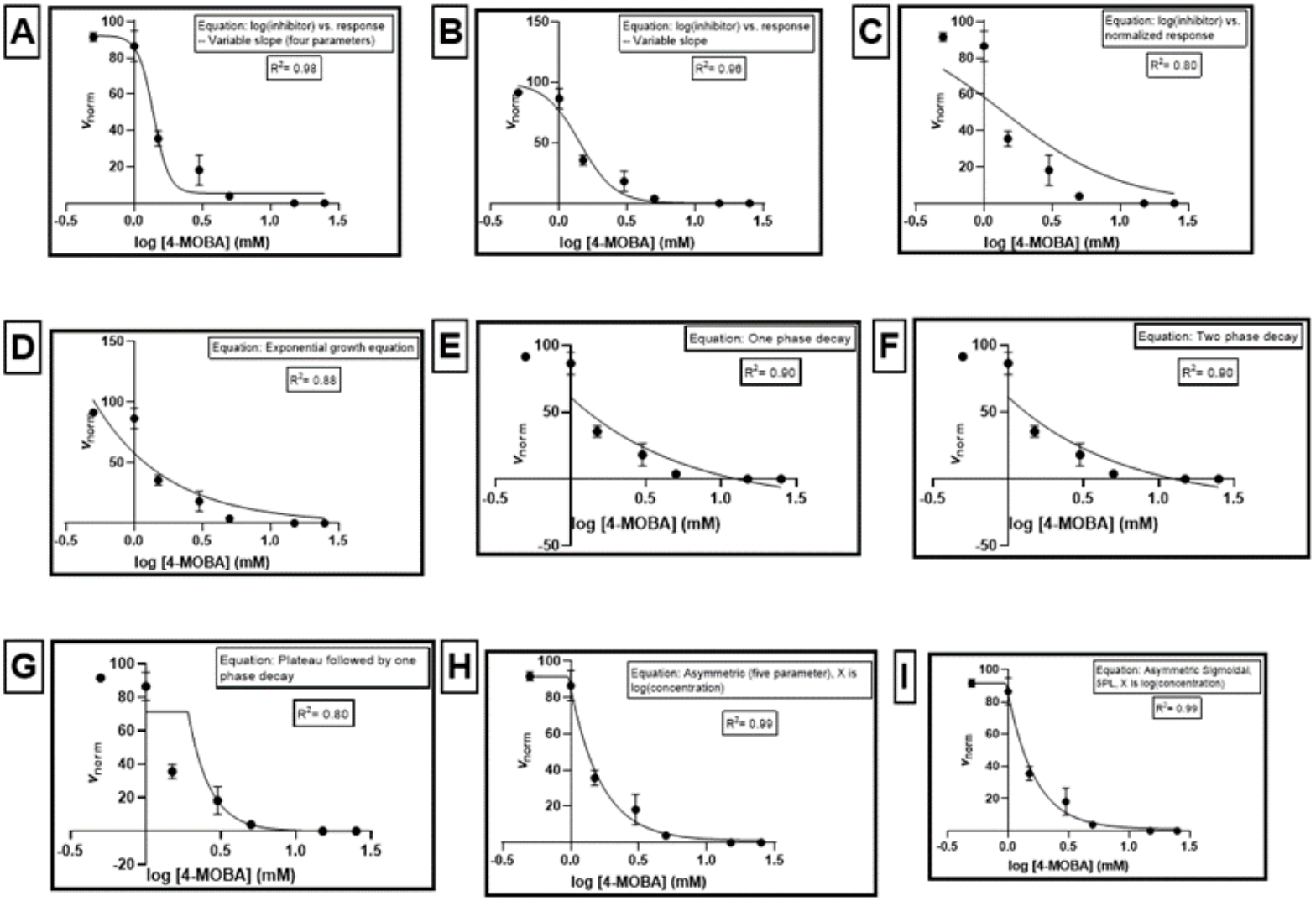

Figure 2.10. 4-MOBA (8) Dose-Response R^2 Comparison. *Dose-response curves for 4-MOBA (**8**) with different nonlinear regression curves fitted comparing fit based on R^2 Value. V_{norm} (%) as a function of log[4-MOBA] (mM). Rate constants (knorm) were normalized to a PBS control and measured in triplicate. Error bars represent the standard error of the mean (SEM).*

Table 2.2. 4-MOBA (8) Dose-Response R^2 Values Comparison. *Table comparing the R^2 Value based on dose-response curves for 4-MOBA (**8**) with different nonlinear regression curves fitted.*

Graph	Curve Fit Equation	R-Value
A	log(inhibitor) vs. response - Variable slope (four parameters)	0.9770
B	log(inhibitor) vs. normalized response - Variable slope	0.9637
C	log(inhibitor) vs. normalized response	0.8026
D	Exponential growth equation	0.8759
E	One phase decay	0.9004
F	Two phase decay	0.9004
G	Plateau followed by one phase decay	0.7995
H	Asymmetric (five parameter), X is log(concentration)	0.9926
I	Asymmetric Sigmoidal, 5PL, X is log(concentration)	0.9926

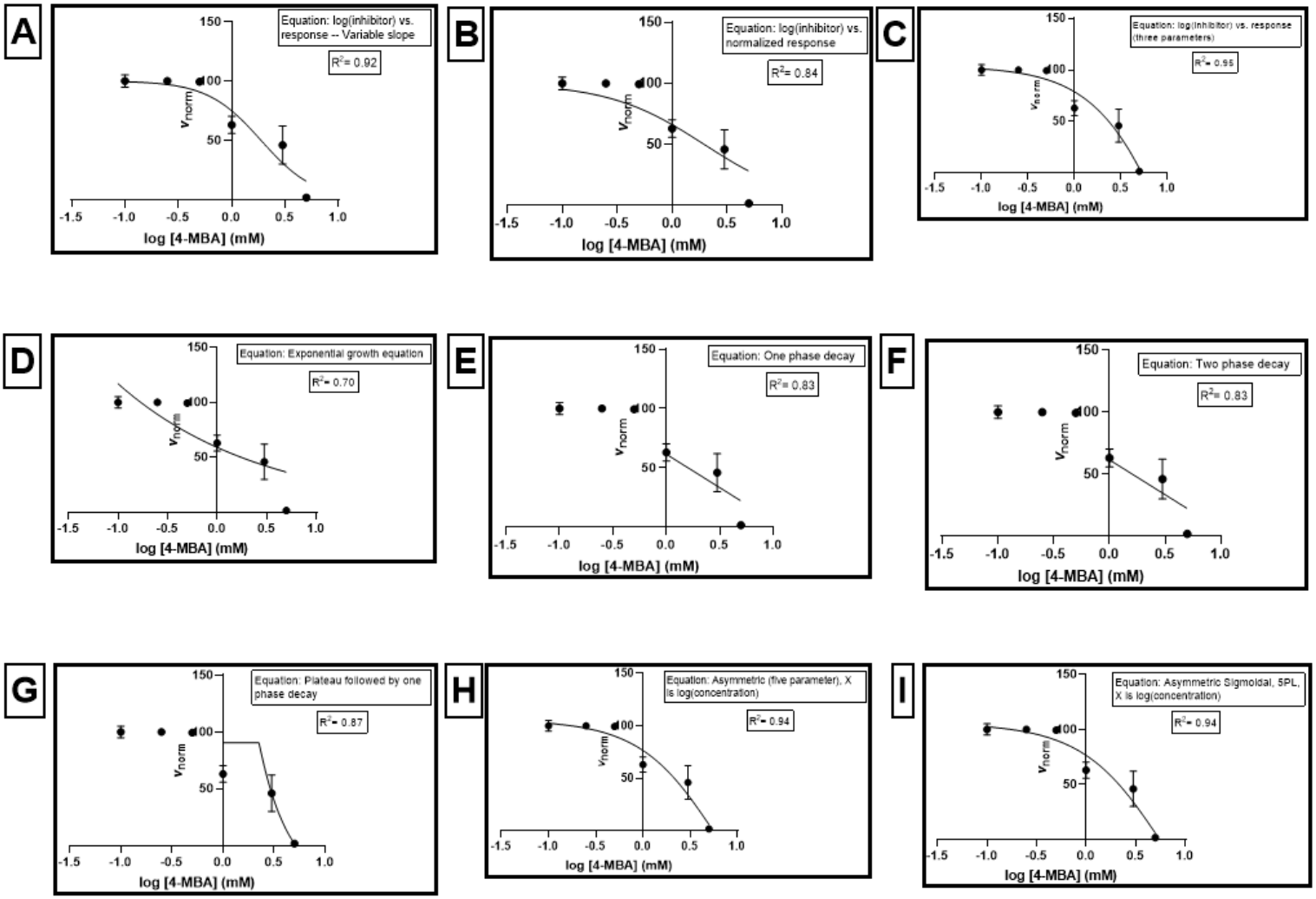

Figure 2.11. 4-MBA (5) Dose-Response R^2 Comparison. *Dose-response curves for 4-MBA (5) with different nonlinear regression curves fitted comparing fit based on R^2 Value. V_{norm} (%) as a function of log[4-MBA] (mM). Rate constants (knorm) were normalized to a PBS control and measured in triplicate. Error bars represent the standard error of the mean (SEM).*

Table 2.3. 4-MBA (5) Dose-Response R^2 Values Comparison. *Table comparing the R^2 Value based on dose-response curves for 4-MBA (5) with different nonlinear regression curves fitted.*

Graph	Curve Fit	R-Value
-	log(inhibitor) vs. response -- Variable slope (four parameters)	0.951
A	log(inhibitor) vs. normalized response -- Variable slope	0.9185
C	log(inhibitor) vs. response (three parameters)	0.948
B	log(inhibitor) vs. normalized response	0.8371
D	Exponential growth equation	0.7006
E	One phase decay	0.8324
F	Two phase decay	0.8323
G	Plateau followed by one phase decay	0.8724
H	Asymmetric (five parameter), X is log(concentration)	0.9448
I	Asymmetric Sigmoidal, 5PL, X is log(concentration)	0.9448

Both the 4-CBA (**7**) and 4-MOBA (**8**) results (figures 2.9-10 and tables 2.1-2) suggest that the curves with the best fit are the 4PL and the asymmetric five parameter dose-response curve, also known as the Richard's five-parameter dose-response curve.[13,14] This was determined by comparing the R^2 value of each nonlinear regression curve. This confirms that IRIs follow a sigmoidal curve trend as there are several points on the graphs that do not fit on the curve lines in figures C-G. In addition, graphs C-G for both derivatives have lower R^2 values indicating that exponential, phase decay, and non-variable slopes are not the most accurate trends for the data. R^2 is a statistical measure of fit that indicates how much variation of a dependent variable is explained by the independent variable(s) in a regression model.[15] Therefore, the closer to 1 (100%), means that all movements of a security are completely explained by movements in the index.[15] In this case, the R^2 values with the least variation of V_{norm} represent the curve with the best fit. The standard dose-response curve using the 4PL equation is one of the most accurate R^2 values, this can be explained as this curve fits four parameters: the bottom and top plateaus of the curve, IC_{50}, and the slope factor (Hill slope).[13,14] The four parameter curves are symmetrical around the midpoint, however, this model does not handle curves that are not symmetrical.[13,14] The Richards equation adds an additional parameter, S, which quantifies the asymmetry.[13,14] This equation is sometimes referred to as a five-parameter logistic equation (5PL).[13,14] S is the unitless symmetry parameter, if S = 1, the curve is symmetrical and identical to the standard dose-response equation, whereas if S is distinct than 1.0, then the curve is asymmetric.[13,14] The 5PL model is able to eliminate most of the lack of-fit error present in fitted 4PL models.[14] A similar comparison of 4-MBA (**5**), which fits the symmetrical sigmodal shape of the 4PL was conducted (figure 2.11 and table 2.3). The results of 4-MBA R^2 values confirmed that the

4PL and 5PL have the best fit with similar R^2 values as **5** follows a symmetric curve. These comparisons confirm that our IRIs follow a dose-response curve, as the exponential and phase decay curves have higher variation of the dependent variable. This provides us with further opportunities to better characterize compounds as the dose response curves obtained for IRIs fits a minimum of 4 parameters and in some cases may not have the typical symmetrical sigmodal shape.

2.5 Cytotoxicity of N-Aryl-β-D-aldonamides and N-Benzyl-β-D-gluconamides within HepG2 Cell Lines

As discussed in section 1.6, ideally the optimal CPA should also exhibit little to no cytotoxicity. Thus, from the library of compounds used in this thesis we sought to examine the cytotoxicity of the N-Aryl-β-D-aldonamides and N-Benzyl-β-D-gluconamides. The cytotoxicity exhibited by the small molecule carbohydrate-based IRIs was determined using an AlamarBlue™ (resazurin) assay on HepG2 cells. This is a colorimetric assay that measures cellular metabolic activity as a means of assessing cell viability.[16] It is based on the ability of mitochondrial and cytosolic dehydrogenase enzymes in metabolically active cells to reduce the water-soluble blue non-fluorescent dye resazurin to the pink, highly fluorescent resorufin.[16] Fluorescence is measured using a spectrophotometer to quantify cell viability.[16]

Both N-3-Fluorophenyl-β-D-gluconamide (3FA) (**2**) and N-2-Fluorophenyl-β-D-gluconamide (2FA) (**3**) are N-Aryl-β-D-aldonamides that were initially investigated by Dr. Briard. Compound **3** has favorable cytotoxicity profiles and has reduced cell damage induced by ice recrystallization in cord blood units.[9] Compound **2** has recently been investigated by our lab in structure function analysis to determine how the position of the fluorine effects the IRI activity. As neither of these compounds have undergone AlamarBlue™ experimentation,

the cytotoxicity of the IRI active N-Aryl-β-D-aldonamides over a range of concentrations is shown in figure 2.12. Both N-Aryl-β-D-aldonamides showed similar low cytotoxicity profiles with the lowest % cell viability being their solubility limits. A 1 mM solution of **2** resulted in a cell viability of 98.8% (±0.03 SD) and increasing this concentration to 15 mM decreased viability to approximately 70.3% (±0.03 SD). Similarly, **3** at 1 mM had a cell viability of 100% (±0.01 SD) and increasing this concentration to 20 mM decreased viability to approximately 69.6% (±0.03 SD).

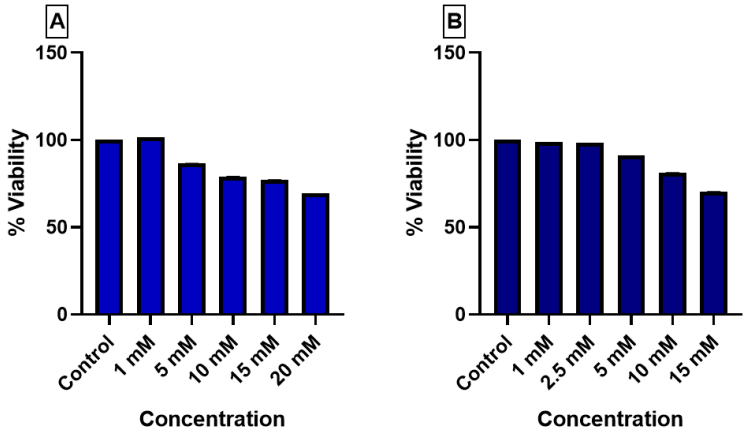

Figure 2.12. N-Aryl-β-D-aldonamides % Cell Viability Resazurin Cytotoxicity Assay. *Cytotoxicity assay using resazurin to measure cell death as a result of IRI presence in solution. HepG2 cells in MEM treated with various concentrations of A) 2FA (**3**), B) 3FA (**2**), incubated for 12 hours at 37 °C with 5% CO_2. The positive control was incubated in MEM and is set to 100%. Excitation at 530 nm and fluorescence measured at 590 nm. Error bars represent the standard deviation (SD), n = 7, N = 2.*

In addition to the N-Aryl-β-D-aldonamides, all the N-Benzyl-β-D-gluconamides investigated for IRI activity were also assayed for cytotoxicity. The cytotoxic effect of derivatives **4**-**8** were determined by assessing cell viability in HepG2 cells at various concentrations (figure 2.13). Interestingly, comparing all the compounds at 10 mM **6** had the largest toxic effect whereas **4** had the least toxic effect, at 61.1% (±0.05 SD) and 95.5% (±0.01 SD) cell viability respectively. Compounds **5** and **7** were both limited in the ability to test higher concentrations due to their solubility limits, whereas **8** was able to be heated (37

°C) and remain in solution long enough to add to cells. Compound **7** was also relatively non-cytotoxic with the lowest cell viability being 83.4% (±0.03 SD). Although all of the tested N-Benzyl-β-D-gluconamides are relatively non-cytotoxic at low concentrations. Concentrations above 90 mM of BA (**4**), 30 mM of 4-MOBA (**8**), 25 mM of 4-MBA (**5**), and 20 mM of 2,6-DFB (**6**) are all moderately to highly toxic resulting in cell viability less than 50%.

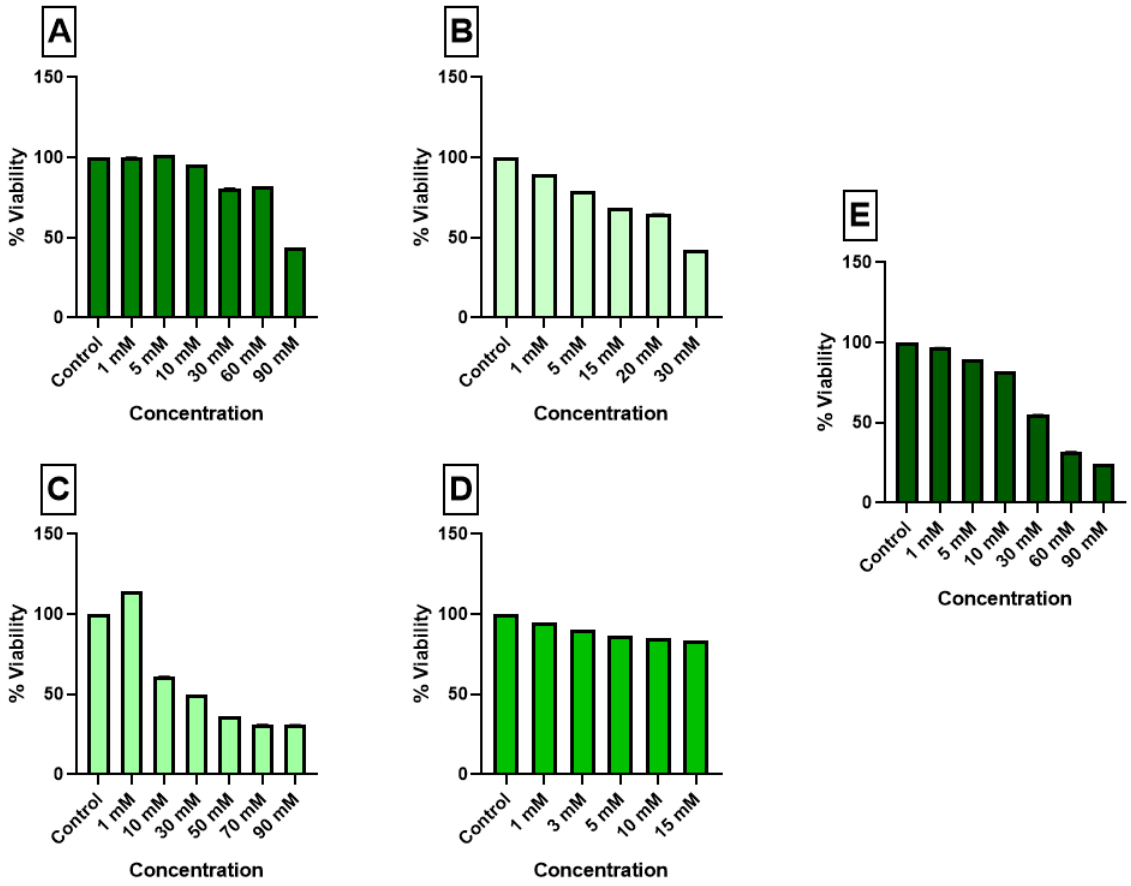

Figure 2.13. N-Benzyl-β-D-gluconamides % Cell Viability Resazurin Cytotoxicity Assay. *Cytotoxicity assay using resazurin to measure cell death as a result of IRI presence in solution. HepG2 cells in MEM treated with various concentrations of A) BA (**4**), B) 4-MBA (**5**), C) 2,6-DFB (**6**), D) 4-CBA (**7**), E) 4-MOBA (**8**), incubated for 12 hours at 37 °C with 5% CO_2. The positive control was incubated in MEM and is set to 100%. Excitation at 530 nm and fluorescence measured at 590 nm. Error bars represent the standard deviation (SD), n = 7, N =2.*

2.6 Compound Assessment Discussion

The first objective of this thesis was to assess a small library of compounds for cytotoxicity and IRI activity-based on the modified splat cooling assay to produce the

optimal dose-response curves. The previous sections have extensively covered the results of those experiments and have provided us with new insights to compound properties. Including how the structure of N-Benzyl-β-D-gluconamides effects the IRI function of these small molecules. A table summarizing the characterization of the compounds tested throughout this thesis can be found below (table 2.4).

Table 2.4. Compound Property Summary Table. *Table comparing the structure, molecular weight, IC_{50}, max solubility, and LD_{50} of all compounds used throughout this thesis. IC_{50} value is based on dose-response curves with their respective nonlinear regression curves fitted. Max solubility determined by the maximum concentration of the solute that can dissolve within PBS without the formation of a visible second phase rich in solute. IC_{50} (± SEM) is based on nonlinear regression curves fitted to cytotoxicity assay results.* ***SL*** *indicates an inability to determine LD_{50} values due to the solubility limit of the compound inhibiting higher concentrations being tested. NOGlc, pBrPhGlc, 2FA, and 3FA data obtained from Kayla Newell, Poisson[16] and Briard[10].*

Compound Name	Compound Structure	Molecular Weight (g/mol)	IC_{50} (mM)	Max Solubility (mM)	LD_{50} (mM)
N-Octyl-β-D-gluconamide (NOGlc)	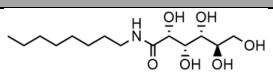	307.39	0.09	1	**SL**
N-4-Bromophenyl-β-D-glucopyranoside (pBrPhGlc)	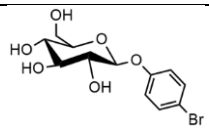	335.15	15	55	~ 2
N-2-Fluorophenyl-β-D-gluconamide (2FA)	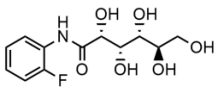	289.26	3.1	25	**SL**
N-3-Fluorophenyl-β-D-gluconamide (3FA)	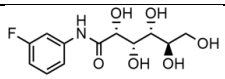	289.26	8.5	15	**SL**
N-Benzyl-β-D-gluconamide (BA)	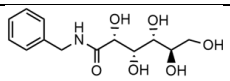	285.30	5.8 (±0.05)	90	81
N-2,6- Difluorobenzyl-β-D-gluconamide (2,6-DFB)	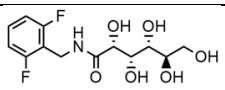	321.28	25 (±3.63)	90	25
N-4-Methylbenzyl-β-D-gluconamide (4-MBA)	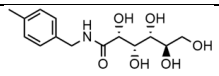	299.32	1.1 (±0.02)	50	26
N-4-Chlorobenzyl-β-D-gluconamide (4-CBA)	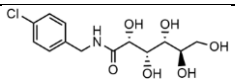	319.74	0.48 (±0.34)	15	**SL**
N-4-Methoxybenzyl-β-D-gluconamide (4-MOBA)	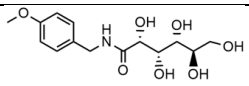	315.32	1.4 (±0.58)	40	40

In section 2.2 and 2.3 the IRI activity of N-Benzyl-β-D-gluconamides with various substituents was assessed to investigate if this group of compounds could improve solubilities relative to NOGlc (**1**) while maintaining IRI activity. It was previously determined that Benzyl-β-D-gluconamides are IRI active and more soluble than **1**, which has a solubility limit of 1 mM.[10] This increase in solubility is hypothesized to be related to the hydrocarbon chain being shortened to 6 carbons and a ring structure being substituted for either a phenyl (N-Aryl-β-D-aldonamides) or benzyl group (N-Benzyl-β-D-gluconamides). This structural change increases the compound solubility without abolishing IRI activity, although the substituents of the ring influence activity. BA (**4**), the parent structure of the N-Benzyl-β-D-gluconamides family, has IRI activity (IC_{50} = 5.8 mM ±0.05 SEM) comparable to the activity of 2FA (**3**) and 3FA (**2**) with their IC_{50} values being 3.1 mM and 8.5 mM respectively. BA (**4**) can be considered an important structure which further investigation can be beneficial to further understand the mechanism of action IRIs use. Despite not testing all permutations, for the three *para* compounds tested an interesting observation is that in addition to being active the addition of substituents to the *para* position on the benzyl ring of BA (**4**) increases activity for the compounds. This increase in activity despite different electronic properties of the substituents indicates that the *para* position may play a role in the function and activity of this family of compounds. The addition of substituents to the benzyl ring also increases the cytotoxicity as **4** is the least toxic, by a significant margin, of all the N-Benzyl-β-D-gluconamides tested. More functional groups should be tested as there is currently no clear trend that can be determined between the type of functional group added and IRI activity. Both 2,6-DFB (**6**) and 4-CBA (**7**) include a halogen on the benzyl ring, but **7** is significantly more active while **6** is the least active of the tested N-Benzyl-β-D-

gluconamides. The electron withdrawing function may play a role in the activity as we see an activity increase as the functional groups become more electron withdrawing in the three *para* substituent compounds. The removal of the oxygen between 4-MOBA (**8**) and 4-MBA (**5**) gives way to an activity increase and again between **5** and **7** we see an increase of activity for the latter compound.

As no clear trend could be determined from the variation of substituents, other metrics such as solubility and electronic properties were considered. Compound **7** had IRI activity and the lowest solubility of all the N-Benzyl-β-D-gluconamides. As **1** had previously shown a similar trend with IRI activity inhibited by solubility limit, an investigation of how solubility effects the activity of N-Benzyl-β-D-gluconamides was sought. Figure 2.14 outlines the relationship between solubility and IC_{50} values of the compounds. Compounds **5**, **7**, and **8** which have the lowest IC_{50} values of the tested N-Benzyl-β-D-gluconamides have the lowest solubility limits. Although, despite **5** being more active than **8**, **8** has a lower solubility limit. The hydrophobicity of the benzyl group must play an important role in disrupting the bulk layer, but this property also decreases the solubility of the compounds. No clear trend can be observed from these finding, however, they reaffirm previous finding that the amphiphilicity of the compound is an important aspect of IRI activity. Further investigation of how different substituents effect the solubility and IC_{50} may provide insight into how these two properties play a role in the function of our IRIs.

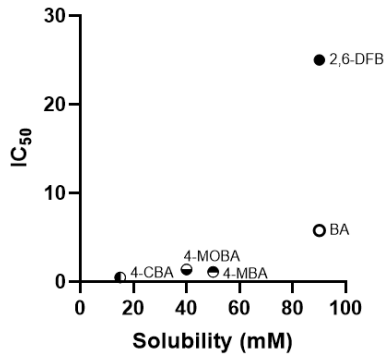

Figure 2.14. Relationship Between IC_{50} and Solubility Limit of Benzyl-β-D-gluconamides*. Scatter plot comparing the IC_{50} to the max solubility of ◐ 4-CBA (**7**), ◓ 4-MBA (**5**), ◒ 4-MOBA (**8**), ● 2,6-DFB (**6**), and ○ BA (**4**). IC_{50} (mM) was determined by nonlinear regression curves from each respective compounds dose-response curve generated from IRI activity. Solubility limit determined by the maximum concentration of the solute that can dissolve within PBS without the formation of a second phase rich in solute.*

In addition to structure and function analysis the method of quantifying IRI activity through dose-response curves was investigated. The best parameter to approximate the changes in ice during recrystallization was acquired using several parameters of ice crystals obtained by using a modified splat cooling assay with PBS.[12] The next step is to select the one curve that best explains the data out of the entire family of possible curves that the curve model can produce.[14] This is accomplished by fitting the curve.[14] Fitting a curve is the process of adjusting the free parameters of the function until the function parameters approximate the assay's true curve better than any other parameter set.[14] In our labs previous findings, the 4PL equation produced the curve with the best fit yielding a sigmodal curve. However, because derivatives **7** and **8** data did not precisely fit the symmetrical curve produced by the 4PL function, in section 2.4 we underwent the process of curve fitting. Our findings, which are in agreement with previous studies, were that in cases that the 4PL curve does not provide the best fit the 5PL function, which includes a fifth parameter, may permit asymmetry to be effectively modeled.[14] The 4PL function is the standard dose-response curve used to model enzyme activity, which typically follows a symmetrical curve. IRIs however are hypothesized to work through a physical change in the system (disrupting the

bulk water) rather than a chemical process observed with enzymes. Therefore, there is a possibility that IRIs may produce asymmetrical curves making the 5PL a more accurate fit. However, to validate that finding, more concentrations would have to be tested to populate the curves as fully as possible, as currently, the 4PL and 5PL curves have similar R^2 values. From section 2.4 we know that the dose response curves must fit a minimum of 4 parameters. The sigmodal curve was confirmed to be the trend that IRIs most accurately follow as the exponential, phase decay, and non-variable slopes have lower R^2 values and worse curve fits.

Lastly, in section 2.5 the cytotoxicity results are encouraging as many of the small molecule IRIs assessed for cytotoxic effects with HepG2 were determined to be relatively non-toxic. These molecules were designed to be less toxic than the N-Alkyl-β-D-aldonamides by replacing the long alkyl chains with an aromatic ring.[10] Both **6** and **8** previously underwent cytotoxicity testing and performed better than compounds **1** and pBrPhGlc (**9**).[10] Compound **1** is largely non-toxic at doses below 1 mM, resulting in cell viabilities of more than 85%; moderately toxic at 2 mM, resulting in 55% cell viability; and highly toxic at 5 mM, resulting in less than 4% of HepG2 cells surviving the incubation time.[6] Additionally, **9** is very cytotoxic even at low concentrations; at 1 mM, cell viability is 77%, at 5 mM, viability is significantly reduced to about 10%, and at 20 mM and above, viability is 0%.[16] Therefore, discovering compounds that are just as active but non-toxic is ideal. The results found in this thesis confirmed that **2** and **3** have low cytotoxicity at concentrations below their solubility limit. As well, all of the tested N-Benzyl-β-D-gluconamides are relatively non-toxic at low concentrations only becoming moderately toxic at higher concentrations which are much larger than their IC_{50} values. These are encouraging

results as all tested compounds are IRI active and with the knowledge that they are non-toxic, gives the opportunity to test these compounds in biological material.

2.7 References

1 Balcerzak, A. K., Capicciotti, C. J., Briard, J. G. & Ben, R. N. Designing ice recrystallization inhibitors: from antifreeze (glyco)proteins to small molecules. *RSC Adv.* **4**, 42682-42696, doi:10.1039/c4ra06893a (2014).

2 J, C., Doshi, M. & N, R. (InTech, 2013).

3 Tae Hoon Jang, S. C. P., Ji Hyun Yang, Jung Yoon Kim, Jae Hong Seok, Ui Seo Park, Chang Won Choi, Sung Ryul Lee, and Jin Han. Cryopreservation and its clinical applications. *Integrative Medicine Research* **6**, 12-18, doi:https://doi.org/10.1016%2Fj.imr.2016.12.001 (2017).

4 Pegg, D. E. 3-19 (Springer New York, 2015).

5 Nishaka William, J. P. A. Cryoprotectant-dependent control of intracellular ice recrystallization in hepatocytes using small molecule carbohydrate derivatives. *Cryobiology* **97**, 123-130, doi:https://doi.org/10.1016/j.cryobiol.2020.09.008 (2020).

6 Capicciotti, C. *The Rational Design of Potent Ice Recrystallization Inhibitors for Use as Novel Cryoprotectants* Doctorate in Philosophy degree in Chemistry thesis, University of Ottawa, (2014).

7 Ghobadloo, S. M. *et al.* Carbohydrate-Based Ice Recrystallization Inhibitors Increase Infectivity and Thermostability of Viral Vectors. *Scientific Reports* **4**, doi:10.1038/srep05903 (2015).

8 Poisson, J. S., Acker, J. P., Briard, J. G., Meyer, J. E. & Ben, R. N. Modulating Intracellular Ice Growth with Cell-Permeating Small-Molecule Ice Recrystallization Inhibitors. *Langmuir* **35**, 7452-7458, doi:10.1021/acs.langmuir.8b02126 (2019).

9 Suria Jahan, M. K. A., Javed K. Manesia, Emily Doxtator, Robert N. Ben, Nicolas Pineault. Inhibition of ice recrystallization during cryopreservation of cord blood grafts improves platelet engraftment. *Transfusion* **60**, 769-778, doi:https://doi.org/10.1111/trf.15759 (2020).

10 Briard, J. G. *The Rational Design and Use of Novel Small-Molecule Ice Recrystallization Inhibitors for the Cryopreservation of Hematopoietic Stem Cells and Red Blood Cells* Department of Chemistry and Biomolecular Sciences thesis, University of Ottawa, (2016).

11 Ampaw, A. A., Sibthorpe, A. & Ben, R. N. 271-283 (Springer US, 2021).

12 Abraham, S. *Development and Implementation of a Kinetic Quantitative Analysis of Novel Small Molecule Ice Recrystallization Inhibitors* MSc degree in Chemistry thesis, University of Ottawa, (2015).

13 Jesús Giraldo, N. M. V., Elisabet Vila, Albert Badia. Assessing the (a)symmetry of concentration-effect curves: empirical versus mechanistic models. *Pharmacology & Therapeutics* **95**, 21-45, doi:https://doi.org/10.1016/S0163-7258(02)00223-1 (2002).

14 Paul G. Gottschalk, J. R. D. The five-parameter logistic: A characterization and comparison with the four-parameter logistic. *Analytical Biochemistry* **343**, 54-65, doi:https://doi.org/10.1016/j.ab.2005.04.035 (2005).

15 Nakagawa, S. & Schielzeth, H. A general and simple method for obtaining R2 from generalized linear mixed-effects models. *Methods in Ecology and Evolution* **4**, 133-142, doi:10.1111/j.2041-210x.2012.00261.x (2013).

16 Poisson, J. S. *Synthesis and In Vitro Applications of Ice Recrystallization Inhibitors* Doctorate in Philosophy degree in Chemistry thesis, University of Ottawa, (2019).

Chapter 3: Assessing Post Freeze-Drying Protein Stabilization After Treatment with Small Molecule Ice Recrystallization Inhibitors

3.1 Introduction

The scientific community's focus underwent a significant shift in 2020 with the emergence of COVID. As viruses utilize both structural and enzymatic proteins as their main building components, proteins have become one of the key areas of research.[1] In contrast to other biological materials, proteins have a unique and interesting history in cryopreservation. These complexities are due to the wide range of chemical reactions that proteins can undergo in aqueous solutions.[2] Among such reactions, which tend to reduce specific biological activity, are hydrolysis, disulfide rearrangements, oxidation, cross-linking and aggregation.[2] In the dry state such reaction can be substantially decelerated, therefore the most commonly used method for preparing solid protein pharmaceuticals is lyophilization (freeze-drying).[2,3] Since this process of freezing, followed by ice sublimation are performed at low temperatures and are less likely to harm labile bioproducts than drying at ambient or higher temperatures, they have become the preferred route of water removal.[2] Although, as previously mentioned in section 1.4, lyophilization causes a number of stressors, including changes in pH, ice crystal formation, solute concentration, and others that tend to destabilize or unfold/denature an unprotected protein.[3] In addition, different proteins tolerate freezing and/or drying stresses to various degrees.[3] Thus, stabilizers are often required in a protein formulation to protect protein stability during both processes.[3]

One of the most commonly used stabilizers for long term storage of solid proteins is the disaccharide trehalose (figure 3.1).[3] As used in both cryoprotection and lyoprotection, trehalose stands out as particularly excellent for a wide range of biologically significant

storage properties.[3,4] These benefits include slowing the rate of protein aggregation, high recovery of protein function after cryostorage and an excellent ability to protect lipid bilayers to low and high temperatures (freeze-thaw) or dehydration.[4,5] Whereas, when heated from the cryogenic storage temperature, concentrated DMSO solutions can cause protein aggregation and damage.[6] Trehalose also possesses a number of other favourable characteristics, such as structural conformation, reduced hygroscopicity, a lack of internal hydrogen bonding that facilitates more flexible creation of hydrogen bonds with proteins, and extremely low chemical reactivity.[3] Trehalose currently appears to provide the highest level of bio-protection due to the cooperative action of all these elements.[5]

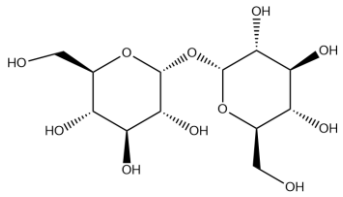

Figure 3.1. Structure of Trehalose.

One important aspect of trehalose is it forms a glass state at -138 °C.[4,7] At concentrations above 30 wt% trehalose has a de-structuring effect on the hydrogen bonded network of water which is related to its ability to prevent water crystallization.[4] Various theories have been proposed to explain the physical and chemical properties of trehalose which are beneficial for cryopreservation, with "preferential exclusion theory" being the most widely recognised (figure 3.2).[5] According to this theory there is no direct interaction between trehalose and protein.[5] Trehalose forms structures close to the surfaces of proteins, sequestering bulk water molecules away from the protein and reducing its hydrated radius. These structures also form numerous hydrogen bonds with a water layer on the protein surfaces.[4,5] In this model the water is entrapped in a layer between the protein surfaces and the surrounding trehalose structures.[4] Thus, the more rigid trehalose-water complexes and

increased compactness are linked to the protein's dynamics via the water layer, slowing down the protein dynamics and increasing the protein's stability.[4,5] The protein can maintain its native state owing to this interaction, preventing denaturation after heat shock, desiccation, and cold storage.[4]

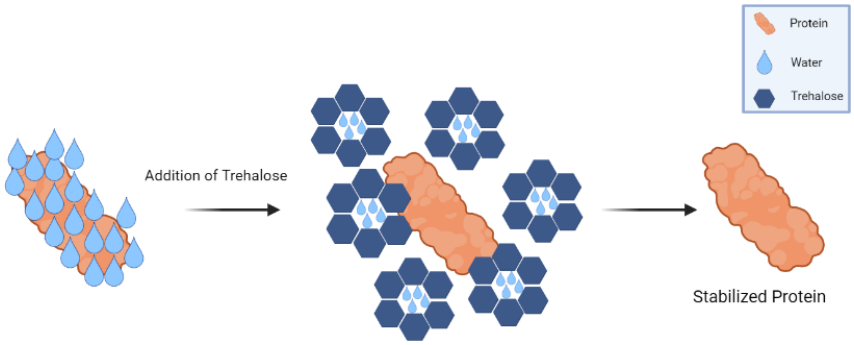

Figure 3.2. Mechanism of Action of Trehalose. *Figure adapted using BioRender ©.*[5]

While trehalose is able to enhance the recovery of proteins, it fails to control the growth of ice.[3] This background leads into the query if small molecule carbohydrate-based IRIs are capable of protein stabilization as both a cryoprotectant and lyoprotectant, comparable to the current industry standard trehalose. Global immunisation campaigns and viral-based therapy have been significantly hampered by viral vaccines' failure to maintain adequate thermostability due to the previously mentioned difficulties associated with cryopreservation of proteins.[8] Given that freezing significantly lowers the virus's titer, lyophilization is the standard method for preserving vaccines.[8] In addition, exposure to cold temperatures causes virus aggregation, which renders the vaccine ineffective.[8] In order to minimise damage, techniques that limit ice development during cryopreservation are needed.[8]

Our lab has previously shown the ability of small molecule IRIs successfully applied to cryopreservation of oncolytic viruses, where the addition of IRIs prevented the damage caused by freezing, as discussed in section 1.8.2.[8] In this chapter we assess if small

molecule-based IRIs are capable of protein stabilization using the nucleocapsid gene (N gene) RNA from SARS-CoV-2. In this study, four compounds were examined (figure 3.3), two of which had shown previous success NOGlc (**1**) and pBrPhGlc (**9**). Both **1** and **9**, regulate extracellular ice from recrystallizing, in addition **9** can enter cells and regulate the recrystallization of intracellular ice in RBC.[9,10] As well as two compounds assessed in chapter 2, 4-MBA (**5**) and 2,6-DFB (**6**) as further assessment of their ability to ensure stability of viral proteins after biopreservation.

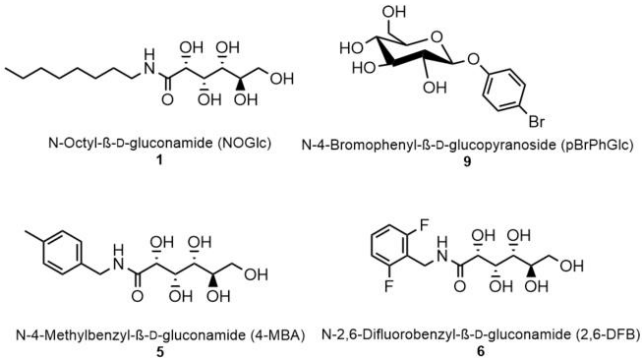

Figure 3.3. Structures of Ice Recrystallization Inhibitors (IRIs) that will be Evaluated.

SARS-CoV-2 is a spherical, pleomorphic enveloped virus containing positive single-stranded RNA associated with a nucleoprotein. All coronaviruses have the S, E, M, and N genes, which are found in the 5' to 3' orientation (figure 3.4). Person to person contact and direct contact with respiratory droplets from an infected person are the two main methods of transmission. The current standard of COVID testing is the collection of an upper respiratory tract specimen, either; nasopharyngeal, deep nasal, or a viral throat swab.[11] The specimen is packed in a sealed bag, kept at 2-8 °C, and shipped on ice prior to transportation.[11] The specimen is frozen to -70 °C and sent on dry ice if transportation is delayed by more than 72 hours.[11] The specimen contains RNA that is extracted and purified.[11] To detect the presence of the virus, RT-qPCR is employed where the purified RNA is reverse transcribed into

cDNA before being amplified by qPCR.[11] RT-qPCR detects various targets as three genes are amplified in the qPCR reaction; the envelope gene (E gene), RNA dependent RNA polymerase gene (RdRp gene), and N gene.[11] Due to freezing of the test samples to -70 ºC or below, there is a potential for degradation of viral DNA caused by the freeze-thaw cycle. As such, a method to prevent cryoinjury of test swabs must be developed.[11]

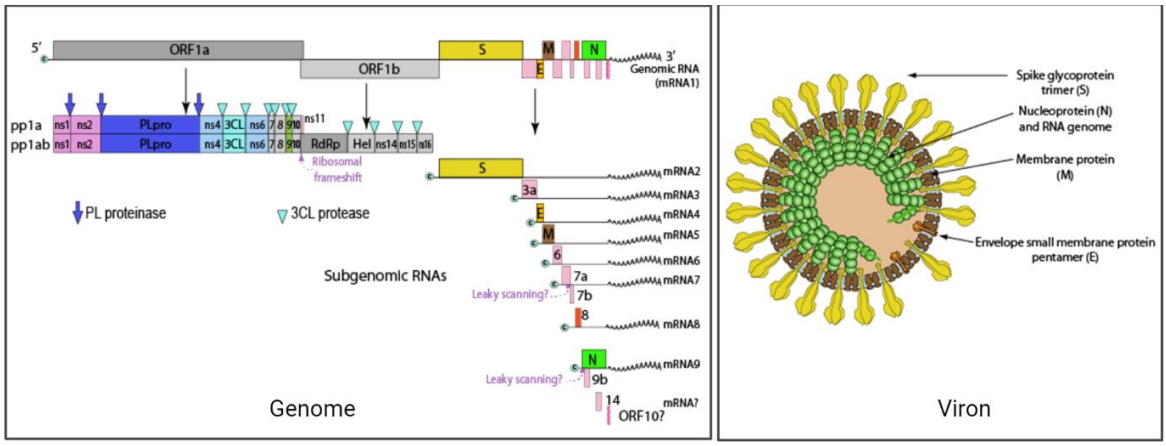

Figure 3.4. Genome and Viron Structure of SARS-CoV-2. *Images adapted from ViralZone © 2020 SIB Swiss Institute of Bioinformatics. Graphic created and edited in BioRender ©.*

In this work, to identify promising compounds we examined the activity and thermostability of master mix (enzymes, oligonucleotides, and RNA) after adding small molecule IRIs during lyophilization and RT-qPCR. To assess the stabilization of qPCR enzymes using the IRIs, the enzymes were freeze-dried in the presence of the IRI's. IRIs were added to master mix, then each solution was added to a qPCR receptacle (chips, plates or, tubes), which was then lyophilized. Template RNA dissolved in water was added to reconstitute the mixture and the RT-qPCR was run (figure 3.5).

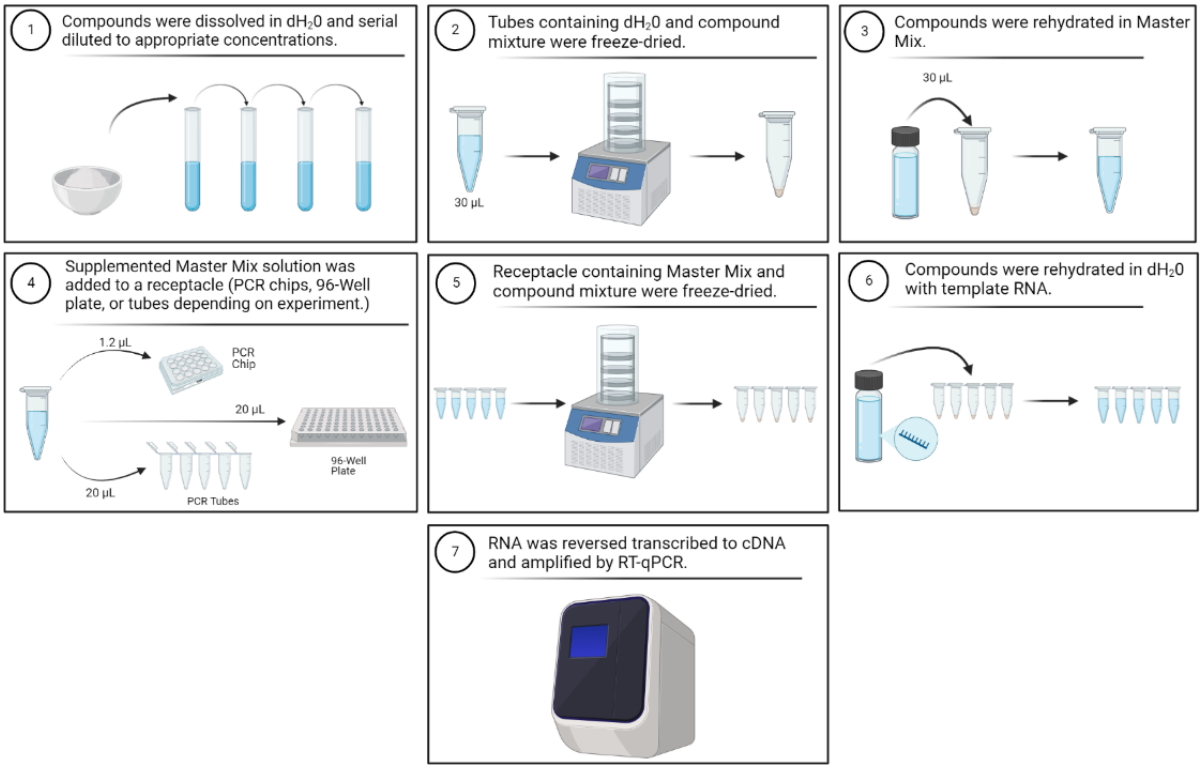

Figure 3.5. RT-qPCR Experimental Design Infographic. *Compounds refer to NOGlc (**1**), 4-MBA (**5**), 2,6-DFB (**6**), and pBrPhGlc (**9**). Image created in BioRender ©.*

3.2 Evaluating Protein Stabilization Ability of Carbohydrate-Based Small Molecule Ice Recrystallization Inhibitors

Given that protein damage due to ice recrystallization is directly responsible for some of the denaturation observed during lyophilization, we sought to explore the ability of the IRIs in this study to act as cryoprotectants.[3] The activity and thermostability of proteins during lyophilization and RT-qPCR using compounds **1**, **5**, **6,** and **9** was examined. Master mix solution contains dNTPs, reverse transcriptase, DNA polymerase, and primers for both the N1 and N2 regions of the N gene which are affected by the freeze-drying process and could benefit from cryo-additives to reduce damage.

In the following experiments the cycle threshold fluorescence (Ct) is determined from RT-qPCR. The Ct value is defined as the number of cycles of amplification (using RT-qPCR) required for the fluorescence of a qPCR target to be detected crossing a threshold, which is above the background signal (a low-level signal that is present in the assay regardless of whether target is present).[12] If target is present in the sample, then each round of amplification results in a doubling of the amount of target present.[12] As a result, amplification occurs exponentially, producing an exponential curve of amplification.[12] This exponential amplification is visualized using a fluorescent nucleic acid probe.[12] Probes are fluorescently labelled DNA oligonucleotides, which bind to the target.[12] As amplification proceeds, more targets become available for binding by the fluorescent probe, increasing the fluorescent signal.[12] In general, the amount of fluorescent signal observed increases as amplification proceeds and is related to the amount of target present in the sample.[12] Amplification is considered significant, and equates with 'detection' of the target, if the threshold of fluorescence is reached.[12] For a positive test result, Ct must be reached within 40 amplification cycles. A decrease in percent mean threshold cycle correlates to increased enzyme stabilization.

3.2.1 Assessing Protein Stabilization Ability of of *N*-Octyl-β-D-gluconamide (**1**) and *N*-4-Bromophenyl-β-D-glucopyranoside (**9**)

Preliminary testing was done using the IC_{50} concentration of compounds **1** and **9** (0.09 mM and 15 mM respectively), to determine if either IRI has the ability to reduce mean cycle value to reach threshold fluorescence. The ability for **1** and **9** to stabilize qPCR enzymes was compared to the trehalose control at 292 mM (10% w/v), the current industry standard.[3] This sugar has also been found to act as a stabilizer to improve the shelf life of

therapeutic proteins, and it was determined as a known PCR enhancer.[3] The results are shown in figure 3.6.

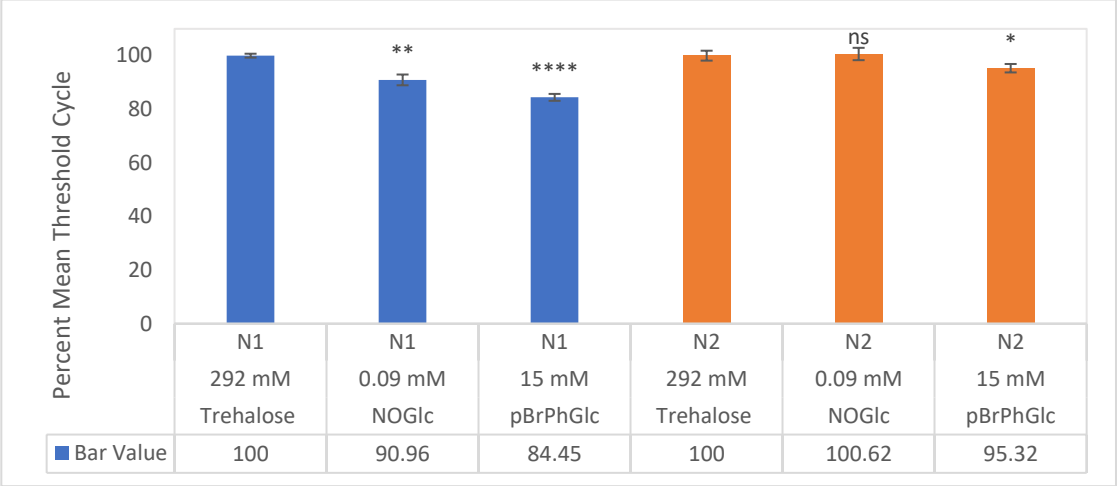

Figure 3.6. Stabilization of RT-qPCR Enzymes in the Presence of NOGlc (1) and pBrPhGlc (9). *qPCR enzymes were lyophilized in the presence of NOGlc (**1**) and pBrPhGlc (**9**), followed by an RT-qPCR chip experiment. The mean cycle (%) to reach threshold fluorescence was graphed. Concentrations were compared to a control of the industry standard, trehalose 292 mM which has been normalize to 100%. The **blue** bars represent N1 region of the N gene results, and **orange** bars represent N2 region of the N gene results as indicated above concentrations on the graph. Error represents SEM, (n = 3). **** $P \leq 0.0001$, *** $P \leq 0.001$, ** $P \leq 0.01$, * $P \leq 0.05$, ns $P > 0.05$.*

Results demonstrate that compared to the trehalose control which was normalized to 100% (±0.73 SEM) the mean cycle value to reach threshold fluorescence for N1 **1** and **9** decreased to 90.9% (±2.01 SEM) and 84.5% (±1.29 SEM), respectively. For the N2 region, there was an increase in the percent mean cycle to reach threshold fluorescence (100.6% ±2.30 SEM) when NOGlc (**1**) was used, and there was a decrease to 95.3% (±1.57 SEM) when pBrPhGlc (**9**) was introduced. Both compounds are effective at stabilizing the RT-qPCR enzymes during a freeze-dry cycle, evident through the decrease in the number of cycles required to reach threshold fluorescence. It is significant to note that the IRIs tested did not affect the ability for the amplification to occur nor interfere with any of the qPCR process. If the process was affected, through damage to (inactivation of) the enzymes or oligonucleotides then amplification would not occur, and the amount of fluorescence detected would not reach the threshold value or threshold cycle values would increase

compared to the standard. In addition, there is a noticeable difference in N1 region results compared to N2 region, with the mean threshold values being larger for the latter. To determine optimal concentration to achieve maximum enzyme stabilization, varying concentrations above and below the IC_{50} of **1** and **9** were tested against two concentrations of trehalose (0.5% and 10%). The second control of trehalose at 15 mM (0.5% w/v) was included to compare the IRIs to a similar concentration. The results of the most active concentrations of the compounds are shown in figures 3.7 and 3.8.

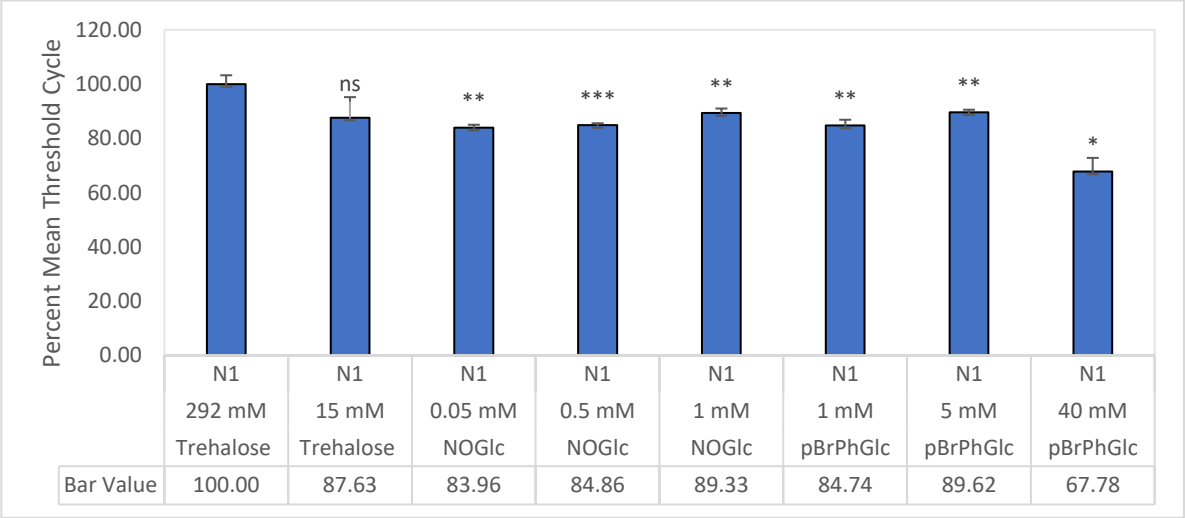

	N1 292 mM Trehalose	N1 15 mM Trehalose	N1 0.05 mM NOGlc	N1 0.5 mM NOGlc	N1 1 mM NOGlc	N1 1 mM pBrPhGlc	N1 5 mM pBrPhGlc	N1 40 mM pBrPhGlc
Bar Value	100.00	87.63	83.96	84.86	89.33	84.74	89.62	67.78

Figure 3.7. Stabilization of RT-qPCR Enzymes in the Presence of NOGlc (1) and pBrPhGlc (9) N1 Region Data. *qPCR enzymes were lyophilized in the presence of NOGlc (**1**) and pBrPhGlc (**9**), followed by an RT-qPCR plate experiment. The mean cycle (%) to reach threshold fluorescence was graphed. Concentrations were compared to a control of the industry standard, trehalose 292 mM which has been normalize to 100%. Error represents SEM, (n = 3). **** $P \leq 0.0001$, *** $P \leq 0.001$, ** $P \leq 0.01$, * $P \leq 0.05$, ns $P > 0.05$.*

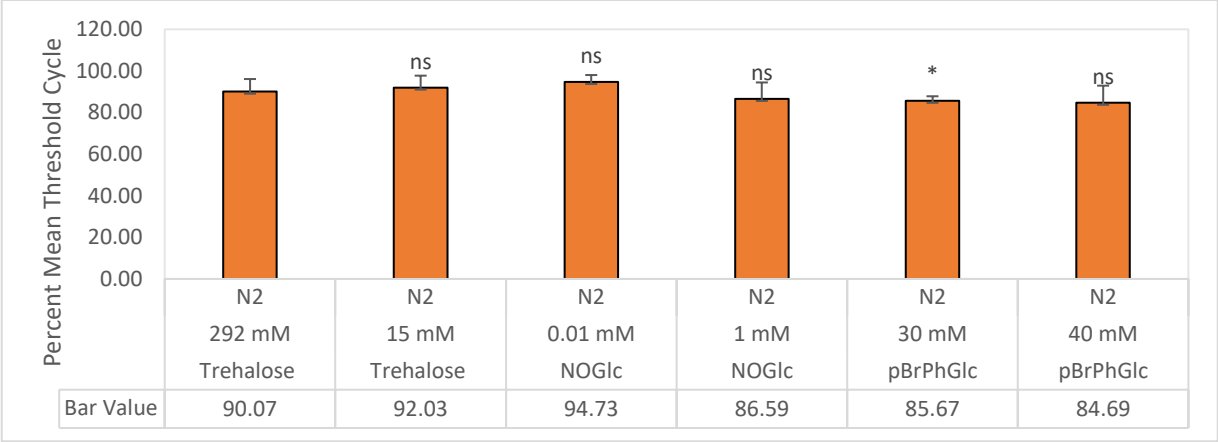

Figure 3.8. Stabilization of RT-qPCR Enzymes in the Presence of NOGlc (1) and pBrPhGlc (9) N2 Region Data. *qPCR enzymes were lyophilized in the presence of NOGlc (**1**) and pBrPhGlc (**9**), followed by an RT-qPCR plate experiment. The mean cycle (%) to reach threshold fluorescence was graphed. Concentrations were compared to a control of the industry standard, trehalose 292 mM which has been normalize to 100%. Error represents SEM, (n = 3). **** $P \leq 0.0001$, *** $P \leq 0.001$, ** $P \leq 0.01$, * $P \leq 0.05$, ns $P > 0.05$.*

Figures 3.7 and 3.8 confirmed the three main results discovered in preliminary testing. The first being that both **1** and **9** can stabilize the proteins during a freeze-dry cycle. Although, not all concentrations tested produced significant results, for example 0.09 mM of NOGlc (**1**) and 15 mM of pBrPhGlc (**9**) in figure 3.6 was significant but was not in further testing, this could be due to a change in qPCR receptacle as the preliminary results were run on a qPCR chip. The significant of change in receptacle from chip to plate was further investigated in section 3.3. Secondly, the compounds do not interfere with the qPCR process at any concentration with the concentration presented in figures 3.7 and 3.8 showing statistically relevant reduction of the mean threshold cycle value. Thirdly, the variance observed between N1 and N2 regions was consistent with N2 having statistically less relevant IRI concentrations, additionally all tested compounds (including the control) had noticeably different percent mean threshold values despite being normalized. This indicates that there is a difference between the N1 and N2 regions during the qPCR process. In conclusion the most effective IRI was **9** at 40 mM for N1 and **9** at 30 mM for N2 with a

decreased of the percent mean cycle to reach threshold of 67.8% (±5.03 SEM) and 85.7% (±2.15 SEM), respectively.

3.2.2 Determining Shelf-Life Stability of Proteins Supplemented with Ice Recrystallization Inhibitors

The long-term storage of proteins is a significant obstacle currently in the pharmaceutical industry, as the longer a protein is stored the harder it is to maintain the integrity.[3] Thus, in order to compare the cryoprotectant and lyoprotectant properties of IRIs to trehalose a shelf-life assay was performed. Our objective was to determine room temperature shelf-life stabilization analysis at varying time points of 1-, 3-, 7-, and 14-days of compounds **1** and **9**. The three concentrations which performed best in previous experiments were used to determine room temperature shelf-life stabilization of qPCR enzymes after a freeze-dry cycle. To determine the amount of time the proteins could be stored after a freeze-drying cycle, IRIs were added to master mix, and 20 µL was aliquoted into a 96-well plate (n = 3), which was then lyophilized. After freeze drying plates were stored at room temperature at the time points of 1-, 3-, 7-, and 14-days before the RT-qPCR was run (table 3.1).

Table 3.1. Shelf-Life Stabilization Cycle Number Data. *PCR enzymes were lyophilized in the presence of NOGlc (**1**) and pBrPhGlc (**9**), the well plates were then stored for their respective shelf-life test (1-, 3-, 7-, and, 14-days) followed by an RT-qPCR plate experiment. The mean cycle (%) to reach threshold fluorescence was average for each value (n = 3) and the values for each condition (compound/concentration/gene) were then compared to determine the highest to lowest value under each condition.*

Conditions		Plate Storage			
		1-Day	3-Days	7-Days	14-Days
Compound	Gene	Mean Threshold Cycle			
Trehalose 292 mM	N1	18.82	23.55	20.49	21.40
Trehalose 292 mM	N2	14.40	18.58	21.96	29.14
pBrPhGlc 40 mM	N1	14.90	30.16	29.61	28.38
pBrPhGlc 40 mM	N2	15.87	30.12	29.49	30.20
Trehalose 15 mM	N1	17.55	21.27	21.58	24.75
Trehalose 15 mM	N2	17.76	21.13	23.57	23.78
pBrPhGlc 30 mM	N1	17.69	21.77	28.65	27.90
pBrPhGlc 30 mM	N2	15.86	24.51	28.10	25.84
NOGlc 1 mM	N1	20.22	23.01	23.83	26.44
NOGlc 1 mM	N2	17.70	23.13	25.49	30.20
pBrPhGlc 15 mM	N1	18.69	19.29	19.27	26.10
pBrPhGlc 15 mM	N2	17.13	22.93	24.72	28.76
NOGlc 0.5 mM	N1	16.98	22.91	23.03	26.06
NOGlc 0.5 mM	N2	20.21	25.54	22.67	24.42
pBrPhGlc 1 mM	N1	16.53	20.91	21.78	24.74
pBrPhGlc 1 mM	N2	17.32	22.55	21.67	24.85
NOGlc 0.05 mM	N1	17.66	24.31	25.10	27.54
NOGlc 0.05 mM	N2	19.34	22.31	23.11	27.66

Legend	
	Highest Value
	Lowest Value

Table 3.1 is a comparison of the mean threshold cycle values of days stored at room temperature for each individual condition (compound, concentration, and gene). Based on the days stored each condition is compared to itself to determine the lowest and highest mean threshold cycle values. This is displayed by the colour gradients listed in the legend to determine a trend of the most effective threshold cycle for each condition based on at varying time points of 1-, 3-, 7-, and 14-days. The main trend seen from the table is that at 1-day of storage, all conditions have the lowest mean threshold cycle value indicating that the compounds are most effective at this time point. For example, trehalose at 15 mM for day 1, 3, 7, and 14 had values of 18, 21, 22, 25 respectively. Therefore day 1 has the lowest percent mean cycle and day 14 has the highest. Table 3.1 results demonstrate 100% of the time the 1-day plate had the lowest percent mean cycle value, the 3-day plate had the 2nd lowest percent mean cycle values, the 7-day plate had the 2nd highest percent mean cycle values, and the 14-day plate had the highest percent mean cycle values for majority of the conditions. The overall results demonstrated that the longer the plates are stored at room temperature between lyophilization and when the RT-qPCR is run, the higher the percent mean cycle to reach

threshold fluorescence. This shows that the increase in shelf storage time decrease the effectivity of the compounds to stabilize the enzymes. As all the mean threshold cycle numbers are under the 40 amplification cycles positive test result limit, all concentrations at all time points equates with 'detection' of target gene. Therefore, despite being less effective at 14 days post lyophilization all conditions are able to reach threshold value indicating that the cryo-additives are effective stabilizers for 2 weeks. In addition, the IRIs tested, **1** and **9**, are comparable to the stabilization seen with trehalose. This is an encouraging result as the IRIs used were dissolved in distilled water and did not need to be supplemented with trehalose to be effective.

3.2.3 Assessing Protein Stabilization Ability of of *N*-4-Methylbenzyl-β-D-gluconamide (5) and *N*-2,6-Difluorobenzyl-β-D-gluconamide (6) in qPCR Tubes

Due to the effective thermostability of proteins observed in previous sections, to further assess if different classes of IRI can effectively stabilize proteins, compounds **5** and **6** were also tested. In addition, assessment of the cryoprotectant abilities of *N*-Benzyl-β-D-gluconamides in biological material has yet to be investigated. Therefore, to determine optimal concentration to reduce mean cycle value to reach threshold fluorescence, varying concentrations, above and below the IC_{50}, of **5** and **6** (1 mM ±0.02 SEM and 25 mM ±3.63 SEM respectively) were tested against two concentrations of trehalose (15 mM and 292 mM). The protocol was optimized, and the experiments were carried out in qPCR strip tubes. The results of the most active concentrations of the compounds are shown in figures 3.9 and 3.10.

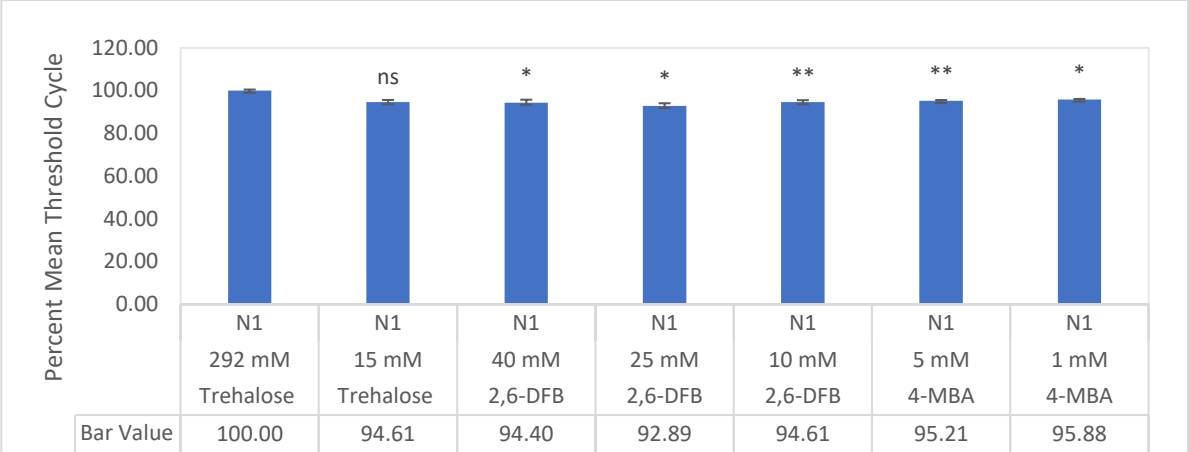

Figure 3.9. Stabilization of RT-qPCR Enzymes in the Presence of 2,6-DFB (6) and 4-MBA (5) N1 Region Data. *qPCR enzymes were lyophilized in the presence of 2,6-DFB (**6**) and 4-MBA (**5**), followed by a RT-qPCR tube experiment. The mean cycle (%) to reach threshold fluorescence was graphed. Concentrations were compared to a control of the industry standard, trehalose 292 mM which has been normalize to 100%. Error represents SEM, (n = 3). **** P ≤ 0.0001, *** P ≤ 0.001, ** P ≤ 0.01, * P ≤ 0.05, ns P > 0.05.*

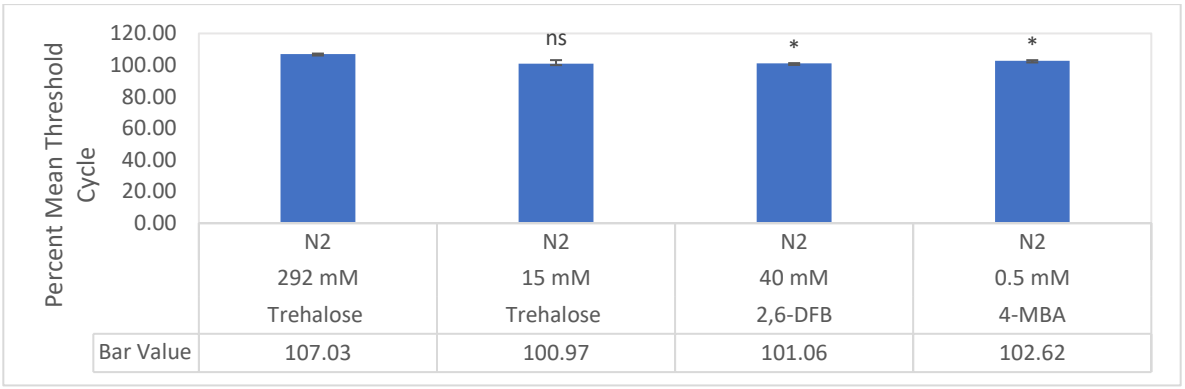

Figure 3.10. Stabilization of RT-qPCR Enzymes in the Presence of 2,6-DFB (6) and 4-MBA (5) N2 Region Data. *qPCR enzymes were lyophilized in the presence of 2,6-DFB (**6**) and 4-MBA (**5**), followed by a RT-qPCR tube experiment. The mean cycle (%) to reach threshold fluorescence was graphed. Concentrations were compared to a control of the industry standard, trehalose 292 mM which has been normalize to 100%. Error represents SEM, (n = 3). **** P ≤ 0.0001, *** P ≤ 0.001, ** P ≤ 0.01, * P ≤ 0.05, ns P > 0.05.*

The results demonstrated that **5** and **6** can both effectively decrease the mean threshold value. In addition to our previous two compounds, we can see that the two tested Benzyl-β-D-gluconamides do not interfere with the qPCR process as a threshold value was reached and Ct values decreased compared to the control. This shows that a variety of classes of IRIs can be used to stabilize proteins during a freeze-dry cycle. The most effective concentration for the N1 region was 5 mM (95.2% ±0.40 SEM) and 25 mM (92.9% ±1.22 SEM) for **5** and **6** respectively. The N2 region only had two statistically relevant

concentrations of **6** at 40 mM (101.1% ±0.16 SEM) and **5** at 0.5 mM (102.6% ±0.48 SEM). This confirms our previous findings of a difference in N1 and N2 regions, where despite testing the same concentrations N2 regions has less relevant results which are not consistent with N1 region results. These results are in agreement that the IRIs tested, **1**, **5**, **6,** and **9** are all comparable to the stabilization seen with trehalose. Despite not being directly comparable due to a difference in qPCR receptacle, which is further explored in the next section, the most effective IRI when compared to the normalized control is **9** at 40 mM.

3.3 Comparing Effectiveness of qPCR Receptacle Methods

Experiments were performed using three different qPCR receptacles qPCR chips, 96-well plates, and qPCR strip tubes (figure 3.11) due to machine breakdown and possible contamination. This probed the investigation if the qPCR receptacle used has an effect on the effectivity of cryo-additives to stabilize proteins during lyophilization and RT-qPCR.

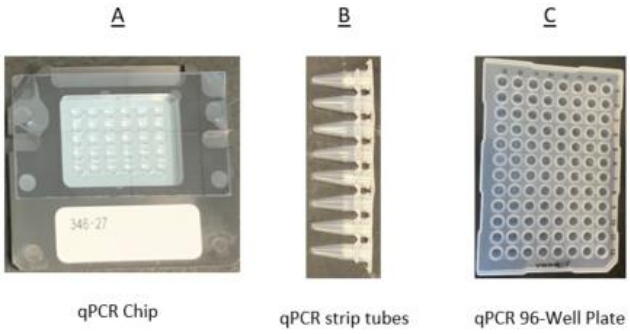

Figure 3.11. Picture of Different qPCR Receptacles. *A) qPCR Chip, B) qPCR strip tubes, and C) qPCR 96-Well Plate.*

Shortly after experiments began the qPCR chip machine broke therefore the experiment was transitioned to qPCR plates. Although, as the qPCR chip and 96-well plate do not have covers or lids, contamination from previous runs or between conditions is a possibility which may account for the variation of results seen between experiments. Therefore, the average results of qPCR tubes, chips, and plates were compared to determine the optimal protocol, as

well to determine if different qPCR receptacles produce comparable results. The mean raw cycle number of trehalose at 15 mM and 292 mM from all experiments were compared as they had the largest number of technical and biological replicates (indicated by N). The raw cycle numbers comparison of the N1 region RT-qPCR enzymes in the presence of trehalose of different qPCR receptacle are shown in figure 3.12.

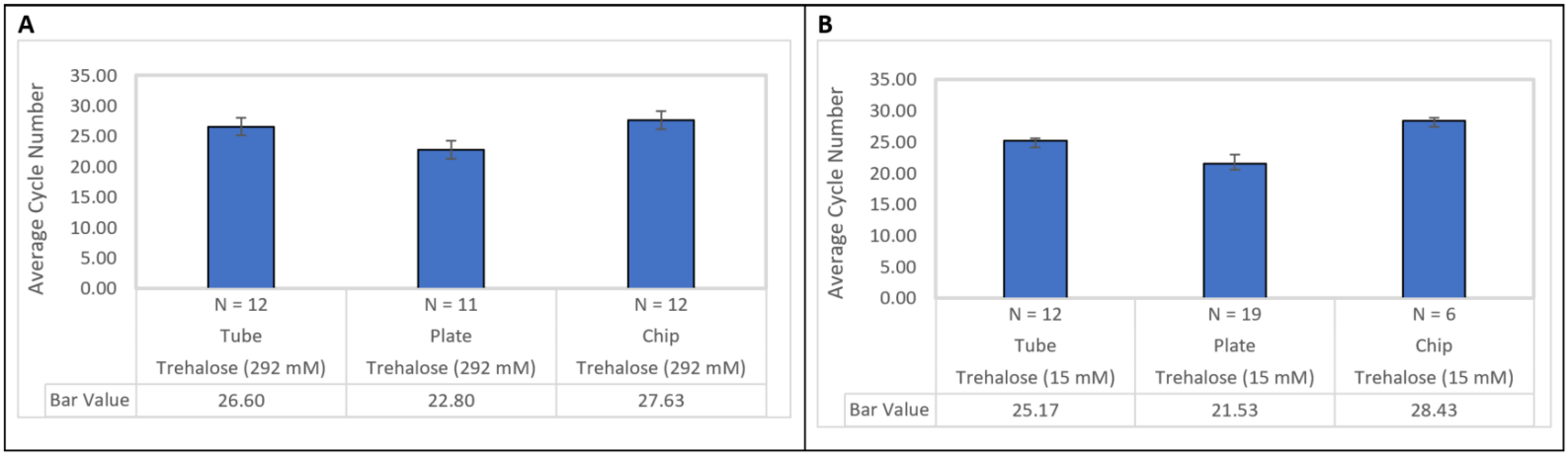

Figure 3.12. Stabilization of RT-qPCR Enzymes in the Presence of Trehalose Comparing PCR Receptacle of the N1 Region. *A) Average Cycle number to reach threshold of industry standard 10% trehalose (292 mM) B) Average Cycle number to reach threshold of 0.5% trehalose (15 mM). qPCR enzymes were lyophilized in the presence of trehalose in different receptacles (tubes, plates, and chips). The average cycle number to reach threshold fluorescence was graphed for each receptacle. Error represents SEM, the technical replicates (N number) of each concentration is indicated on the graph.*

Both panels of figure 3.12 show the same trend when comparing the cycle number of different qPCR receptacles. Under the same conditions qPCR chips take more cycles to reach threshold fluorescence, whereas 96-well plates take the least. The qPCR chips may have a higher average cycle number compared to plate and tubes due to the amount of solution added. qPCR chips use 1.2 µL per well whereas 20 µL are added to both other receptacles. Despite being at the same concentration of template copy numbers (10^6), the temperature changes during the qPCR process would affect the smaller amount of solution differently compared to a larger volume. Due to the difference in average cycle number, we can conclude that the use of different qPCR receptacles means that the different values of cycle

threshold numbers are not directly comparable. Due to the normalization of data to a standard control, the different IRIs values can be directly compared to trehalose and the difference in activity observed can then be compared. In addition, all experiments showed statistically relevant enzyme stabilization after freeze drying in the presence of IRIs at certain concentrations. qPCR tube experiments show more statistical relevance compared to the other two receptacle methods. Due to the lid on the tube strip, the possibility of contamination of conditions is significantly reduced and therefore there is more confidence in the results. Lastly, it was observed that trehalose at 292 mM is not the optimal concentration despite being industry standard as 15 mM performs better when comparing average cycle number of tube and plate experiments. This brings us to our next section as we compare the optimal concentration of trehalose.

3.4 Determining Optimal Trehalose Concentration for Protein Thermostability

The observation that 15 mM of trehalose results in a decrease in mean threshold cycle values indicating more effective enzyme stabilization than 292 mM, led to the query of the optimal trehalose concentration. To determine if lower concentrations of trehalose performed better at reducing cycle numbers a variety of concentrations were tested. The concentrations were chosen based on the IRI concentrations tested (between 0.5 mM – 40 mM) in order to directly compare if trehalose at similar concentrations stabilizes enzymes more efficiently. The ability for various concentrations of trehalose to stabilize qPCR enzymes was compared to the trehalose control at 292 mM, in which a decrease in percent mean threshold cycle correlates to increased enzyme stabilization. The results of the comparison of lower concentrations of trehalose shown in figure 3.13 confirmed our initial hypothesis that 292 mM was not the optimal concentration of trehalose during a freeze-drying qPCR experiment.

All tested concentrations of trehalose 40 mM and below reduced the percent mean threshold cycle indicating more effective protein stabilization. With 15 mM causing the lowest reduction to 94.6% (±0.85 SEM) compared to the normalized 100% of 292 mM. This indicates that the current industry standard is not the most effective concentration of trehalose as lower concentrations increase protein thermostability.

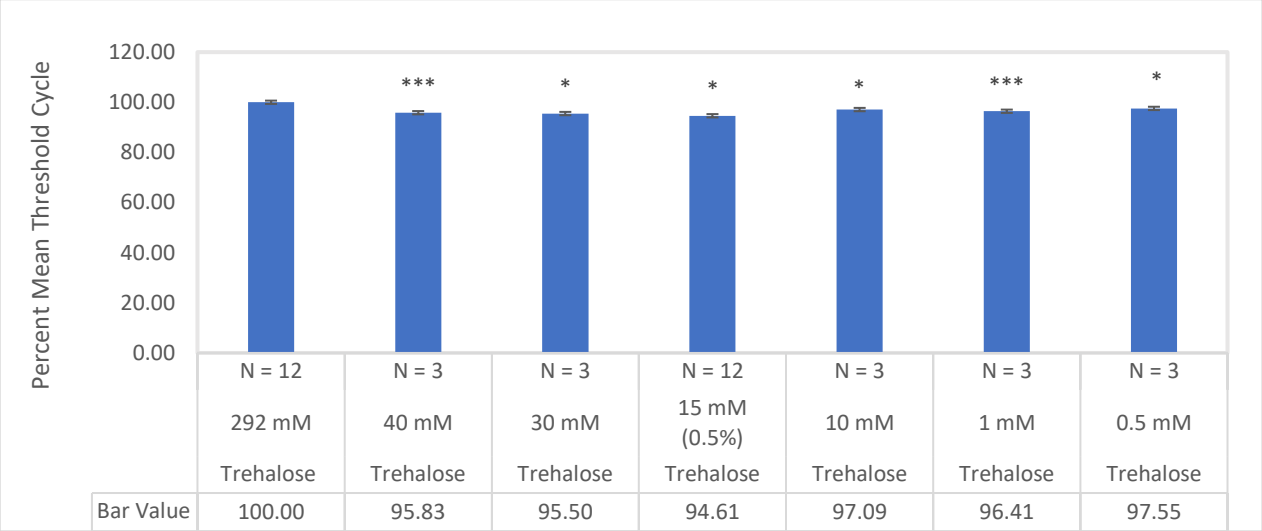

Figure 3.13. Stabilization of RT-qPCR N1 Region Enzymes in the Presence of Varying Concentration of Trehalose. *qPCR enzymes were lyophilized in the presence of trehalose, followed by an RT-qPCR tube experiment. The mean cycle (%) to reach threshold fluorescence was graphed. Error represents SEM, number of technical replicates (N) are indicated above each concentration. *** $P \leq 0.001$, ** $P \leq 0.01$, * $P \leq 0.05$, ns $P > 0.05$.*

3.5 Discussion - Mechanism of Action of Ice Recrystallization Inhibitors to Increase Protein Thermostability

In sections 3.2.1 and 3.2.3, NOGlc (**1**), pBrPhGlc (**9**), 4-MBA (**5**) and 2,6-DFB (**6**) were examined for cryoprotectant ability during freeze-drying. The compounds increased thermostability of the enzymes and oligonucleotides in master mix during the freezing and the lyophilization processes. In these experiments no interference of the qPCR process or decrease in enzyme activity was observed, as all compounds reached a Ct. Therefore, IRIs

did not affect the RNA template or master mix during RT-qPCR as the target gene was detected indicating that amplification occurred. For amplification to occur enzymes and proteins must remain functional. As the IRIs were not supplemented with any lyoprotectant, the compounds must be working in a similar capacity to trehalose which functions as both cryo- and lyoprotectant. This finding is auspicious as PCR is the most prevalent of all molecular tests, and it was shown that IRIs are useful compounds for stabilization of proteins with no seen adverse effects to the RT-qPCR procedure.[12]

However, the target gene plays a role in the effectiveness of the cryo-additives stabilization ability. This was observed in the variance between the N1 region and N2 region results. The N protein contains three dynamic disordered regions, and three independent regions of the SARS-CoV-2 nucleocapsid gene (N1, N2, N3) which where designed by the Centers for Disease Control and Prevention (CDC) for nucleic acid amplification tests.[13,14] In our experiments two of the regions are targeted and because of the difference in each region we hypothesize that the N1 primers interact more effectively with its targeted region. This may indicate that the N2 region is less stable, and the primer does not bind as efficiently compared to the N1 region. Despite this observation both N1 and N2 regions have shown statistically relevant decrease in percent mean threshold cycle number for certain IRI concentrations.

As both our target gene and the qPCR enzymes are proteins, the process of freeze-drying generates both freezing and drying damage which leads to denaturation.[3] Denaturation of the proteins leads to a decrease in protein activity - this would be observed as an increase in cycles to reach threshold during RT-qPCR. To avoid a reduction in enzyme activity trehalose is added to samples, acting as a stabilizer and as a known PCR enhancer.[3]

A concentration of 10% (292 mM) trehalose is commonly used for the stabilization of enzymes.[3] From the data collected, it can be seen that compounds **1**, **5**, **6,** and **9** are effective at stabilizing enzymes during a freeze-dry cycle, evident through the decrease in the number of cycles required to reach threshold fluorescence. All four compounds at their optimal concentrations performed better than 292 mM of trehalose and in some cases 15 mM of trehalose. Compound **9** at 40 mM produced the most effective stabilization as it resulted in the largest reduction of cycles, with a decrease to 67.8% (±5.03 SEM). As mentioned in section 2.6, **9** has been shown to be very cytotoxic at concentrations as low as 10 mM in HepG2 cells.[15] However, **9** is a highly IRI active compound with a IC_{50} of 15 mM which has shown success in increasing post-thaw RBC integrity.[10] Therefore, proteins may be the best application for this compound as it is effective at high concentrations and the toxic effect does not interfere with the protein activity. Using IRIs in protein stabilization may be a way to 'rescue' IRIs which have been previously not viable in cell systems due to cytotoxicity but have cryoprotectant activity.

Small molecule IRIs have shown to be effective cryoprotectants as they modify the size of ice crystals reducing the damage seen during ice recrystallization as mentioned in section 1.7.[3,16] The tested compounds may be acting as IRIs preventing damage to the enzymes caused by ice formation during the freezing process. In addition, these cryoprotectants may potentially be acting as lyoprotectants during the drying steps in lyophilization. In a review by Wang, the mechanism by which surfactants increase thermostability of proteins is outlined; the formation of ice-water interfaces during freezing may cause surface denaturation of proteins.[3] Surfactants may drop surface tension of protein solutions and reduce the driving force of protein adsorption and/or aggregation at these

interfaces.[3] Other stabilization mechanisms were also proposed, including protein binding, which may prevent protein-protein interactions, and aid with protein refolding after thawing.[3] Although those two mechanisms are the main hypothesized, these stabilizers may protect proteins by several other stabilization postulated mechanisms such as replacement of water, formation of a glass, hydrogen bonding, and reduction (instead of elevation) of surface tension.[3] Due to a similar result being seen with the Ben lab's oncolytic virus research, in which the surfactant NOGlc (**1**) produced promising results, the hypothesized mechanism behind the observed qPCR stabilization occurs due to IRIs preventing agglomeration of enzymes in addition to reducing ice recrystallization.[8] Though, further experimentation is required to investigate how the IRIs interact with the proteins during the freezing and drying process.

In addition to mechanism of action, how long the IRIs are effective is an important point of investigation. Proteins in solid state may only have a limited long-term storage stability even after successful lyophilization using a protein stabilizer(s).[3] Storage of protein products after freezing or lyophilization may also lead to denaturation, therefore, for Covid PCR products the current standard is kits must be tested after no longer than 72 hours.[11] A benefit of using trehalose as a stabilizer is that it has been shown to improve the shelf life of therapeutic proteins.[3] One proposed mechanism is that trehalose is able to prevent the oxidation of the proteins during storage by forming a coating around the proteins.[3] In section 3.2.2, shelf-life stabilization at time points of 1-, 3-, 7-, and 14-days were investigated. This experiment was done in order to assess the ability of IRIs in comparison to trehalose to stabilize proteins during storage. The results confirmed that the longer the dried solution is stored the less thermostability of proteins, as there was an increase of cycles to reach

threshold fluorescence. Both compounds **1** and **9**, were able to store the dried mixtures for up to 14 days and are comparable to the stabilization seen with trehalose. At a concentration of 40 mM compound **9** after 1 day of storage was the most effective IRI condition, with 1 mM of **9** having the most effective long-term storage after 14 days. A similar trend was seen with trehalose as the 15 mM trehalose condition was more effective at long term storage than 292 mM. Overall, when using trehalose or IRIs threshold values are reached up to 14 days at room temperature storage, however, increase in shelf storage time decrease the effectivity of the compounds to stabilize the enzymes. IRIs may be working in a similar capacity to prevent the oxidation of the proteins during storage of protein products.

The shelf-life stabilization assay tested both trehalose and IRIs on qPCR plates, whereas other experiments were done on chips or tubes. Due to a variance seen in the results based on qPCR receptacle used, section 3.3 is a comparison of trehalose results to determine if results can be directly compared between receptacles. These results indicated that there is a difference in average cycle number based on the receptacle used. As mentioned, due to the lids on the tube's, contamination is greatly reduced and therefore the most reliable raw data results. In addition, the 15 mM trehalose average cycle number was lower then the 292 mM counterpart for tubes and plates. This led to the hypothesis investigated in section 3.4, that lower concentrations of trehalose stabilize proteins more effectively. The results in figure 3.13 confirmed this, as all tested lower concentrations reduced mean threshold cycle. Further investigation on the optimal trehalose concentration should be performed as all the concentrations tested were below 40 mM leaving a large gap of concentrations between 292 mM and 40 mM to be tested. Due to machine breakdown, contamination, and reproducibility issues all further experiments should be carried out in qPCR tube strips.

In conclusion the observed results confirm our initial hypothesis that compounds **1**, **5**, **6,** and **9** can stabilize proteins after lyophilization. As well, using the IRIs, qPCR enzymes do not lose activity after a freeze-thaw cycle. Additionally, samples which used IRIs as cryoprotectants perform better than trehalose. The compounds tested may also be working as lyoprotectants during the drying process, indicating that the compounds may have further application beyond reducing ice recrystallization during freezing. The benefit to using IRIs in the thermostabilization of proteins is that they are stronger cryoprotectants than trehalose while maintaining lyopotectant and shelf-life storage abilities. Compounds **1** and **9** continue to show success when applied to biological materials, whereas **5** and **6** show new potential as they also successfully stabilized proteins.

3.6 References

1 Soderstrom, K. Physical Chemical Properties of Viruses. *Reference Module in Biomedical Sciences*, 1-4, doi:https://doi.org/10.1016/B978-0-12-801238-3.05232-6 (2014).

2 Franks, F. Freeze-drying of bioproducts: putting principles into practice. *European Journal of Pharmaceutics and Biopharmaceutics* **45**, 221-229, doi:10.1016/s0939-6411(98)00004-6 (1998).

3 Wang, W. Lyophilization and development of solid protein pharmaceuticals. *International Journal of Pharmaceutics* **203**, 1-60, doi:10.1016/s0378-5173(00)00423-3 (2000).

4 Olsson, C. J., Helén; Swenson, Jan. The Role of Trehalose for the Stabilization of Proteins. *The Journal of Physical Chemistry B* **120**, 4723-4731, doi:https://doi.org/10.1021/acs.jpcb.6b02517 (2016).

5 Jain, N. K. & Roy, I. Effect of trehalose on protein structure. *Protein Science*, NA-NA, doi:10.1002/pro.3 (2008).

6 Takekiyo, T., Ishikawa, Y., & Yoshimura, Y. Cryopreservation of Proteins Using Ionic Liquids: A Case Study of Cytochrome c. *The Journal of Physical Chemistry B* **121**, 7614-7620, doi:10.1021/acs.jpcb.7b05158 (2017).

7 Benson, E. E.15-32 (Springer New York, 2008).

8 Ghobadloo, S. M. *et al.* Carbohydrate-Based Ice Recrystallization Inhibitors Increase Infectivity and Thermostability of Viral Vectors. *Scientific Reports* **4**, doi:10.1038/srep05903 (2015).

9 Balcerzak, A. K., Capicciotti, C. J., Briard, J. G. & Ben, R. N. Designing ice recrystallization inhibitors: from antifreeze (glyco)proteins to small molecules. *RSC Adv.* **4**, 42682-42696, doi:10.1039/c4ra06893a (2014).

10 Poisson, J. S., Acker, J. P., Briard, J. G., Meyer, J. E. & Ben, R. N. Modulating Intracellular Ice Growth with Cell-Permeating Small-Molecule Ice Recrystallization Inhibitors. *Langmuir* **35**, 7452-7458, doi:10.1021/acs.langmuir.8b02126 (2019).

11 Ontario, P. H. *Coronavirus Disease 2019 (COVID-19) – PCR*, www.publichealthontario.ca (2022).

12 Ontario, P. H. An Overview of Cycle Threshold Values and their Role in SARS-CoV-2 Real-Time PCR Test Interpretation., 1-14 (2020).

13 Babiker, A., Myers, C. W., Hill, C. E. & Guarner, J. SARS-CoV-2 Testing. *American Journal of Clinical Pathology* **153**, 706-708, doi:10.1093/ajcp/aqaa052 (2020).

14 Cubuk, J. *et al.* The SARS-CoV-2 nucleocapsid protein is dynamic, disordered, and phase separates with RNA. *Nature Communications* **12**, doi:10.1038/s41467-021-21953-3 (2021).

15 Poisson, J. S. *Synthesis and In Vitro Applications of Ice Recrystallization Inhibitors* Doctorate in Philosophy degree in Chemistry thesis, University of Ottawa, (2019).

16 Chaytor, J. L. *et al.* Inhibiting ice recrystallization and optimization of cell viability after cryopreservation. *Glycobiology* **22**, 123-133, doi:10.1093/glycob/cwr115 (2012).

Chapter 4: Evaluating the Ability of Small Molecule Ice Recrystallization Inhibitors to Increase Post-thaw Viability of Tissues and Tissue Components

4.1 Introduction

The largest organ in the body, the skin, is a complex tissue that contains various types of specialised cells and serves a variety of purposes, including acting as a physical barrier, immunological, and sensory functions.[1,2] The epidermis, the skin's outermost layer, is primarily formed of keratinocytes and contains several stem cells (i.e. epidermal and hair follicle stem cells).[1] The dermis contains a large number of fibroblasts, which are involved in a variety of skin homeostasis processes, the most crucial of which is the production of the extracellular matrix.[1,3] The skin is also highly vascularized and innervated, providing solutes to interact with other organs.[1] Skin homeostasis is influenced by each of these elements as well as many more that have not been mentioned (figure 4.1).[1]

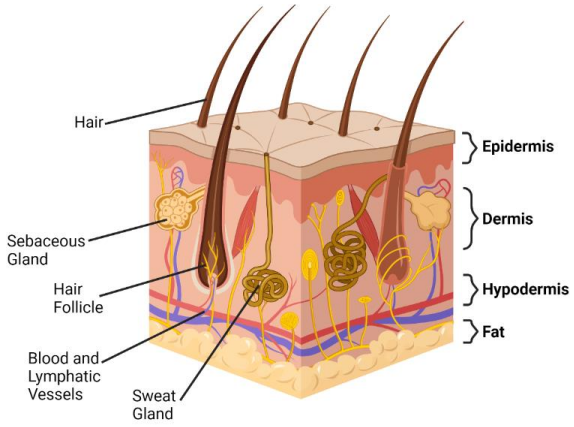

Figure 4.1. Main Components of Human Skin. *Figure adapted using BioRender ©.*[4]

Due to the size and complexity of skin, skin injuries are a major issue with severe injuries resulting in death. Burns are one of the main factors that cause skin damage.[2] Thermal injuries affect more than 1 million persons annually in the United States alone.[5] Of

these, approximately 100,000 are hospitalised and 10,000 patients die.[5] The loss of the barrier that protects the skin and sepsis, which is caused by bacteria entering the body causing an extreme immune reaction, are two factors that contribute to the morbidity and mortality linked to these injuries.[5] Rapid covering of burn wounds utilizing the early excision and grafting procedure is used to minimise damage.[5] Human cultured epidermal cell sheets, both autologous and allogeneic, have been used successfully to cover these wounds.[5]

In order to prevent immunological rejection, restore skin function, and promote wound healing following skin damage, autologous grafts taken directly from the patient are frequently employed.[2] Unfortunately, autologous grafts do not provide adequate healing for wounds that are deep or cover broad areas, as there is a limited amount of skin you can take from the same patient.[2] If there is insufficient autologous skin, allogeneic skin grafts from living donors are thought to be the best alternative as allografts avoid pain and risk of infection from frequent dressing changes; nevertheless, due to their restricted availability, they are rarely used.[6,7] For allografts, keratinocytes and fibroblasts must be cultured for 21 days, and burn patients must tolerate this time in good general health.[6] Allogeneic skin rejection often occurs three to four weeks following the graft.[6] Therefore, major complications persist even though skin grafting is the primary technique for rebuilding full-thickness burns and wound infections.[8] The high total body surface area burn patient, who deserves an elastic, mobile, esthetically pleasing, and robust outcome instead receives the worst prognosis due to a lack of donor sites.[9] This necessitates the development of skin substitutes employing novel methods for skin regeneration.[2]

The development of skin substitutes over time has progressed from simple cultured autologous epidermal sheets to more intricate bilayered cutaneous substitutes.[10] With the

advancement of technology, it may soon be possible to create full-thickness skin constructs that imitate physiological functions by including different skin components, such as the vasculature.[1] It has proven challenging to mimic the skin of a person as nerve endings, capillaries, multi-layered 3D structures, and the countless derivative structures, such as sebaceous glands, sweat glands, and hair follicles must be accommodated.[2] Advances in induced pluripotent stem cell (iPSC) technology and microfabrication methods like 3D printing have made it possible to create more accurate and sophisticated *in-vitro* skin models.[1] 3D bioprinting makes it possible to create replicas of the human skin structure by spatiotemporally patterning different bio-inks and cells.[2]

However, engineering epidermal grafts takes time, similar to allogeneic grafts, as several weeks are needed for cell multiplication to produce a transplantable graft.[11] This delayed timeline make applying these grafts more difficult in vital situations, such as after serious burns or trauma.[11] Thus, the need for quickly accessible tissue structures is critical in order to enhance outcomes. To provide an available supply that can fulfil clinical needs, tissue "banks" of ready-to-use grafts must be developed.[5,11] This would necessitate the use of an effective cryopreservation method that can hold a variety of tissue grafts for several months and be usable immediately after thawing.[11] Current methods of tissue cryopreservation have reduced viability due to previously mentioned cryoinjury. Living cells are not required for all tissue grafts, such as alloplastic grafts or acellular dermal matrices, and suitable preservation techniques are frequently available.[12] Other tissues require living, active cells, such as skin which is generally more immunogenic and less advanced preservation techniques are available.[12,13] Optimised storage techniques must be created in order to facilitate these items in the clinic.[11]

The difficulties in tissue cryopreservation are typically not brought on by the challenges of preserving the living cells, but rather by the characteristics of the integrated cell/matrix systems which tissue function depends upon.[12] Methods of cryopreservation were initially developed for isolated cells (although there are still associated cryoinjuries which effect viability).[14] Each type of cell has a certain set of conditions that are ideal for cryopreservation, as was discussed in section 2.1.[14] However, tissues are intricate multicellular systems made up of various cell types that have different requirements for the best possible preservation.[14] All cell types inside a tissue will experience the identical cooling and thawing parameters during the cryopreservation process.[14] Cell-to-cell and cell-to-matrix interactions, temperature and solute gradients, and the constrained flow of water across cell membranes are additional factors that affect cells within a tissue and may exacerbate freezing injury.[14] When tissues are cryopreserved, extracellular ice, which is mostly harmless to a cell suspension, is present within the matrix and can cause structural disruption.[14] Consequently, densely packed cells within a tissue are more likely to be harmed by cryopreservation-induced mechanical stresses than are dilute cell suspensions due to this matrix effect that can be observed in complex rigid matrices.[14,15]

One way to reduce matrix effect is to increase cryoprotectant concentrations as the two are inversely related because thicker sheets present penetration problems.[5,15] Higher concentrations are an issue as the current approach of tissue cryopreservation uses low doses of DMSO (~2-10%), which already results in a low survival rate due to DMSO being highly toxic.[11,14] Therefore, for all tissue cells and sheets two major problems still need to be overcome, cryoprotectant cytotoxicity and recrystallization during rewarming.[12] This work is carried out in collaboration with Dr. Moulin's Laval group as outline in the statement of

contribution. Our groups hypothesize that IRIs will be able to address these concerns increasing the post-thaw viability of a variety of tissue products by reducing damage associated with cryopreservation while being less toxic than current cryo-additives. The goal of this chapter is to use a ground up approach to assess the ability of six IRIs (figure 4.2), synthesized by the Ben lab, to cryopreserve *in-vitro* tissue constructs using simplified tissue models of different thicknesses cultured by the Laval Lab.

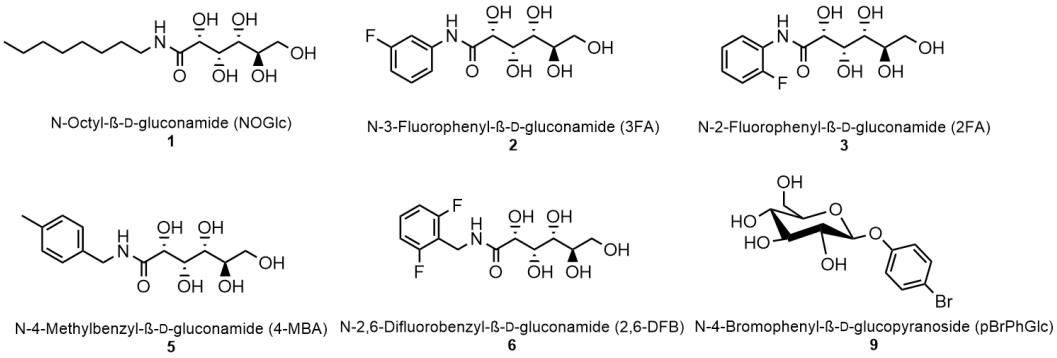

Figure 4.2. Structures of Ice Recrystallization Inhibitors (IRIs) that will be Evaluated.

4.2 Optimal Cooling Rate and Post-Thaw Viability of Autologous Dermal Sheets

Optimal cooling rate, which is dependent on the water permeability of the cell membrane and the surface area to volume ratio of the cell, differs between cell types.[14] Mazur's inverted "U" theory, mentioned in section 1.6, describes the phenomenon which can be summarized as: slow cooling rates results in cryoinjury via the solution effects and high cooling rates leads to cryoinjury due to lethal IIF.[16] For the majority of cell-types, any significant quantity of intracellular ice is lethal but as mentioned the more complex a tissue the more lethal both extracellular and intracellular ice.[15] Cellular damage of this nature accounts for 75-85% of the cellular injury/death associated with cryopreservation.[17] A freezing rate of 1 °C/minute has been previously utilized for cryopreservation of vascular tissues.[14] Thus, preliminary testing was performed on cryosettes at a cooling rate of 1 °C/min

in a rate controlled freezer, to test the effect of freezing on autologous dermal sheet samples. Autologous dermal sheets were cultured in 1.5% Bovine Serum Albumin (BSA) or 90% FBS (serum), both conditions were supplemented with 10% DMSO as a cryoprotectant. Figure 4.3 confirmed that a cooling rate of 1 °C/min on BSA and serum cryosettes could be achieved. The effect of the cooling rate on BSA and serum samples were then assessed in two biological replicates as both a cooling rate of 1 °C/min and viability assays have been extensively reported on in the literature.

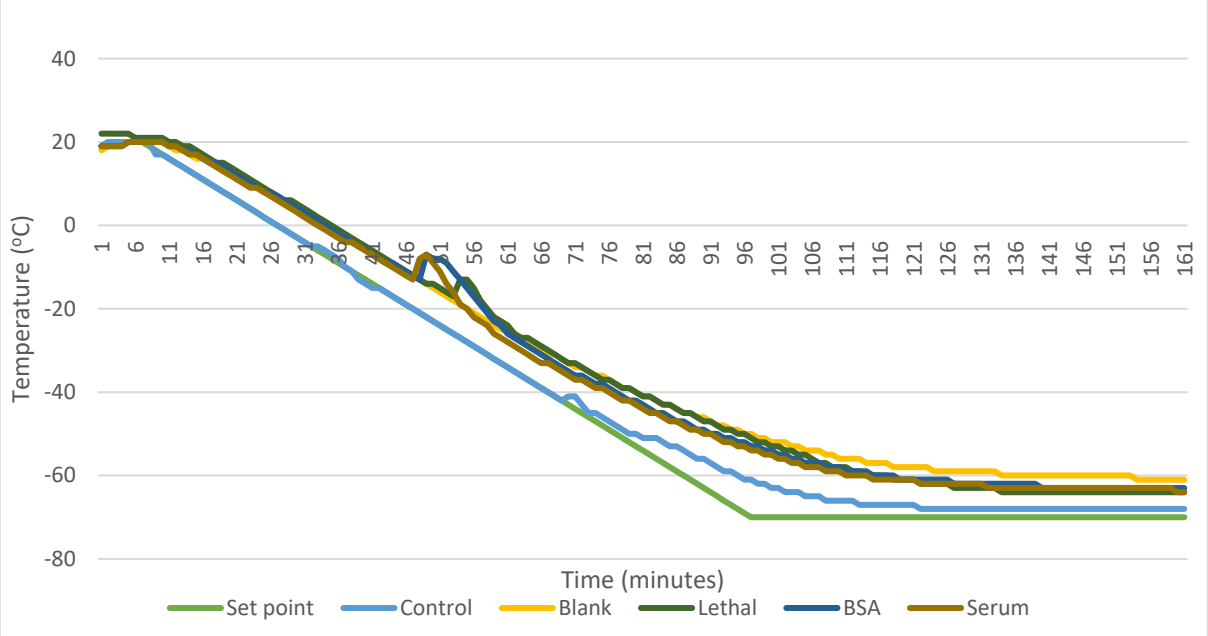

Figure 4.3. Temperature of Cryosette Samples in a 1 °C/min Rate Controlled Freezer. *Cooling rates of controls, serum dermal sheet sample, and BSA dermal sheet sample following approximately a -1 °C/min cooling rate. This experiment was done from RT to -160 °C. The set point indicates the desired cooling rate curve. N = 2*

Following the freeze-thaw process, samples were stained using SYTOX Green a DNA staining assay that quantifies mortality through visualization of the mortality distribution within the tissue images (figure 4.4). SYTOX Green is a high-affinity nucleic acid stain which only penetrates cells with compromised plasma membranes, therefore, it is an indicator of dead cells within a population.[18] In addition, post-thaw viability was determined using an AlamarBlue™ viability assay. This is a colorimetric assay that measures

cellular metabolic activity as a means of indirectly assessing cell viability within the tissues.[19] SYTOX Green mortality assays were performed in conjunction with AlamarBlue™ viability assay throughout this chapter, as the mortality assay considers the amount of nonviable cells before cryopreservation providing us with the overall recovery of cells. Fluorescence of BSA and serum samples were compared to three controls: a heated lethal sample, a blank, and a non-frozen control (as described in section 6.3). The % post-thaw viability of the autologous dermal sheets was then calculated and presented in table 4.1. The results show a decrease in viability of 73.5% and 62.6% for BSA and serum cultured dermal sheets, respectively. This large decrease in viable cells displays the need for better cryopreservation protocols as more than half of the cells in the samples are non-functional following freezing. The majority of damage causing the decrease of cell viability can be attributed to ice recrystallization during cooling and thawing of the samples.[15] Therefore, in order to increase the post-thaw viability, the following sections will investigate the ability of IRI supplemented tissue products (cell suspension and autologous dermal sheets) to increase post-thaw viability.

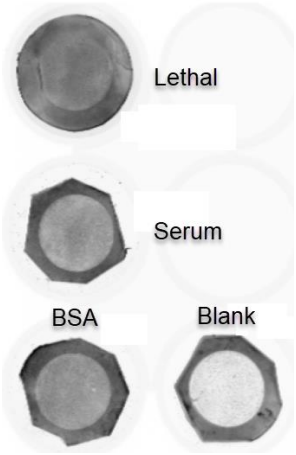

Figure 4.4. Images of Tissue Samples in Cryosettes Under Different Conditions Post-Thaw Using SYTOX Green Staining.

Table 4.1. Post-thaw Percent Viability of Autologous Dermal Sheets Samples. *Post-thaw % viability of autologous dermal sheets following a AlamarBlue™ viability assay. A comparison of the % viability of 1.5% BSA-10% DMSO sample, 90% Serum-10% DMSO sample, a blank, a negative control lethal sample, and an unfrozen positive control (CTRL). N = 2*

Treatment	CTRL	BSA	Serum	Lethal	Blank
% Viability	100	26.5	37.42	1.1	0.98

4.3 Assessing the Ability and Cytotoxicity of Current Tissue Media Additives in the Cryopreservation of Tissue Components

The most common method of cryopreservation of fibroblasts and autologous dermal sheets includes culturing the cells in BSA or serum supplemented with 10% DMSO.[20] Serum which is composed of various nutrients (e.g., amino acids, nucleotides, and sugar), growth factors, adhesion factors, minerals, proteins, lipids, and hormones, is a culture media additive to help cell proliferation and growth.[20,21] Serum is not a cryoprotectant, whereas BSA can help protect cells during the freezing process as it contains proteins which help dehydrate the cells and stabilize the membrane while acting as antioxidants.[21] In addition, BSA and serum are potential sources of biological contamination, increasing the probability of animal health problems such as bovine spongiform encephalopathy (BSE), disease transmission, and viral infections.[21] As well, DMSO is a highly toxic cryo-additive that can decrease cell survival at high concentrations.[20,21] Due to these issues, BSA, serum, and DMSO are often removed through a lengthy washing process post-thaw.[20,21] However, the removal of DMSO from solution does not prevent all side effects after the cells have been thawed as it is a permeating cryoprotectant. The effects of BSA, serum, and DMSO on dermal tissue sheets post-thaw must be investigated to determine cytotoxicity that these products may have on a tissue matrix.

The best cryopreservation protocol for each type of tissue can be determined through cryopreservation trials.[22] These protocols' enables the selection of parameters appropriate for the cryopreservation of 3D models, enabling the development of the perfect mixture of cryo-additives for each organ and its constituent tissues and cells.[22] Therefore, each trial in the following sections has been tested on cells in differing structural complexity (cell suspension & dermal sheets). Testing will initially be done in cell suspension as obvious toxic effects can be more easily identify in the simpler constituent.

4.3.1 Determining Effects of Culture Media Additives in the Cryopreservation of Cell Suspension

In order to determine the effects of BSA and serum on fibroblast recovery post-thaw, the cells were cryopreserved in BSA, or serum supplemented with 10% DMSO. Immediately following thawing a SYTOX Green mortality assay was performed on the cell suspension to quantify mortality of the cells, seen in panel A of figure 4.5. The % mortality of the BSA sample has a value of 5.6% (±1.4 SD), whereas the serum sample had 7.3% (±2.0 SD) mortality, indicating a 1.7% (±1.2 SD) decrease in mortality using BSA. In addition, cell proliferation was investigated via Trypan blue staining and cell counts. Proliferation was investigated 96 hours post-thaw, to ensure cells are back to regular metabolism prior to the assay.[23] This assay determines any long-term negative effects the additive may have on cell growth. The results of the number of fibroblasts per well 96 hours after a freeze-thaw cycle are shown in panel B of figure 4.5. For all replicates tested, serum promotes better cell proliferation than BSA. BSA may have a better % mortality as the proteins increase BSA's ability to reduce damage associated with cryopreservation, whereas serum has better cell proliferation as the nutrients in the serum help the cells grow post-thaw. Therefore, in cell

suspension BSA should be the media supplement with IRIs in further testing for the best possible reduction of cryoinjury.

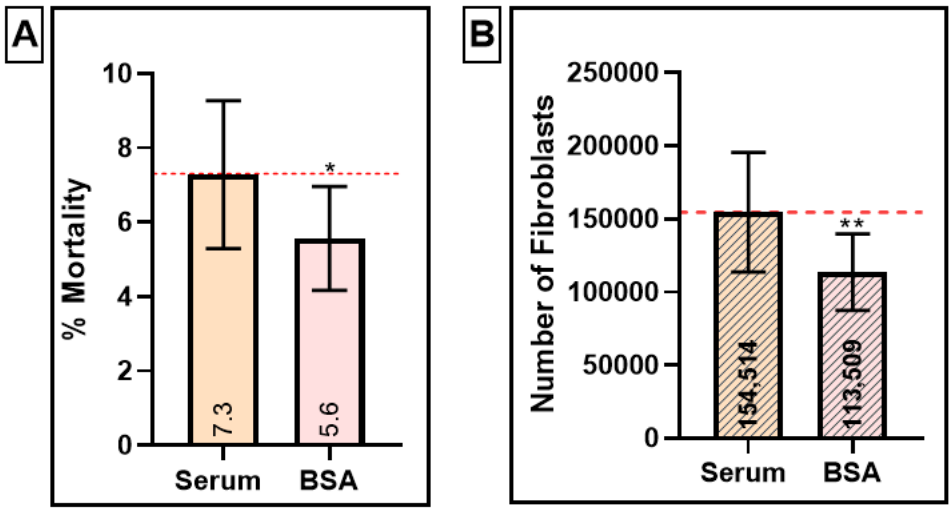

Figure 4.5. Post-Thaw Mortality and Proliferation of Fibroblast Cell Suspension. *A) SYTOX Green post-thaw mortality of fibroblasts cryopreserved in BSA or serum. B) Trypan Blue post-thaw cell proliferation after 96 hours incubation of fibroblasts cryopreserved in BSA or serum. Error represents SD, n = 4, N = 3. T-test, **** P ≤ 0.0001, *** P ≤ 0.001, ** P ≤ 0.01, * P ≤ 0.05.*

To determine the toxic effect of DMSO on fibroblasts cell suspension, three different donors (replicates) were tested for 96 hours post-thaw cell mortality. A time dependent lethality assay was performed on fibroblast cells which were incubated at room temperature in 10% DMSO preceding cryopreservation. The % mortality of the cells was assessed at incubation time points of 0, 20, 40, 60, and 80 minutes. The results of the post-thaw mortality can be seen in panel A of figure 4.6. No discernible difference in mortality was seen for the three donors examined below a threshold of 60 minutes. The percentage of mortality in the three replicates does, however, significantly increase at 80 minutes compared to 0 minutes, increasing by 81.3% (±2.6 SD). In addition, for the second replicate 96 hours post-thaw proliferation was evaluated for each time point, shown in panel B of figure 4.6. As expected, as time increases the number of fibroblasts per well decreases with a significant decrease in cells at 80 minutes in comparison to no incubation in DMSO preceding

cryopreservation. The results indicate that cells can be incubated in DMSO for up to 60 minutes without increasing the amount of damage caused by the cryo-additive.

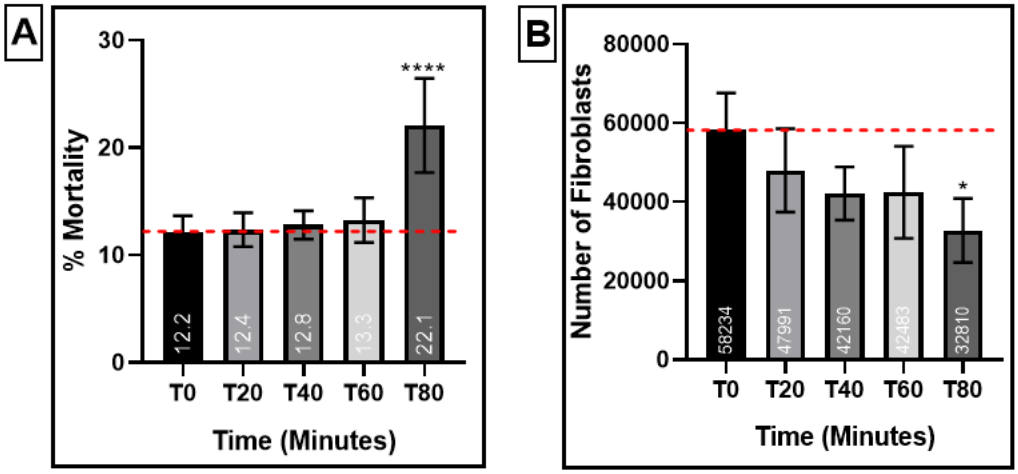

Figure 4.6. Post-Thaw Mortality and Proliferation of Fibroblast Cell Suspension Incubated in DMSO. *A) SYTOX Green post-thaw % mortality of fibroblasts incubated in DMSO at time points of 0, 20, 40, 60, and 80 minutes. B) Trypan Blue post-thaw cell proliferation of time points of 0, 20, 40, 60, and 80 minutes after 96 hours post-thaw of fibroblasts cryopreserved in DMSO. Error represents SD, n = 4, N = 1. 1-way Anova, **** $P \leq 0.0001$, *** $P \leq 0.001$, ** $P \leq 0.01$, * $P \leq 0.05$.*

4.3.2 Determining Effects of Culture Media additives in the Cryopreservation of Autologous Dermal Sheets

The next experiments assessed the effects of BSA and serum on single dermal sheets viability post-thaw. Dermal sheets followed the same protocol as cell suspension and were cryopreserved in BSA or serum supplemented with 10% DMSO. An AlamarBlue™ viability assay was performed on the dermal sheets 96 hours post-thaw, to ensure cells are back to regular metabolism. This assay quantifies metabolic activity of cells within the tissue, seen in figure 4.7. BSA appears to have better post-thaw tissue viability than serum, with a statistically relevant difference of 5.5% viability (±1.9 SD). Due to similar results in section 4.2, the immediate post-thaw mortality increase seen in section 4.3.1 and better post-thaw

viability of dermal sheets for BSA, it was determined that BSA will be the control to test our IRIs against. Therefore, in the following sections serum was no longer used as a control.

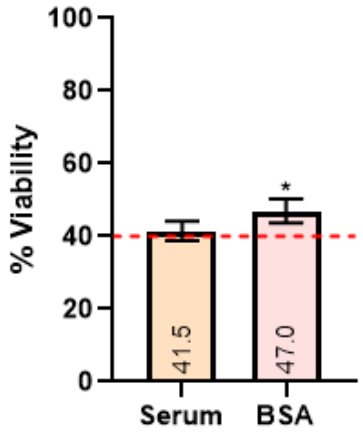

Figure 4.7. Post-Thaw Viability of Autologous Dermal Sheets. *Post-thaw viability determined through an AlamarBlue™ viability assay of dermal sheets cryopreserved in BSA or serum. Error represents SD, n = 4, N = 1. T-test, **** P ≤ 0.0001, *** P ≤ 0.001, ** P ≤ 0.01, * P ≤ 0.05.*

Lastly, to determine the toxic effect of DMSO on single dermal sheets, a time dependent viability assay was performed on the tissues which were incubated at room temperature in 10% DMSO preceding cryopreservation. An AlamarBlue™ viability assay was performed on the dermal sheets and the % viability of the dermal sheets were assessed at incubation time points of 0, 20, 40, 60, and 80 minutes. The results of the % post-thaw viability can be seen in figure 4.8. No discernible difference in viability was seen. The increasing viability drift up to 60 minutes was not significant which is followed by an expected decrease at 80 minutes. The results indicate that dermal sheets can be incubated in DMSO for up to 80 minutes without decreasing the viability of the cells within the tissue.

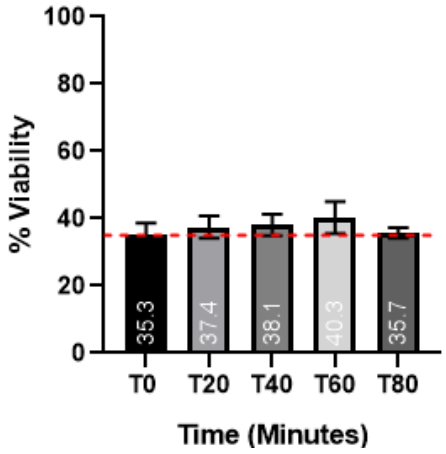

Figure 4.8. Post-Thaw Viability of Autologous Dermal Sheets Incubated in DMSO. *Post-thaw % viability of dermal sheets incubated in DMSO at time points of 0, 20, 40, 60, and 80 minutes then cryopreserved. Post-thaw viability determined through an AlamarBlue™ viability assay. Error represents SD, n = 4, N = 1. 1-way Anova, P-value <0.05.*

4.4 Assessing the Ability of Small Molecule Ice Recrystallization Inhibitors to Cryopreserve Tissue Components

It is possible to reach the optimal conditions for the cryopreservation of a homogeneous cell population or a one cell-layer tissue, however the percentage of initial cells is greatly reduced by damage associated with freezing.[22] As tissues increase in complexity successful cryopreservation of the composite becomes more diffcult.[22] During cryopreservation, the transition of liquid to a solid state during freezing is a concern as the proportion of liquid in biological tissues may reach 70% of the volume.[22] The solid state ice after freezing within the cells and tissues matrix is the reason that cells are irreparably damaged, caused by the uncontrolled growth (recrystallization) of ice during freezing and thawing.[17] Conventional cryoprotectant solutions, such as DMSO, fail to prevent this form of injury thus improved cryopreservation approaches are urgently required.[24] As previously mentioned, DMSO is cytotoxic causing disruption of intracellular signaling reducing post-thaw recovery.[11] Thus, it is fundamental that the cryopreserving agents used be adapted and specific to the tissue to reduce risks of direct cellular toxicity.[22]

Therefore, the goal is to investigate a variety of IRIs that inhibit extracellular (and in some cases intracellular) ice recrystallization thereby mitigating the cellular damage associated with cryopreservation. Preventing cryoinjury from the uncontrolled growth of ice during freezing and thawing would enable the successful long-term storage and transport of these constructs prior to transplant. Given that ice recrystallization figures prominently in cryoinjury, IRIs are uniquely positioned to improve cryopreservation outcomes, as IRI technology has been shown to improve cryopreservation in a number of aforestated cellular systems.[25-29] Very little is known about the cytotoxicity in fibroblasts of the carbohydrate-based IRIs proposed in this study. Consequently, we will investigate the cytotoxic nature of the IRIs over a wide range of concentrations above and below the IC_{50} values. Given that increased recovery post-cryopreservation is a delicate balance between concentration of adjuvant, cytotoxicity, and cryopreservation abilities, this specific aim will provide useful data towards optimization of conditions for further *in-vitro* studies. In the following sections due to the beneficial effects of inhibition of ice recrystallization the IRIs; NOGlc (**1**), 3FA (**2**), 2FA (**3**), 4-MBA (**5**), 2,6-DFB (**6**), and pBrPhGlc (**9**), will be tested in fibroblasts and dermal sheets. This investigation is undergone with the objective of increasing the post-thaw recovery by reducing nucleation or freezing damage after a freeze-thaw cycle.

4.4.1 Assessing the Ability of Ice recrystallization Inhibitors to Cryopreserve Fibroblast Cell Suspension

To determine if IRIs are effective as cryoprotectants initial testing was performed using compounds **1**, **3**, or **9** supplemented cell media in fibroblasts cell suspension, to investigate cell mortality and post-thaw cell proliferation. 96 hours following thawing a SYTOX Green mortality assay was performed on the cell suspension to quantify mortality of

the cells, seen in panel A of figure 4.9. The results indicate that each class of IRI performs differently during cryopreservation of fibroblasts. These results are expected as previous results have indicated that IRIs do not work in every system, for example **9** has been toxic in HepG2 cells but successful in RBCs.[28,30] All concentrations of **3** were not effective at decreasing cell mortality compared to BSA. Whereas 0.01 mM, 0.1 mM, and 1 mM of **1** all significantly decreased % mortality, with the most effective concentration of 1 mM decreasing up to 12% (±1.6 SD) compared to BSA. Lastly, 15 mM and 40 mM of **9** significantly increased post-thaw mortality indicating cytotoxic effect. In addition to post-thaw mortality, cell proliferation was investigated via Trypan blue staining and cell counts. Proliferation was investigated 96 hours post-thaw to assure regular metabolism before the mortality assay, to determine any delayed cytotoxic effects the IRIs may have on cells. The results of the number of fibroblasts per well 96 hours after a freeze-thaw cycle are shown in panel B of figure 4.9. Similar results as the mortality were observed with no change in cell growth using **3**, a significant increase in cell proliferation with **1**, and a significant decrease in proliferation with **9** compared to BSA. For both 15 mM and 40 mM of **9** more than 90% of cells were dead indicating that compound **9** has a significant toxic effect on fibroblasts.

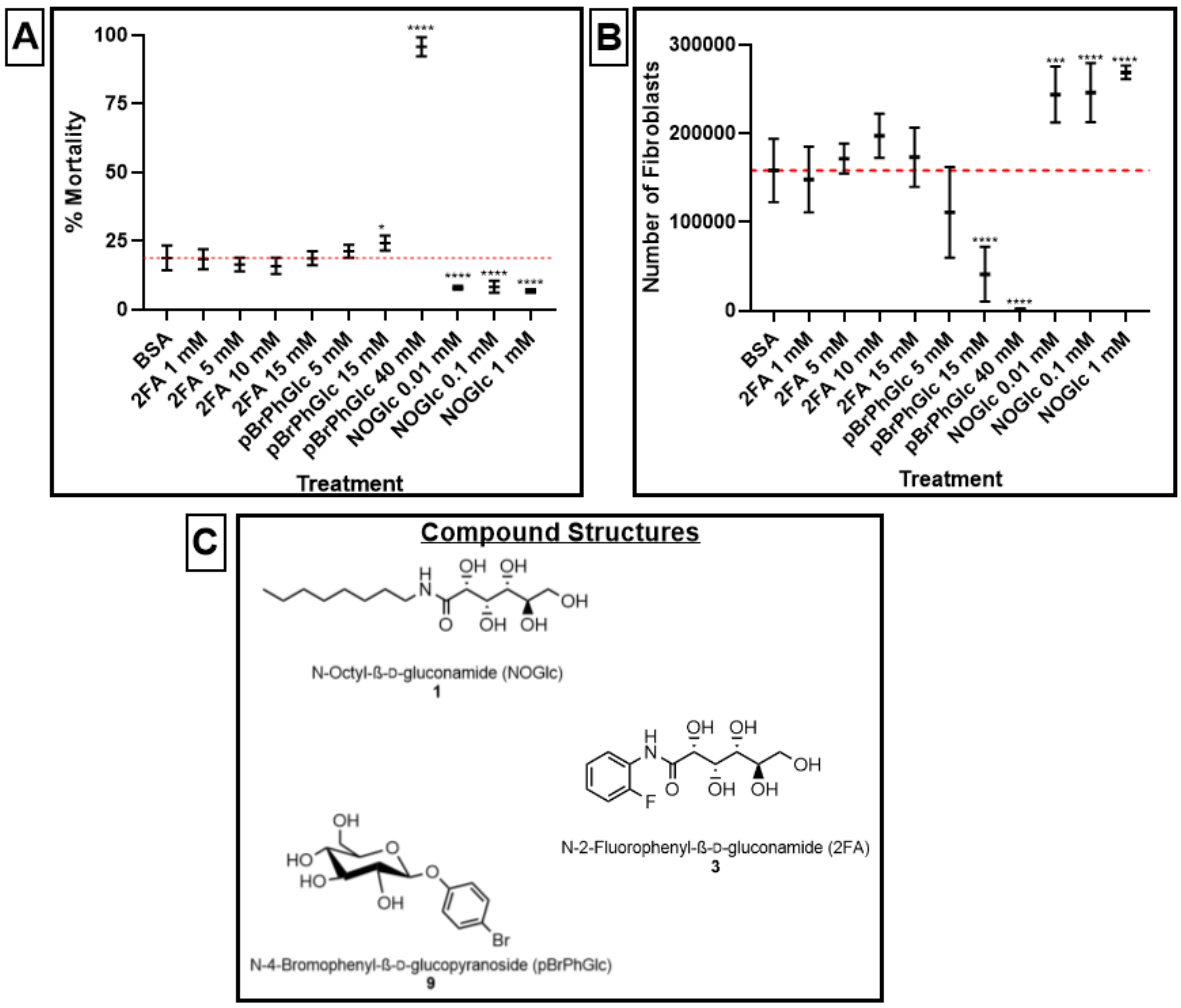

Figure 4.9. Post-Thaw Mortality and Proliferation of Fibroblast Cell Suspension Following IRIs Supplementation. *A) Post-thaw mortality determined through a SYTOX Green mortality assay of fibroblasts cryopreserved in IRI supplemented cell media. The IRIs 2FA (**3**), pBrPhGlc (**9**), and NOGlc (**1**) were tested at various concentrations and compared to a control of BSA. B) Post-thaw proliferation determined through Trypan blue staining and cell counts of fibroblasts cryopreserved in IRI supplemented cell media. The IRIs 2FA (**3**), pBrPhGlc (**9**), and NOGlc (**1**) were tested at various concentrations and compared to a control of BSA.* C) Compound structures and numbers. *Error represents SD, n = 3, N = 2. 1-way Anova, **** P ≤ 0.0001, *** P ≤ 0.001, ** P ≤ 0.01, * P ≤ 0.05.*

As each class of IRI performed differently, further testing to determine how 3FA (**2**), 4-MBA (**5**) and 2,6-DFB (**6**) would perform as cryoprotectants was investigated. IRI supplemented cell media in fibroblasts cell suspension was used to investigate immediate cell mortality using a SYTOX Green mortality assay. The results seen in figure 4.10, indicate that both **2** and **6** were not effective at decreasing cell mortality compared to BSA. However, 1 mM and 5 mM of **5** significantly decreased % mortality, with the most effective

concentration of 1 mM decreasing up to 7.8% (±2.4 SD) compared to BSA. Proliferation was investigated 96 hours post-thaw and the results of the number of fibroblasts per well 96 hours after a freeze-thaw cycle are shown in panel B of figure 4.10. A significant increase in cell proliferation with **5** at 5 mM and **6** at 5 mM and 30 mM compared to BSA was observed.

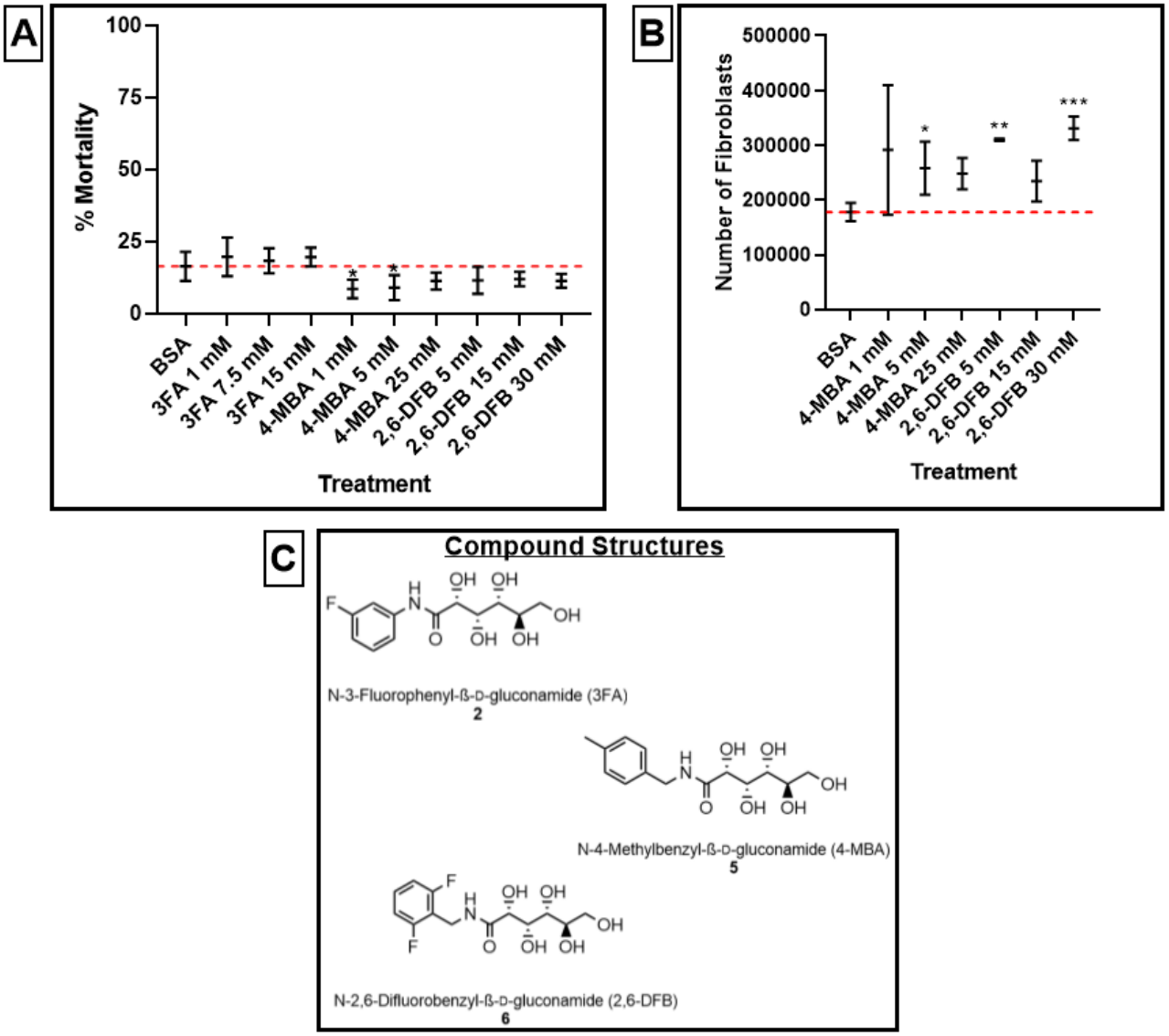

Figure 4.10. Post-Thaw Mortality of Fibroblast Cell Suspension Following IRIs Supplementation. *Post-thaw % mortality determined through a SYTOX Green mortality assay of fibroblasts cryopreserved in IRI supplemented cell media. The IRIs 3FA (**2**), 4-MBA (**5**), and 2,6-DFB (**6**) were tested at various concentrations and compared to a control of BSA. n = 3, N = 2. B) Post-thaw proliferation determined through Trypan blue staining and cell counts of fibroblasts cryopreserved in IRI supplemented cell media. The IRIs 4-MBA (**5**) and 2,6-DFB (**6**) were tested at various concentrations and compared to a control of BSA. n = 3, N = 1.* C) Compound structures and numbers. *Error represents SD, 1-way Anova. **** P ≤ 0.0001, *** P ≤ 0.001, ** P ≤ 0.01, * P ≤ 0.05.*

4.4.2 Assessing the Ability of Ice recrystallization Inhibitors to Cryopreserve Autologous Dermal Sheets

The next stage of testing was to evaluate the ability of IRIs to cryoprotect single layer autologous dermal sheets. The compounds used in further testing were NOGlc (**1**), 4-MBA (**5**), and 2,6-DFB (**6**). Both **1** and **5** showed a significant reduction of damage observed in fibroblast cell suspension post-thaw. However, **6** did not show significance despite reducing the % mortality, this compound was chosen to continue testing to assess if cell suspension and dermal sheets produce contrasting results. Both % viability and % mortality were investigated for the dermal sheets after cryopreservation with IRI supplemented cell media. % Viability was conducted using an AlamarBlue™ viability assay to quantify metabolic activity of cells within the tissue and % mortality was conducted using SYTOX Green to quantify mortality distribution within the tissues. Figure 4.11 shows the results of % viability and % mortality of each NOGlc (**1**) donor tested. Viability of the dermal sheets, shown in panels A-C, was increased at 0.01 mM by 20.4% (±2.9 SD) in the first replicate, by 33.6% (±2.6 SD) at 0.1 mM and by 22.9% (±2.0 SD) at 1 mM in the second replicate. However, a decrease in viability in the third replicate of 26.7% (±1.2 SD) at 0.01 mM was observed. It should be noted that the control for the third replicate was particularly high which may contribute to the decrease observed with **1**. For mortality of the dermal sheets, seen in panels a-c, a decrease of 13.6% (±2.6 SD) at 0.01 mM and of 10.3% (±2.3 SD) at 1 mM was observed for the first replicate. Figure 4.12 shows the results of % viability and % mortality of each 4-MBA (**5**) donor tested. Viability of the dermal sheets, seen in panels A-C, was increased at 5 mM by 27.7% (±2.6 SD) and by 22.0% (±2.8 SD) at 25 mM for the first replicate. The second replicate saw a viability increase by 29.7% (±3.2 SD) at 1 mM. For

mortality of the dermal sheets, shown in panels a-c, supplemented with compound **5**, a decrease of 16.8% (±3.9 SD) at 25 mM and 8.5% (±1.3 SD) at 5 mM was observed with the first and third replicate respectively. Figure 4.13 shows the results of % viability and % mortality of each 2,6-DFB (**6**) donor tested. Viability of the dermal sheets, shown in A-C, was increased at 5 mM by 14.3% (±2.9 SD) and by 21.7% (±3.1 SD) at 15 mM for the first replicate. 30 mM showed a significant increase in viability of 14.7% (±2.1 SD) and 16.4% (±2.2 SD) with the second and third replicate respectively. For mortality of the dermal sheets supplemented with **6**, seen in a-c, only 5 mM for the second replicate shows a significant decrease of 15.8% (±2.7 SD). Overall, **5** has the most significant reduction of mortality and **1** the most significant increase of viability in dermal sheets. Although, each IRI tested in dermal sheets at certain concentrations shows a reduction in freeze associated damage compared to dermal sheets not supplemented with IRIs.

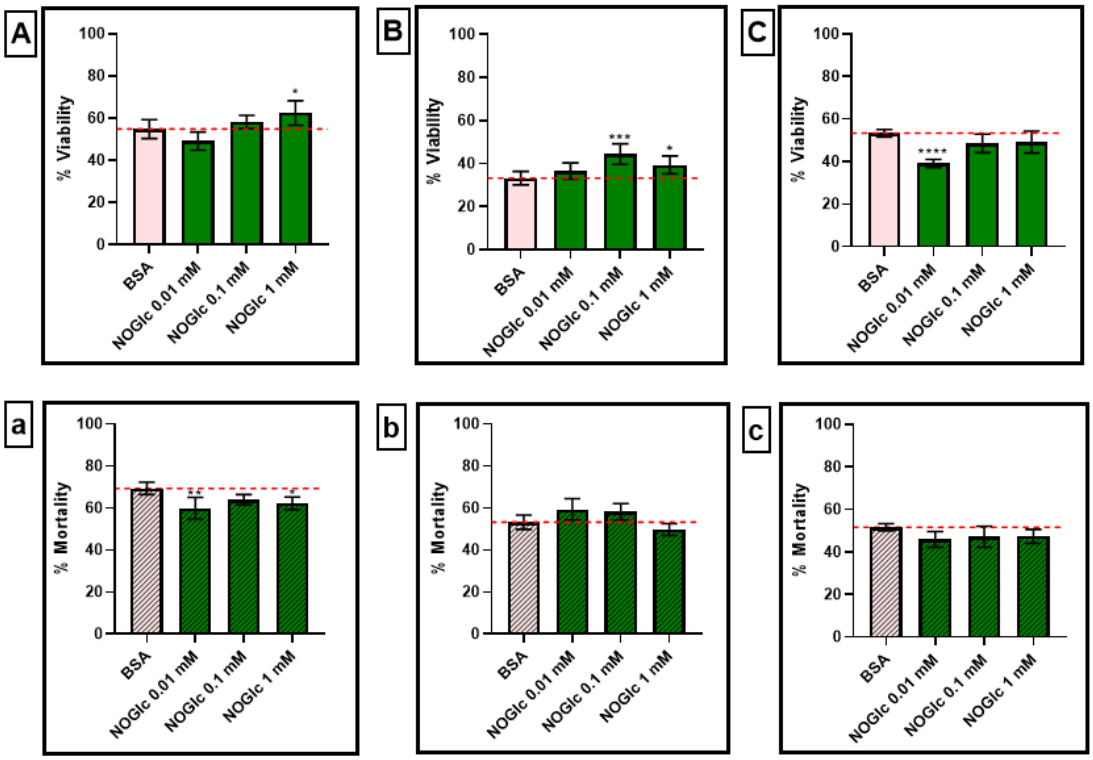

Figure 4.11. Post-Thaw Viability and Mortality of Autologous Dermal Sheets Following NOGlc* (1) *Supplementation. *Solid graphs (A-C) indicate post-thaw % viability determined through an AlamarBlue™ viability assay of dermal sheets cryopreserved in NOGLc* (**1**) *supplemented cell media compared to a control of BSA. Hatched Graphs (a-c) indicate post-thaw % mortality determined through a SYTOX Green mortality assay of dermal sheets cryopreserved in NOGLc* (**1**) *supplemented cell media compared to a control of BSA. Error represents SD, n = 5, N = 1. 1-way Anova, **** $P \leq 0.0001$, *** $P \leq 0.001$, ** $P \leq 0.01$, * $P \leq 0.05$.*

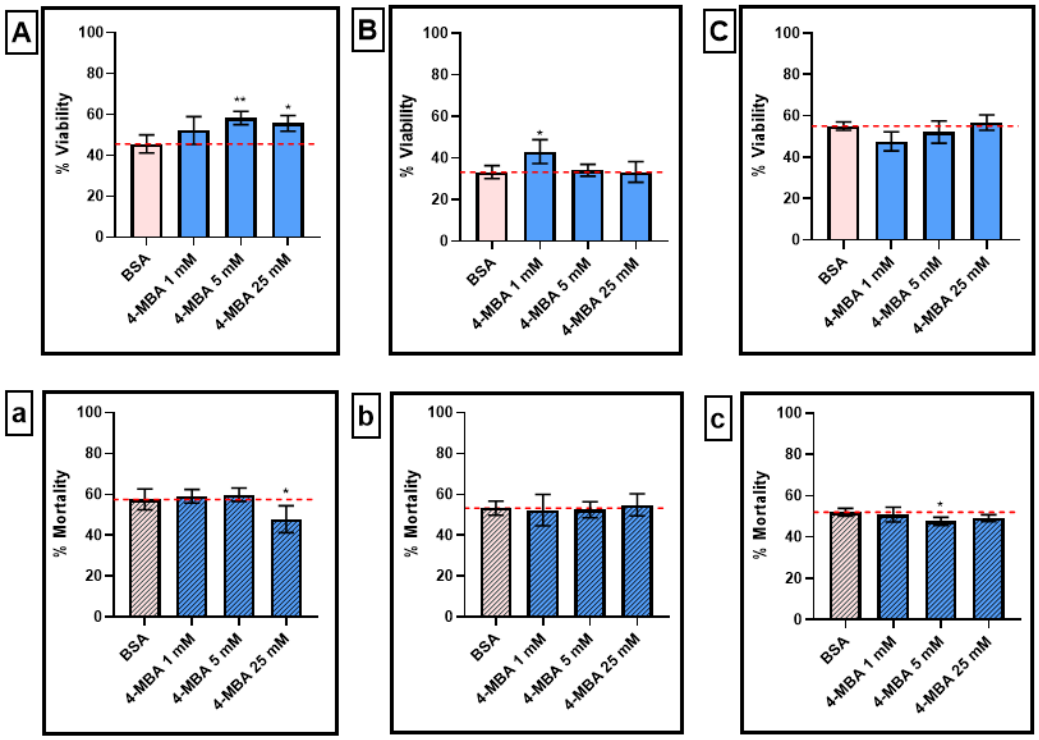

Figure 4.12. Post-Thaw Viability and Mortality of Autologous Dermal Sheets Following 4-MBA* (5) *Supplementation. *Solid graphs (A-C) indicate post-thaw % viability determined through an AlamarBlue™ viability assay of dermal sheets cryopreserved in 4-MBA* (5) *supplemented cell media compared to a control of BSA. Hatched graphs (a-c) indicate post-thaw % mortality determined through a SYTOX Green mortality assay of dermal sheets cryopreserved in 4-MBA* (5) *supplemented cell media compared to a control of BSA. Error represents SD, n = 5, N = 1. 1-way Anova, **** P ≤ 0.0001, *** P ≤ 0.001, ** P ≤ 0.01, * P ≤ 0.05.*

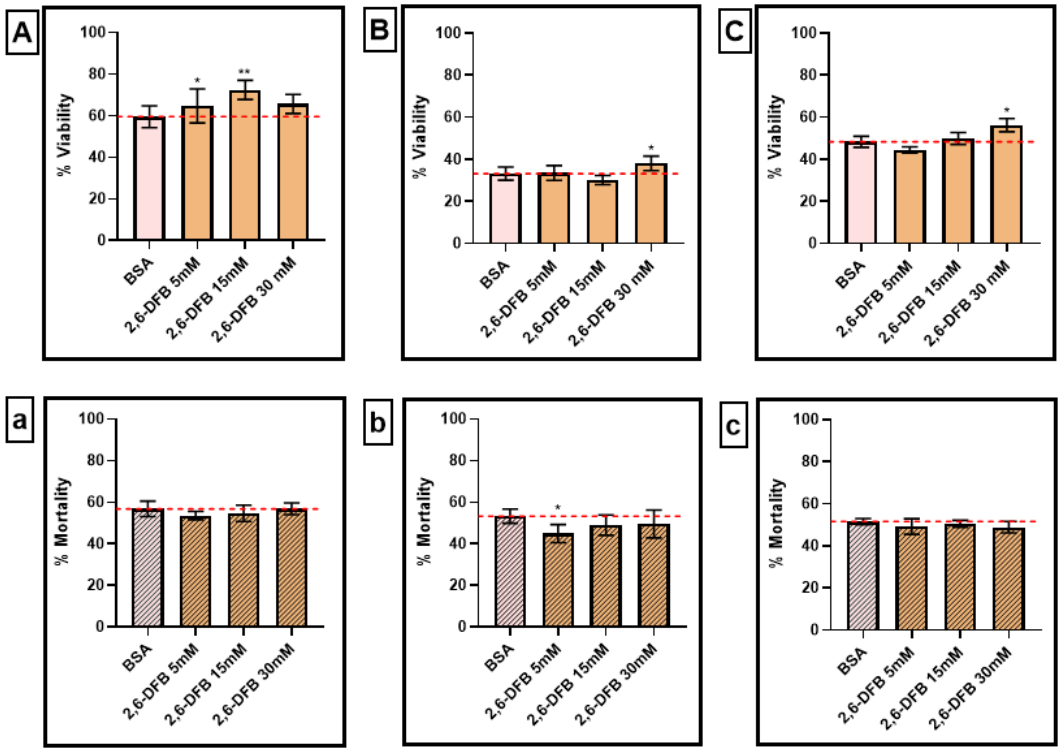

Figure 4.13. Post-Thaw Viability and Mortality of Autologous Dermal Sheets Following 2,6-DFB* (6) *Supplementation. *Solid graphs (A-C) indicate post-thaw % viability determined through an AlamarBlue™ viability assay of dermal sheets cryopreserved in 2,6-DFB* (6) *supplemented cell media compared to a control of BSA. Hatched graphs (a-c) indicate post-thaw % mortality determined through a SYTOX Green mortality assay of dermal sheets cryopreserved in 2,6-DFB* (6) *supplemented cell media compared to a control of BSA. Error represents SD, n = 5, N = 1. 1-way Anova, **** P ≤ 0.0001, *** P ≤ 0.001, ** P ≤ 0.01, * P ≤ 0.05.*

4.5 Discussion - Outlook for Ice Recrystallization Inhibitors in Tissue Cryopreservation

The best cryopreservation protocol for each type of tissue can be determined through cryopreservation trials with baseline testing as the first step. Sections 4.2 and 4.3, investigate the current cryopreservation protocols used for both fibroblasts and autologous dermal sheets. An optimal cooling rate of 1 °C/min was achieved when freezing BSA and serum dermal sheets begetting post-thaw viability results. The decrease in post-thaw viability to 37.4% and 26.5% for BSA and serum respectively, clearly outlines the issue with cryopreserving tissues, being the major reduction in cell viability. In addition, cytotoxicity trials of serum, BSA, and DMSO in both fibroblasts and autologous dermal sheets led to new insights. Such as, in comparison to BSA, serum increases post-thaw mortality leading to a greater loss of cells during cryopreservation, however it promotes better cell proliferation post-thaw. It is relevant to note that the role of serum components has not been fully determined. The biggest drawbacks in the use of sera are their untested biological safety and the added costs of supplementing basic media. In addition, the presence of serum in culture broth has complicated the isolation and purification of valuable products, such as culture-produced therapeutics. Therefore, there is a need to develop an affordable substitution for sera.[20] Another insight was that significant damage associated with DMSO only increases past 60 minutes of incubation. Nevertheless, DMSO is still toxic to cells at lower incubation time points reducing the number of cells post-thaw when compared to alternative cryo-additives.[31] These sections outline the need for cryo-additive alternatives, due to cryoprotectant cytotoxicity and ice recrystallization during rewarming which causes major reduction in the amount of viable cells post-thaw.

To address these concerns section 4.4 investigated the ability of NOGlc (**1**), 3FA (**2**), 2FA (**3**), 4-MBA (**5**), 2,6-DFB (**6**), and pBrPhGlc (**9**) to increase the post-thaw viability of a variety of tissue products by reducing damage associated with cryopreservation, while being less toxic than current cryo-additives. Fibroblasts were cultured in IRI supplemented cell media containing 1.5% BSA and 10% DMSO. Two of the six IRIs tested resulted in a decrease in fibroblast mortality. Compounds **2** and **3** did not show any significance, producing similar results to the not supplemented BSA control. As mentioned in previous chapters, **9** has shown to be toxic, therefore the results that **9** increased cell mortality and was highly toxic to fibroblasts significantly reducing post-thaw cell growth were in agreement with previous findings.[30] Figure 4.14 shows the fold change in the % mortality of fibroblasts in suspension compared to BSA according the IRIs **1**, **5**, and **6**. The results show **6** has no significant effect, at 0.01 mM **1** reduces mortality by 42% (±0.3 SD), and at 5 mM **5** reduces mortality by 37% (±0.2 SD). With the most significant result being a 52% (±0.3 SD) reduction of fibroblast mortality by **1** at 1 mM. Overall, the results indicate that not all classes or concentrations of IRIs are effective at reducing the damage associated with freezing in fibroblasts. Although only one of the tested IRIs was cytotoxic causing an increase in mortality, with all other compounds being neutral (having similar results to the control) or effective indicating they are potentially good CPAs by reducing mortality. In addition, where **9** decreased cell growth after cryopreservation **1**, **5**, and **6** were shown to increase post-thaw cell proliferation compared to BSA (figure 4.9 B and figure 4.10 B). The most notable results are those of NOGlc (**1**) and 4-MBA (**5**) which are extremely effective at reducing post-thaw mortality, with **1** reducing mortality by over half compared to the current methods using BSA and DMSO.

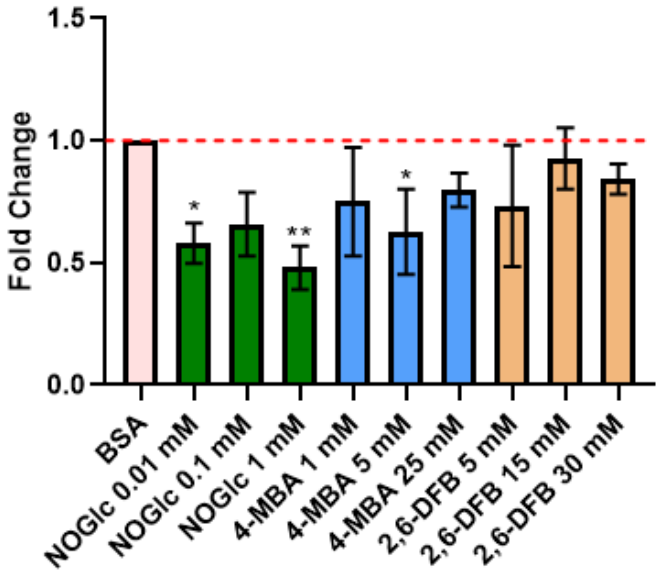

Figure 4.14. Fold Change Comparing Post-Thaw Mortality of Fibroblast Cell Suspension Following IRIs Supplementation. *Post-thaw mortality determined through a SYTOX Green mortality assay of fibroblasts cryopreserved in IRI supplemented cell media. The IRIs NOGlc (**1**), 4-MBA (**5**), and 2,6-DFB (**6**) were tested at various concentrations and compared to a control of BSA. Error represents SD, n = 3, N = 3. 1-way Anova, **** $P \leq 0.0001$, *** $P \leq 0.001$, ** $P \leq 0.01$, * $P \leq 0.05$.*

Thick cell sheets can present unique problems with regard to penetration of cryoprotectants and freezing characteristics.[5] As complexity of the tissues increases so do cell-to-cell and cell-to-matrix interactions contributing to increased cell injury caused by ice, this damage is associated with both the cell packing effect (section 1.4) and the matrix effect.[14] Section 4.4.2 investigated the ability of **1**, **5**, and **6** to cryoprotect autologous single dermal sheets. In dermal sheets, all of the tested IRIs at certain concentrations showed an increase in cell viability and decrease in mortality when supplemented in cell media. With the most significant result being a reduction in mortality of 16.8% (±3.9 SD) at 25 mM for **5** and an increase in viability of 33.6% (±2.6 SD) at 0.1 mM for **1** compared to solely BSA and DMSO. Increase viability of dermal sheets is important as these cultured sheets allow for the survival of severely burned patients when there are insufficient donor sites for the classical therapeutic approach necessitating the harvesting of spared sites.[10] Although, skin substitute is the desired goal for a more definitive treatment of burn patients and many other

problematic skin wounds.[10] An interesting observation that **6** which had no significant increase of viability in cell suspension did have significance in single dermal sheets. Therefore, the difference in complexity of the tissue products may account for the effectiveness of the IRI used. In future testing this may be an important insight, IRIs which show no significance in fibroblasts cell suspension does not indicate that it will be ineffective in more complex tissues. As the thickness of the tissues increases the most effective concentration of the IRI also increases. The observed effectiveness of higher concentration is connected to the matrix effect, which is dependent on cryoprotectant concentration and is reduced at higher concentrations as they are able to better penetrate the tissue matrix.[15] The matrix effect may explain why **1** was not as significant in dermal sheets as it was in cell suspension, as the compound has a low solubility limit of 1 mM. Therefore, as we increase complexity from cell suspension to dermal sheets, the most effective concentration also increases in molarity, indicating that higher concentrations should be the focal point of future testing in dermal equivalents.

Cryopreservation plays an important role in tissue banking and will assume even greater importance as the prevalence of tissue engineering increases.[12] Therefore, more effective cryoprotectants which are less toxic and address the issue of ice recrystallization are a necessity for better cryopreservation protocols of tissue products. Overall, IRIs have been shown to be effective cryo-additives in various complexities of tissue samples. With, **1** increasing fibroblast proliferation 96 hours post-thaw. Both **1** and **5** showed a significant reduction of damage to cells and increase viability at both levels of complexity. It is important to note that each replicate is carried out on cells that are seeded from different donors therefore variation of results is expected due to the lack of standardization of the

cells. In addition, % recovery of cells in suspension or matrices should be used in following experiments as it provides a more accurate representation by considering the total number of cells damaged before and after cryopreservation. The results obtained in this chapter are notable as dermis cryopreserved using IRIs retain enough properties to produce relevant bioengineered self-assembled skin substitutes in a timely manner. The ultimate goal for cryopreservation of tissues is the uniform cryopreservation of all tissue components of a composite organ.[22] IRIs are a promising approach which may be the key to achieving this goal, as they are nontoxic compounds which are able to reduce ice recrystallization within the matrix and cells.

4.6 References

1 Abaci, H., Guo, Z., Doucet, Y., Jacków, J. & Christiano, A. Next generation human skin constructs as advanced tools for drug development. *Experimental Biology and Medicine* **242**, 1657-1668, doi:10.1177/1535370217712690 (2017).

2 Gu, B. K., Choi, D. J., Park, S. J., Kim, Y.-J. & Kim, C.-H. 15-28 (Springer Singapore, 2018).

3 Wong, T., McGrath, J. A. & Navsaria, H. The role of fibroblasts in tissue engineering and regeneration. *British Journal of Dermatology* **156**, 1149-1155, doi:10.1111/j.1365-2133.2007.07914.x (2007).

4 Urciuolo, F., Casale, C., Imparato, G. & Netti, P. A. Bioengineered Skin Substitutes: The Role of Extracellular Matrix and Vascularization in the Healing of Deep Wounds. *Journal of Clinical Medicine* **8**, 2083, doi:10.3390/jcm8122083 (2019).

5 Madden, M. R. M. L., Anthony A. MD; Hajjar, David P. PhD; Staiano-Coico, Lisa PhD. Transplantation of Cryopreserved Cultured Epidermal Allografts. *The Journal of Trauma and Acute Care Surgery* **40**, 743-750 (1996).

6 Diana Kitala, M. K., Agnieszka Klama-Baryła, Wojciech Łabuś, Małgorzata Kraut, Justyna Glik, Ireneusz Ryszkiel, Marek P. Kawecki, Mariusz Nowak. Allogeneic vs. Autologous Skin Grafts in the Therapy of Patients with Burn Injuries: A Restrospective, Open-label Clinical Study with Pair Matching. *Advances in Clinical and Experimental Medicine* **25**, 923-929, doi:10.17219/acem/61961 (2016).

7 Gupta S, M. D., Chittoria RK, Subbarayan E, Reddy SK, Chavan V, Aggarwal A, Reddy LC. Human Skin Allograft: Is it a Viable Option in Management of Burn Patients? *J Cutan Aesthet Surg* **12**, 132-135, doi:https://doi.org/10.4103%2FJCAS.JCAS_83_18 (2019).

8 Plichta, J. K. *et al.* Cutaneous Burn Injury Promotes Shifts in the Bacterial Microbiome in Autologous Donor Skin. *Shock* **48**, 441-448, doi:10.1097/shk.0000000000000874 (2017).

9 Greenwood, J. The evolution of acute burn care – retiring the split skin graft. *Royal Collage of Surgeons of England* **99**, 432-438, doi:https://doi.org/10.1308/rcsann.2017.0110 (2017).

10 François A. Auger, F. B., Véronique Moulin, Roxane Pouliot, Lucie Germain. Tissue-engineered skin substitutes: from in vitro constructs to in vivo applications. *Biotechnology and Applied Biochemistry* **39**, 263-275, doi:10.1042/ba20030229 (2010).

11 Fanfan Chen, W. Z., Wei Wu, Yuqing Jin, Lian Cen, James D. Kretlow, Weicheng Gao, Zhenpeng Dai, Jiaming Wang, Guangdong Zhou, Wei Liu, Lei Cui, Yilin Cao. Cryopreservation of tissue-engineered epithelial sheets in trehalose. *Biomaterials* **32**, 8426-8435, doi:https://doi.org/10.1016/j.biomaterials.2011.07.008 (2011).

12 D.E. Pegg, M. D. The current status of tissue cryopreservation. *Europe PMC* **22**, 105-114 (2001).

13 Mark A. Moore, B. S., Julie McLean. Chapter 5 - Allograft Tissue Safety and Technology. *Biologics in Orthopaedic Surgery*, 49-62, doi:https://doi.org/10.1016/B978-0-323-55140-3.00005-9 (2019).

14 Müller-Schweinitzer, E. Cryopreservation of vascular tissues. *Organogenesis* **5**, 97-104, doi:10.4161/org.5.3.9495 (2009).

15 D.E. Pegg, M. D. The relevance of ice crystal formation for the cryopreservation of tissues and organs. *Cryobiology* **60**, S36-44, doi:https://doi.org/10.1016/j.cryobiol.2010.02.003 (2010).
16 Benson, E. E. 15-32 (Springer New York, 2008).
17 Barry J. Fuller, N. L., Erica E. Benson. *Life in the Frozen State (1st ed.)*. (CRC Press, 2004).
18 Roth, B. L., Poot, M., Yue, S. T. & Millard, P. J. Bacterial viability and antibiotic susceptibility testing with SYTOX green nucleic acid stain. *Applied and Environmental Microbiology* **63**, 2421-2431, doi:doi:10.1128/aem.63.6.2421-2431.1997 (1997).
19 Rampersad, S. N. Multiple Applications of Alamar Blue as an Indicator of Metabolic Function and Cellular Health in Cell Viability Bioassays. *Sensors* **12**, 12347-12360 (2012).
20 Cao, T.-T. & Zhang, Y.-Q. The potential of silk sericin protein as a serum substitute or an additive in cell culture and cryopreservation. *Amino Acids* **49**, 1029-1039, doi:10.1007/s00726-017-2396-3 (2017).
21 Isobe, T., Ikebata, Y., Onitsuka, T., Do, L. T. K., Sato, Y., Taniguchi, M., & Otoi, T. Cryopreservation for bovine embryos in serum-free freezing medium containing silk protein sericin. *Cryobiology* **67**, 184-187, doi:https://doi.org/10.1016/j.cryobiol.2013.06.010 (2013).
22 Bakhach, J. The cryopreservation of composite tissues. *Organogenesis* **5**, 119-126, doi:10.4161/org.5.3.9583 (2009).
23 Murray, K. A. & Gibson, M. I. Post-Thaw Culture and Measurement of Total Cell Recovery Is Crucial in the Evaluation of New Macromolecular Cryoprotectants. *Biomacromolecules* **21**, 2864-2873, doi:10.1021/acs.biomac.0c00591 (2020).
24 Giwa, S. *et al.* The promise of organ and tissue preservation to transform medicine. *Nature Biotechnology* **35**, 530-542, doi:10.1038/nbt.3889 (2017).
25 Briard, J. G. *The Rational Design and Use of Novel Small-Molecule Ice Recrystallization Inhibitors for the Cryopreservation of Hematopoietic Stem Cells and Red Blood Cells* Department of Chemistry and Biomolecular Sciences thesis, University of Ottawa, (2016).
26 Briard, J. G. *et al.* Small-Molecule Ice Recrystallization Inhibitors Improve the Post-Thaw Function of Hematopoietic Stem and Progenitor Cells. *ACS Omega* **1**, 1010-1018, doi:10.1021/acsomega.6b00178 (2016).
27 Ghobadloo, S. M. *et al.* Carbohydrate-Based Ice Recrystallization Inhibitors Increase Infectivity and Thermostability of Viral Vectors. *Scientific Reports* **4**, doi:10.1038/srep05903 (2015).
28 Poisson, J. S., Acker, J. P., Briard, J. G., Meyer, J. E. & Ben, R. N. Modulating Intracellular Ice Growth with Cell-Permeating Small-Molecule Ice Recrystallization Inhibitors. *Langmuir* **35**, 7452-7458, doi:10.1021/acs.langmuir.8b02126 (2019).
29 Robert Ben, J. G. B., Jessica S. Poisson, Tracey R. Turner, Jayme D.R. Kurach, Jason P. Acker. Ice recrystallization inhibitors – Mitigating cellular damage during freezing, transient warming and thawing. **71**, 171, doi:https://doi.org/10.1016/j.cryobiol.2015.05.031 (2015).
30 Poisson, J. S. *Synthesis and In Vitro Applications of Ice Recrystallization Inhibitors* Doctorate in Philosophy degree in Chemistry thesis, University of Ottawa, (2019).

31 Capicciotti, C. *The Rational Design of Potent Ice Recrystallization Inhibitors for Use as Novel Cryoprotectants* Doctorate in Philosophy degree in Chemistry thesis, University of Ottawa, (2014).

Chapter 5: Conclusions and Future Outlook

5.1 Conclusions

The work described in this thesis aimed to evaluate IRIs in appropriate and clinically relevant biological applications to determine if they are beneficial for preventing mechanisms of cryoinjury and biocompatible, while maintaining low cytotoxicity. The development of IRIs which possess these attractive qualities could significantly enhance the methods and protocols used in cryopreservation today. Thus, the overall goals of this thesis were: (1) to elucidate additional structural features that are important for the IRI activity of N-Aryl-β-D-gluconamides while increasing solubility and assessing curve fit; (2) investigate the capacity of small molecule carbohydrates to efficiently preserve proteins during freeze-drying; and (3) to explore the cryopreservation potential of small molecule IRIs in simplified human tissue models.

The first objective was achieved by synthesizing N-Aryl-β-D-aldonamide and N-Benzyl-β-D-gluconamide analogues, with a variety of aromatic substituents, then testing IRI activity. These analogues were previously found to be IRI active but lacked current and complete chemical property assessment.[1] Through IRI and cytotoxicity evaluation it was determined that all tested analogues were IRI active with lower cytotoxicity than pBrPhGlc (**9**).[2] In addition, compared to NOGlc (**1**) both groups of compounds had increased solubility. Overall, N-Benzyl-β-D-gluconamides proved to be a promising class of compounds with the *para* derivatives being more IRI active than all other tested compounds except **1**. In chapter 2 it was outlined that the *para* position may play an important role in the IRI activity. The combination of significant ice inhibition with the increased solubility addresses a major issue seen with the application of **1**, as well, the low cytotoxicity observed addresses issues seen

with **9**.[2,3] As both **1** and **9** are effective IRIs which have been applied in various cryopreservation protocols, the decrease in adverse effects makes this class of compounds favourable.[4,5] Lastly, dose-response curves of 4-CBA (**7**) and 4-MOBA (**8**) provided new insights validating that IRIs follow a sigmodal curve, however in some cases the trend is not symmetrical. As our compounds do not undergo a chemical change during the cryopreservation process their function may result in an asymmetrical curve. Therefore, The 5PL function, which contains a fifth parameter, enables asymmetry to be properly approximated when the 4PL curve does not provide the greatest fit.[6]

The next objective of this work involved the investigation of a small library of IRIs ability to cryopreserve proteins during the freeze-drying process. The storage of proteins through lyophilization presents unique challenges as freezing and drying both effect proteins, which require specific conditions to maintain their structure.[7] Therefore, **1**, 4-MBA (**5**), 2,6-DFB (**6**), and **9** were examined for their ability to limit denaturation of proteins. The data showed that the IRIs did not interfere with the qPCR process and were effective cryoprotectants during the lyophilization process: as all compounds were able to reach or even reduced the threshold cycle number. When compared to the most effective concentration of trehalose, certain concentrations of IRIs increased the thermostability of the proteins. The most effective IRI was **9** at 40 mM increasing the activity by ~30%, reducing the number of cycles to reach threshold value. Compound **9** is highly cytotoxic in cells leading to 0% viability at concentrations as low as 10 mM, but the cytotoxicity does not affect the proteins or qPCR process.[2] Therefore, it may be ideal to use **9** in the application of cryopreservation of protein products. As chapter 3 was a preliminary test of IRIs ability to stabilize proteins during both processes, many of the results did not result in large changes

except for 40 mM of pBr. In following experiments, ideally a decrease in cycle number of 30-50% would be significant enough improvement of outcomes to change protocols. The most significant contribution of this work was the discovery that carbohydrate-based small molecules may be working in more than one mechanism. Inhibitors of ice recrystallization may be working to protect the proteins from harm brought on by ice formation during freezing. Additionally, it is possible that these cryoprotectants also function as lyoprotectants during the lyophilization process' drying stages. Lyoprotectants or compounds that serve as both cryoprotectants and lyoprotectants, such as trehalose, are utilized due to the distinct drying stressors on proteins during lyophilization that are not always protected by cryoprotectants.[7] Therefore, it is suggested that IRIs may be stabilizing proteins via both processes as IRIs were not combined with a lyoprotectant during testing.

Finally, this work explored the ability for IRIs to cryopreserve tissue products of various complexity. Current cryo-additives used, such as DMSO and BSA, do not inhibit ice recrystallization which causes the majority of the damage during the storage of tissue products.[8] Preliminary tests of IRI supplemented cell media indicated that IRIs can increase viability and reduce mortality in cell suspension and single dermal sheets. Compounds **1** and **5** produced the best results as they had no significant cytotoxicity and increased post-thaw growth of cells. As the complexity of the tissues increased, higher concentrations of IRI were needed, therefore, **5** recovered cells better in complex tissues due to the low solubility limit of **1**.[3] Although, **1** due to its higher IRI activity increases viability more significantly in less complex systems. IRIs may not change the biological activity of the tissues but work on a physiochemical basis. As the tissues increase in complexity or change cell type of tissue morphology, such as through vascularization of bioengineered skin substitutes or seeding

epidermal bilayers, the IRIs should hypothetically still be effective cryoprotectants. Overall, in simple one cell type thin tissue matrix both **1** and **5** are effective cryo-additives reducing the damage associated with freezing and increasing viability of the cells within the system.

Combined, the findings highlight the complexity of cryopreservation and imply that while ice recrystallization inhibition is advantageous for a cryoprotectant, specific derivatives are better suited as cryoprotectants for particular biological materials. Overall, the results of the cryopreservation investigations showed that, in addition to being strong inhibitors of ice recrystallization, small molecules may also be strong lyoprotectants, demonstrating the variety of ways in which these compounds may aid in biopreservation. IRIs offer enormous potential to advance current cryopreservation techniques, which are currently constrained by the usage of trehalose or cytotoxic DMSO, two routinely employed cryoprotectants that do not prevent ice recrystallization.

5.2 Future Outlook

Throughout this thesis, several different classes of small molecule IRIs were confirmed as effective inhibitors of ice recrystallization, that can help direct future research in the field. Collectively, the results from this thesis have established that small-molecule IRIs have tremendous potential for improving upon current cryopreservation protocols for freeze-drying proteins and tissue products such as dermal sheets.

With the current global pandemic, the results obtained from the protein thermostability assays in chapter 3 are pertinent. With further testing, IRIs could allow stabilization of COVID test kits more efficiently without compromising the efficacy of the testing procedure when samples are retrieved from infected patients. This leads to the inquiry if IRIs are useful molecules to perhaps stabilize additional protein products, which could

ultimately lead to more effective freezing and storage of mRNA vaccines. In addition, the discovery that IRIs do not negatively affect qPCR and potentially act as lyoprotectants is compelling. The requirement for uniform, quality-controlled frozen or refrigerated materials is one aspect of the qPCR technique that hinders its application.[9] The availability of high-quality, ready-to-use freeze-dried qPCR mixes would make implementation much easier because they offer a one-step reaction format that would lessen issues with unintended contamination.[9,10] As per our observations, freeze-drying enables the creation of qPCR reaction mixes for the detection of RNA that are readily available, preoptimized, premixed, and pre-dispensed and are stable for two weeks at room temperature. Reconstitution of the mixture and template RNA are all that are needed.[9,10] In summation, further investigation will be needed to determine the mechanism of action of IRIs acting as both cryoprotectants and lyoprotectants. Specifically, moving forward with compound **9** derivatives and testing additional IRIs in further protein products, such as test kits.

Simple dermal sheets were successfully cryopreserved in chapter 4. However, the ideal result involves increasing complexity to incorporate a bilayer of dermis and epidermis or even developing more physiological skin constructs by include various skin components, such as vasculature, appendages, pigment, innervation, and adipose tissue.[11] The final goal of the project is to accelerate the grafting of tissue engineered skin substitutes. By cryopreserving allogeneic dermis, which is less immunogenic, autologous keratinocytes could be seeded to create a bilayer reducing tissue culture time from 8 weeks to 2 weeks. These skin substitutes would be less antigenic and present the same histology of regular skin substitutes. This shorter turnaround time and improved protocol would enable the "banking" of cultivated cell sheets for long-term preservation, easy shipping, and quick access for burn

victims when necessary.[12] The immediate next steps include determining the mechanism of action to investigate if the IRIs are entering the cells or only working extracellularly within the cell matrix. Tissues of further complexity and vascularization will need to be tested with IRIs to confirm the initial findings of improved cell viability, specifically investigating compounds **1** and **5** as they are the most promising. Finally, testing if IRIs can reduce the amount of DMSO needed in cell media to avoid cytotoxic effects.

Further investigation within the Ben lab would start at structure function analysis as the main structural features which contribute to IRI activity are still yet to be known. For insight into the mechanism of action, dose-response curves should be further populated to determine if 4PL or 5PL curve fits are more accurate. The importance of the *para* position in N-Benzyl-β-D-gluconamides has been discovered but the connection between the substituents and IRI activity requires further analysis. The chemical properties which contribute to effective cryopreservation would be the foundation of designing future active small molecule IRIs. Due to the success in many biological materials and low cytotoxicity **5** may be a promising new compound to develop for the application of cryopreservation. In addition to further research into other more active benzyl compounds such as **7**.

In summation, there is still a lot of work to be done to pinpoint the precise mechanism of action of these molecules. Understanding how these compounds function as cryoprotectants and potentially as lyoprotectants is more crucial than understanding the mechanism of ice recrystallization inhibition. It is still unknown whether they work solely as cell-permeating cryoprotectants, prevent ice from recrystallizing, maintain cell viability and functionality by interacting in a way that protects cell membranes or perhaps a combination of mechanisms.[1]

5.3 References

1 Briard, J. G. *The Rational Design and Use of Novel Small-Molecule Ice Recrystallization Inhibitors for the Cryopreservation of Hematopoietic Stem Cells and Red Blood Cells* Department of Chemistry and Biomolecular Sciences thesis, University of Ottawa, (2016).

2 Poisson, J. S. *Synthesis and In Vitro Applications of Ice Recrystallization Inhibitors* Doctorate in Philosophy degree in Chemistry thesis, University of Ottawa, (2019).

3 Capicciotti, C. *The Rational Design of Potent Ice Recrystallization Inhibitors for Use as Novel Cryoprotectants* Doctorate in Philosophy degree in Chemistry thesis, University of Ottawa, (2014).

4 Balcerzak, A. K., Capicciotti, C. J., Briard, J. G. & Ben, R. N. Designing ice recrystallization inhibitors: from antifreeze (glyco)proteins to small molecules. *RSC Adv.* **4**, 42682-42696, doi:10.1039/c4ra06893a (2014).

5 Poisson, J. S., Acker, J. P., Briard, J. G., Meyer, J. E. & Ben, R. N. Modulating Intracellular Ice Growth with Cell-Permeating Small-Molecule Ice Recrystallization Inhibitors. *Langmuir* **35**, 7452-7458, doi:10.1021/acs.langmuir.8b02126 (2019).

6 Paul G. Gottschalk, J. R. D. The five-parameter logistic: A characterization and comparison with the four-parameter logistic. *Analytical Biochemistry* **343**, 54-65, doi:https://doi.org/10.1016/j.ab.2005.04.035 (2005).

7 Wang, W. Lyophilization and development of solid protein pharmaceuticals. *International Journal of Pharmaceutics* **203**, 1-60, doi:10.1016/s0378-5173(00)00423-3 (2000).

8 Barry J. Fuller, N. L., Erica E. Benson. *Life in the Frozen State (1st ed.)*. (CRC Press, 2004).

9 Klatser PR, K. S., van Ingen CW, Kolk AH. Stabilized, freeze-dried PCR mix for detection of mycobacteria. *J Clin Microbiol.* **36**, 1798-1800, doi:https://doi.org/10.1128/jcm.36.6.1798-1800.1998 (1998).

10 Colaço, C., Sen, S., Thangavelu, M., Pinder, S. & Roser, B. Extraordinary Stability of Enzymes Dried in Trehalose: Simplified Molecular Biology. *Nature Biotechnology* **10**, 1007-1011, doi:10.1038/nbt0992-1007 (1992).

11 Abaci, H., Guo, Z., Doucet, Y., Jacków, J. & Christiano, A. Next generation human skin constructs as advanced tools for drug development. *Experimental Biology and Medicine* **242**, 1657-1668, doi:10.1177/1535370217712690 (2017).

12 Madden, M. R. M. L., Anthony A. MD; Hajjar, David P. PhD; Staiano-Coico, Lisa PhD. Transplantation of Cryopreserved Cultured Epidermal Allografts. *The Journal of Trauma and Acute Care Surgery* **40**, 743-750 (1996).

Chapter 6: Experimental Procedures and Compound Characterizations

6.1 Experimental Protocols and Characterization Data for Chemical Compounds

***General Materials and Methods for Chemical Synthesis*:**

Reagents were purchased from Sigma-Aldrich and used as received or purified from existing stock prior to use. All anhydrous reactions were performed in flame-dried glassware under a positive pressure of dry argon. Air sensitive reagents were transferred using oven-dried syringes. All flash chromatography was performed with SiliCycle silica gel 60 (230-400 mesh). All solution phase reactions were monitored using thin layer chromatography (TLC) with 0.2 mm pre-coated silica gel aluminum plates 60 F254 (SiliCycle). Components were visualized with short-wavelength (254 nm) ultra-violet light and/or staining (orcinol/sulphuric acid stain solution). All solvents used for anhydrous reactions were distilled. Dichloromethane was dispensed from a SPBT- Bench Top Solvent Purification System (LC Technology Solutions inc.) and stored under argon. ^{1}H-NMR (400 MHz) and ^{13}C-NMR (400 MHz) spectra were recorded at ambient temperature on a Bruker Avance 400 spectrometer. Dimethyl sulphoxide-*d6* ($(CD_3)_2SO$) was used as NMR solvent. Chemical shifts are reported in ppm and corrected using the solvent residual peak as an internal standard. Splitting patterns are designated as follows: s, singlet; d, doublet; dd, doublet of doublets; t, triplet; td, triplet of doublets; q, quartet; m, multiplet; and br, broad. NMR spectra of compounds assessed for IRI activity and of intermediate compounds are provided. High resolution mass spectrometry (HRMS) was performed on quadrupole time-of-flight (Q-TOF) spectrometer with a pump rate of 100 nL/min using electrospray ionization (ESI). Gluconolactone (D-(+)-Gluconic acid-δ-lactone) and 1,2,3,4,6-Penta-*O*-acetyl-β-D-

glucopyranose are commercially available carbohydrates. Compounds were lyophilized using a Labconco FreeZone lyophilizer in dH_2O prior to testing in cells.

N-Octyl-β-D-gluconamide (1)

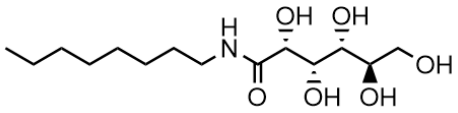

Compound 1 Reaction Scheme:

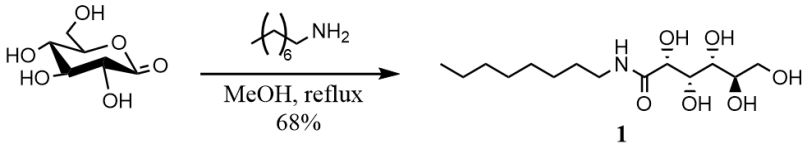

Scheme 6.1. Synthesis of N-Octyl-β-D-gluconamide.

Compound **1** was prepared according to a standard literature procedure.[1] To a solution of D-Gluconic acid-δ-lactone (1.4 g, 7.9 mmol) in MeOH (30 mL) was added n-octylamine (1.3 mL, 7.9 mmol). The mixture was stirred under reflux for 1 hour then cooled in an ice bath. The precipitate was filtered off and washed with cold MeOH to afford **1** as a white powder (1.6 g, 68%). Characterization data is consistent with that previously reported in the literature. ^{1}H NMR (400 MHz, DMSO-d_6): δ 7.56 (t, *J* = 6.0 Hz, 1H), 5.32 (d, *J* = 5.3 Hz, 1H), 4.51 (d, *J* = 5.0 Hz, 1H), 4.44 (d, *J* = 5.0 Hz, 1H), 4.36 (d, *J* = 7.3 Hz, 1H), 4.30 (t, *J* = 6.0 Hz, 1H), 3.93 (t, *J* = 4.5 Hz, 1H), 3.86 (m, 1H), 3.54 (m, 1H), 3.42 (m, 2H), 3.02 (m, 2H), 1.36-1.20 (m, 11 H), 0.82 (t, *J* = 7.0 Hz, 3H). ^{13}C NMR (400 MHz, DMSO-d_6): δ 172.7, 74.1, 72.9, 71.9, 70.6, 63.8, 38.7, 31.7, 29.6, 29.2, 29.1, 26.8, 22.6, 14.4.

Compound 1 NMR Spectra:

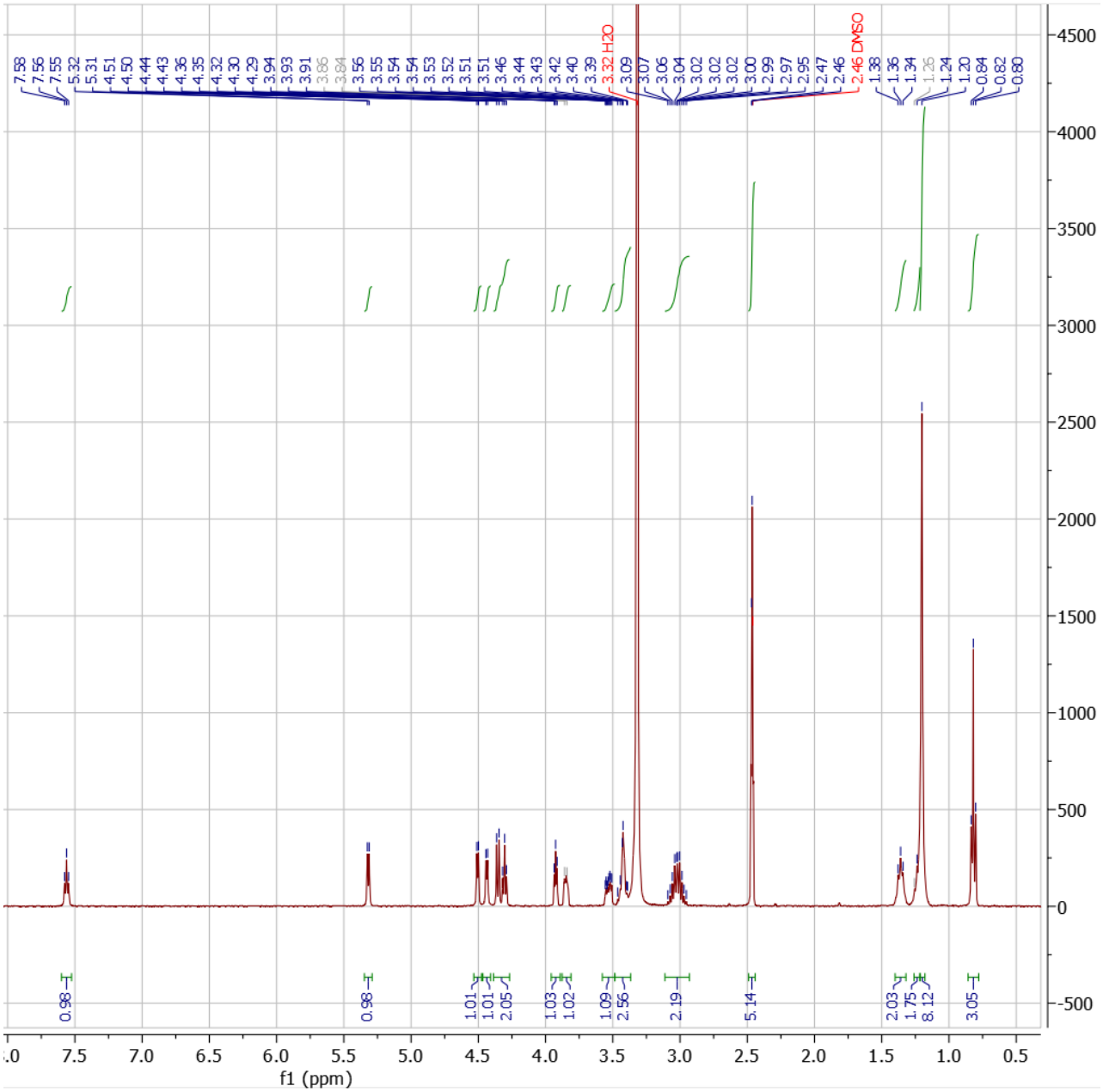

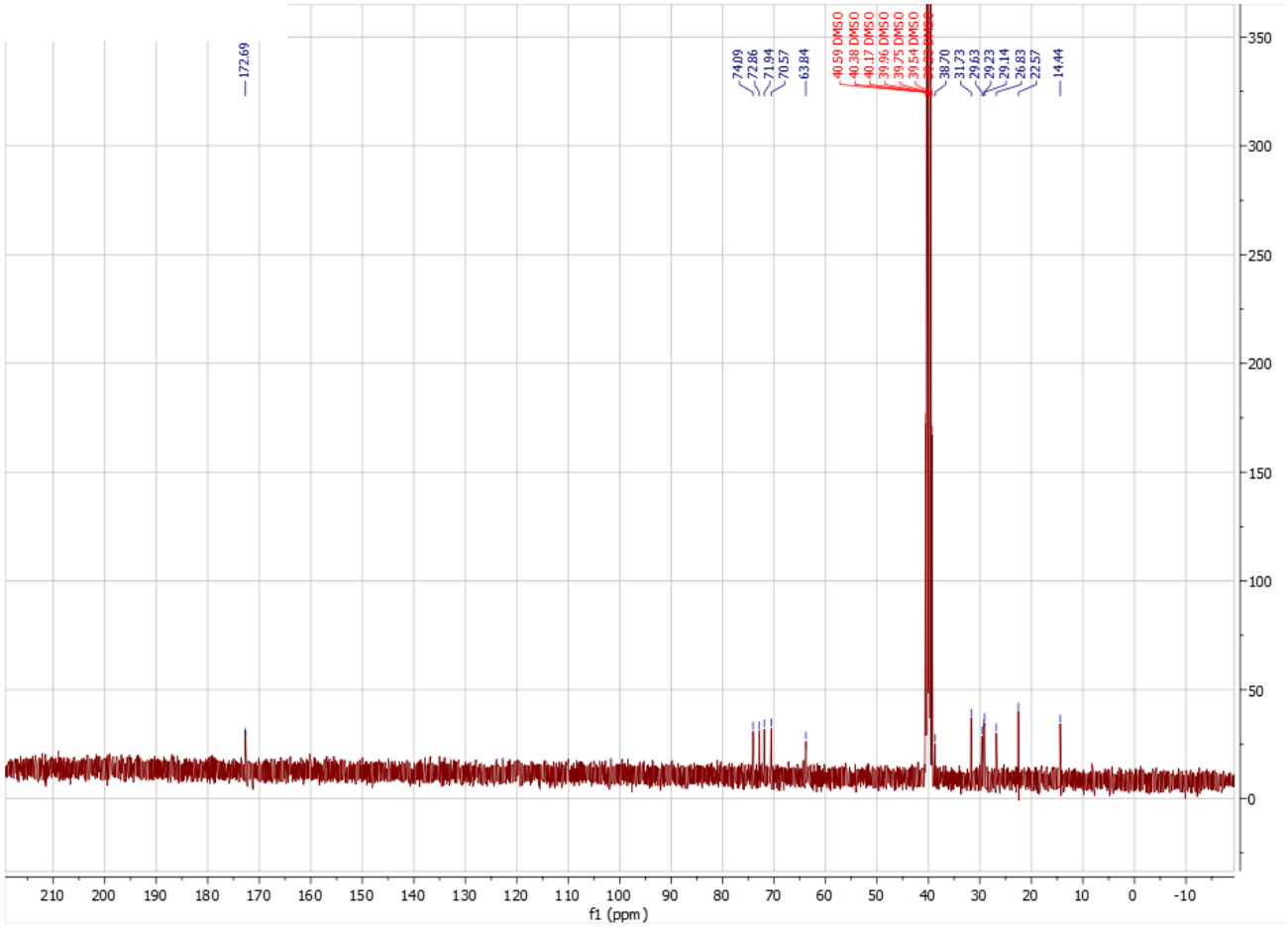
172.69
74.09
72.86
71.94
70.57
63.84
40.59 DMSO
40.38 DMSO
40.17 DMSO
39.96 DMSO
39.75 DMSO
39.54 DMSO
38.70
31.73
29.63
29.23
29.14
26.83
22.57
14.44
f1 (ppm)

N-3-Fluorophenyl-β-D-gluconamide (2)

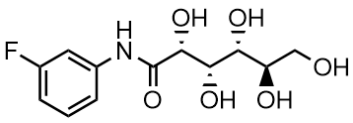

Compound 2 Reaction Scheme:

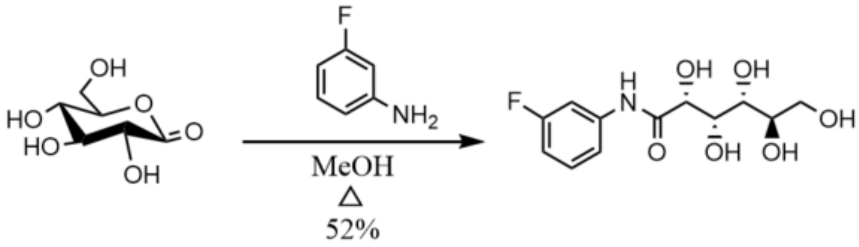

Scheme 6.2. Synthesis of N-3-Fluorophenyl-β-D-gluconamide.

Compound **2** was prepared according to a standard literature procedure.[2] To a solution of D-Gluconic acid-δ-lactone (0.6 g, 3.36 mmol) in acetic acid (30 mL) was added 3-fluoroaniline (1.08 mL, 10.1 mmol). The mixture was stirred under reflux for 3 hours. The solvent was evaporated producing a dark brown solid. The solid was recrystallized in EtOH to afford **2** as a white powder (0.51 g, 52%). Characterization data is consistent with that previously reported in the literature. ^{1}H NMR (400 MHz, DMSO-d_6): δ 9.74 (s, 1H), 7.68 (dt, *J* = 11.8, 2.6 Hz, 1H), 7.48 (m, 1H), 7.29 (m, 1H), 6.84 (m, 1H), 5.74 (s, 1H), 4.54 (m, 2H), 4.34 (m, 1H), 4.14 (br, 1H), 3.97 (br, 1H), 3.55 (m, 1H), 3.47 (s, 1H), 3.37-3.33 (m, 1H). ^{13}C NMR (400 MHz, DMSO-d_6): δ 172.5, 74.7, 72.6, 72.0, 70.8, 63.7.

Compound 2 NMR Spectra:

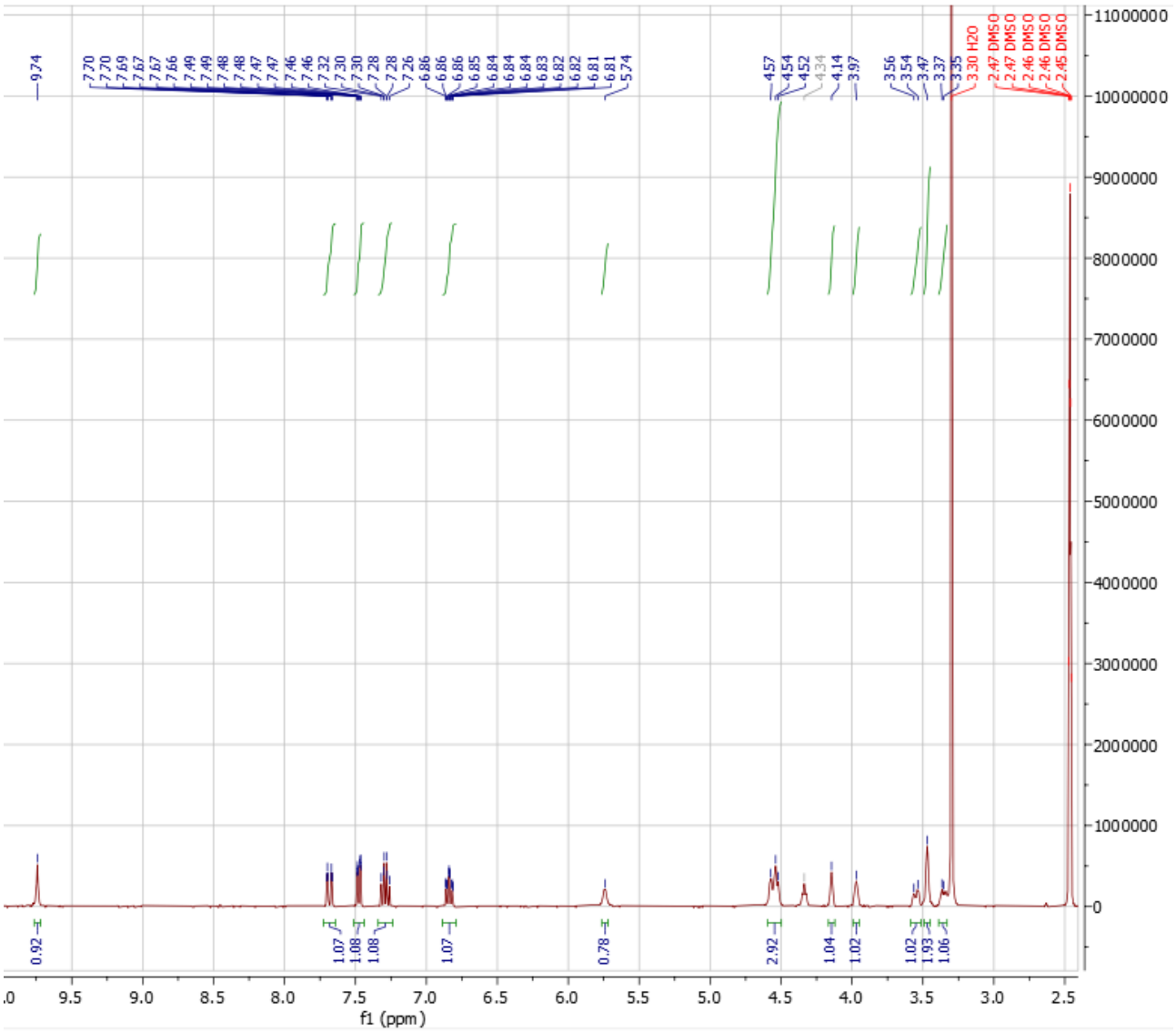

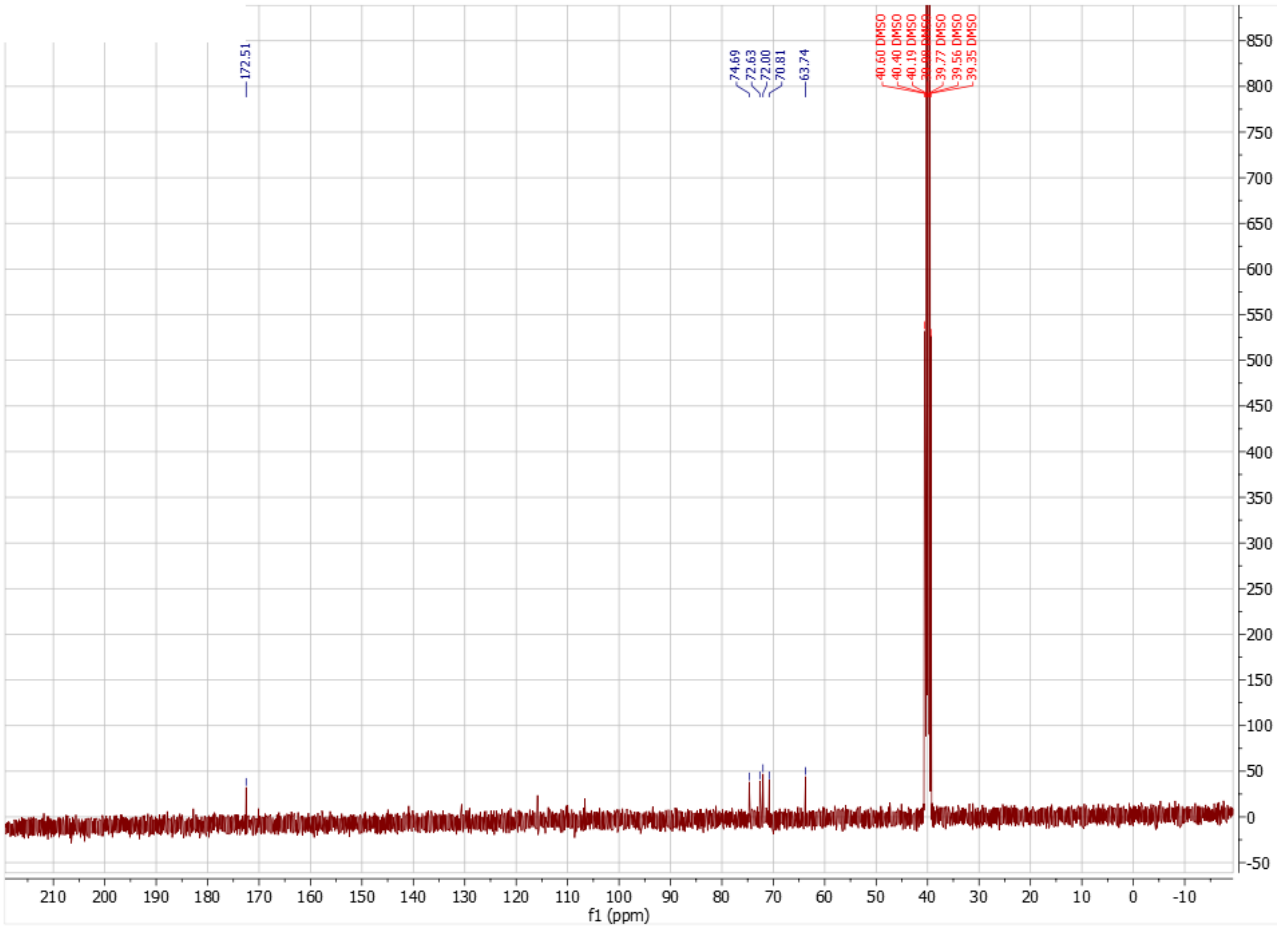
172.51
74.69
72.63
72.00
70.81
63.74
40.60 DMSO
40.40 DMSO
40.19 DMSO
39.77 DMSO
39.56 DMSO
39.35 DMSO
f1 (ppm)

N-2-Fluorophenyl-β-D-gluconamide (3)

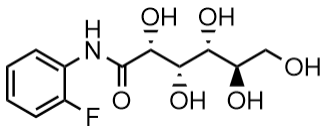

Compound 3 Reaction Scheme:

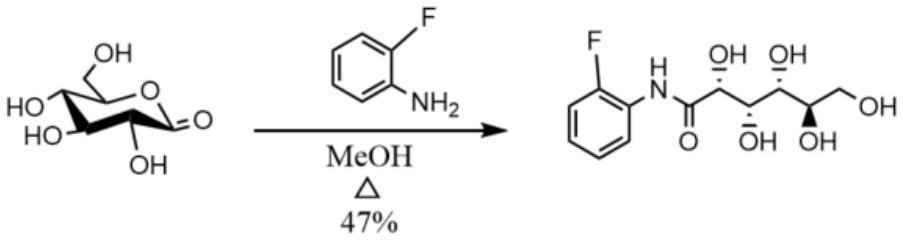

Scheme 6.3. Synthesis of N-2-Fluorophenyl-β-D-gluconamide.

Compound **3** was prepared according to a standard literature procedure.[2] To a solution of D-Gluconic acid-δ-lactone (1 g, 5.62 mmol) in acetic acid (10 mL) was added 2-fluoroaniline (1.62 mL, 16.84 mmol). The mixture was stirred under reflux for 1 hour. The solvent was evaporated producing a dark brown solid. The solid was recrystallized in EtOH to afford **3** as a white powder (0.77 g, 47%). Characterization data is consistent with that previously reported in the literature. ^{1}H NMR (400 MHz, DMSO-d_6): δ 9.17 (s, 1H), 8.09 (td, *J* = 6.0, 2.0 Hz, 1H), 7.27-7.22 (m, 1H), 7.17-7.07 (m, 2H), 5.94 (d, *J* = 4.6 Hz, 1H), 5.64 (d, *J* = 7.5 Hz, 1H), 4.59 (t, *J* = 6.0 Hz, 2H), 4.36 (t, *J* = 5.5 Hz, 1H), 4.20 (m, 1H), 3.99 (m, 1H), 3.58-3.41 (m, 3H), 3.41-3.30 (m, 2H). ^{13}C NMR (400 MHz, DMSO-d_6): δ 172.0, 125.0, 122.5, 115.6, 74.4, 72.7, 72.0, 70.7, 63.7.

Compound 3 NMR Spectra:

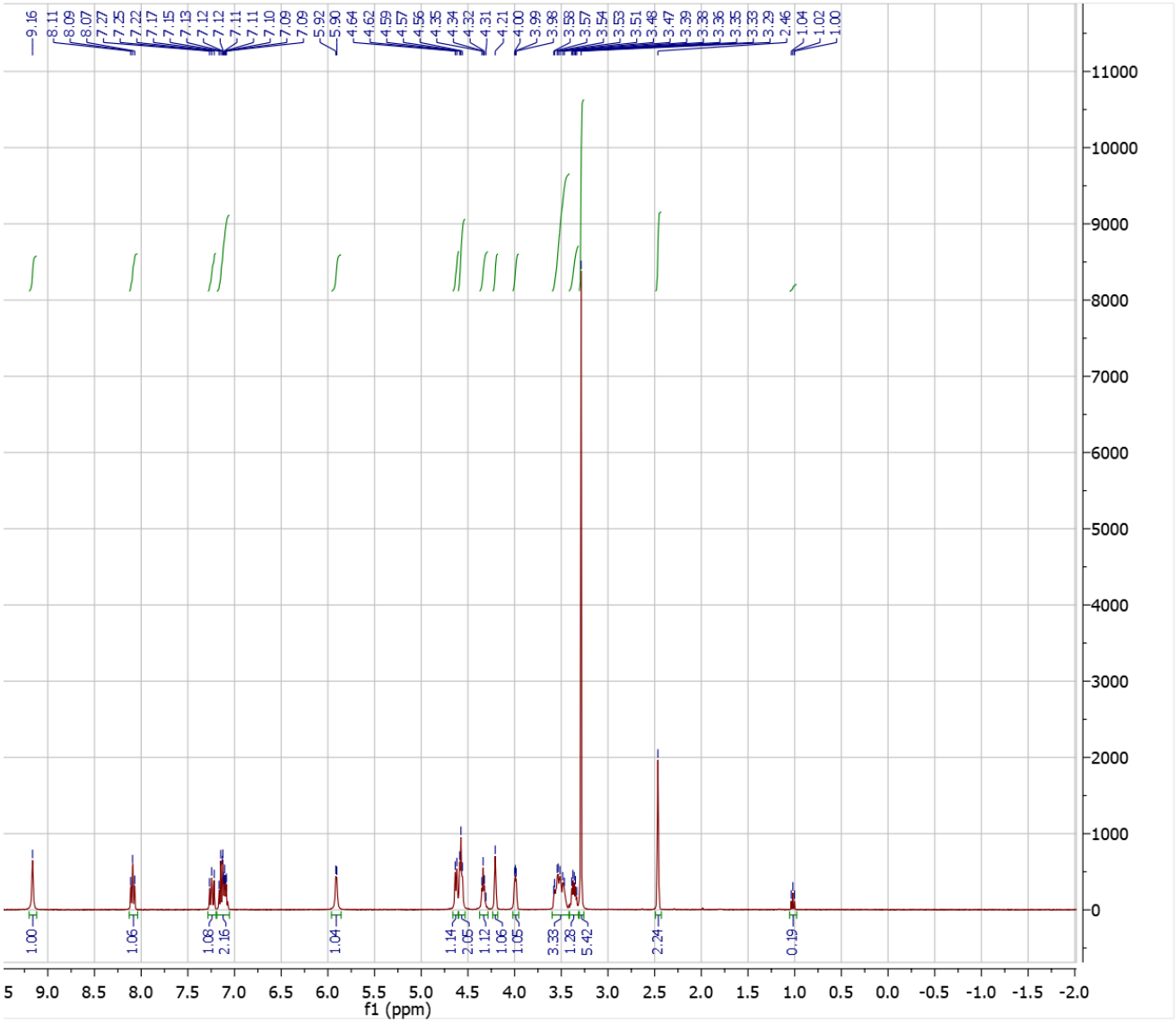

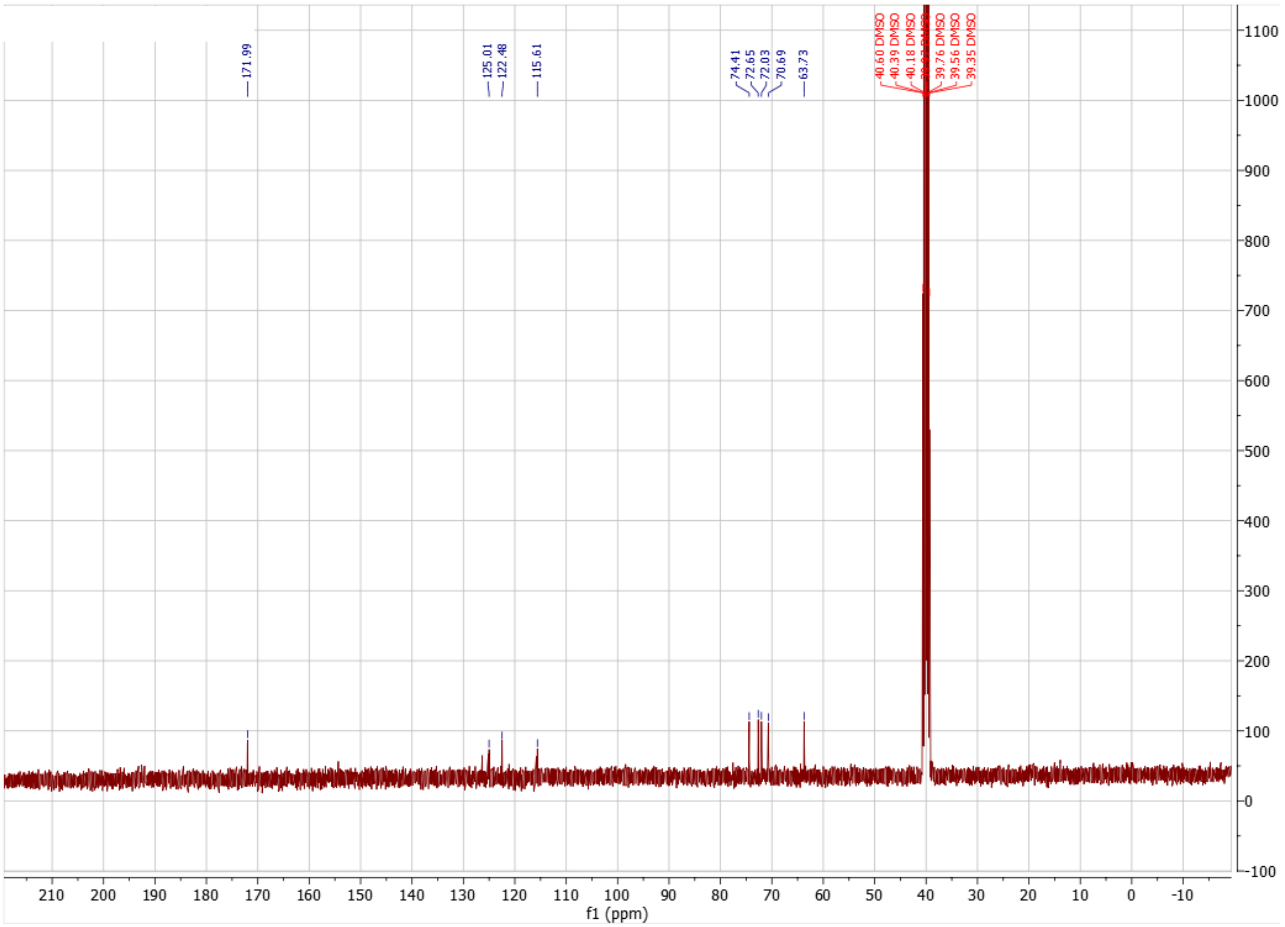
171.99
125.01
122.48
115.61
74.41
72.65
72.03
70.69
63.73
40.60 DMSO
40.39 DMSO
40.18 DMSO
39.76 DMSO
39.56 DMSO
39.35 DMSO
f1 (ppm)

N-Benzyl-β-D-gluconamide (4)

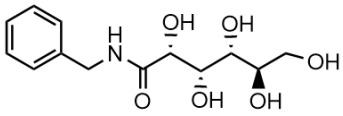

Compound 4 Reaction Scheme:

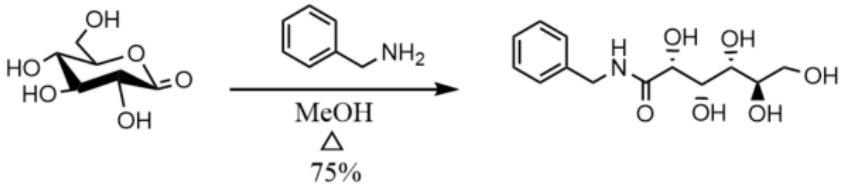

Scheme 6.4. Synthesis of N-Benzyl-β-D-gluconamide.

Compound **4** was prepared according to a standard literature procedure.[2] To a solution of D-Gluconic acid-δ-lactone (1.51 g, 8.5 mmol) in MeOH (60 mL) was added n-benzylamine (1.03 mL, 9.3 mmol). The mixture was stirred under reflux for 24 hours. The solvent was evaporated, and the residue was recrystallized in EtOH to afford **4** as a white powder (1.82 g, 75%). Characterization data is consistent with that previously reported in the literature. ^{1}H NMR (400 MHz, DMSO-d_6): δ 8.13 (t, *J* = 6.3 Hz, 1H), 7.28-7.15 (m, 5H), 5.43 (d, *J* = 5.1 Hz, 1H), 4.55 (m, 1H), 4.49 (m, 1H), 4.44 (d, *J* = 7.3 Hz, 1H), 4.32 (t, *J* = 5.7 Hz, 1H), 4.28 (d, *J* = 6.3 Hz, 1H), 4.03 (t, *J* = 4.3 Hz, 1H), 3.94-3.91 (m, 1H), 3.57-3.52 (m, 1H), 3.44 (br, 2H), 3.36-3.32 (m, 3H). ^{13}C NMR (400 MHz, DMSO-d_6): δ 173.0, 140.0, 128.6, 127.6, 127.0, 74.3, 73.0, 72.0, 70.6, 63.8, 42.2.

Compound 4 NMR Spectra:

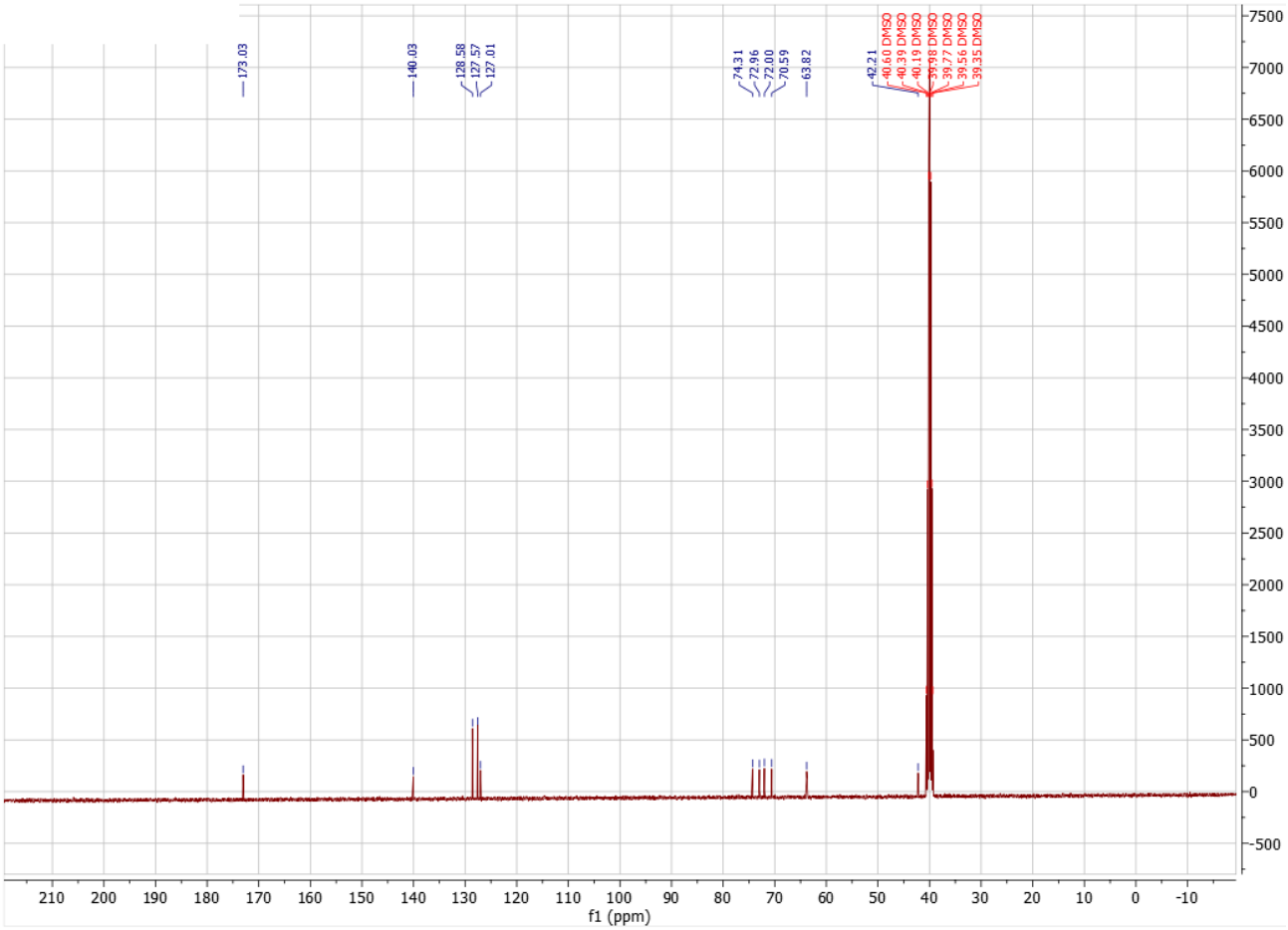
173.03
140.03
128.58
127.57
127.01
74.31
72.96
72.00
70.59
63.82
42.21
40.60 DMSO
40.39 DMSO
40.19 DMSO
39.98 DMSO
39.77 DMSO
39.56 DMSO
39.35 DMSO
f1 (ppm)

N-4-Methylbenzyl-β-D-gluconamide (5)

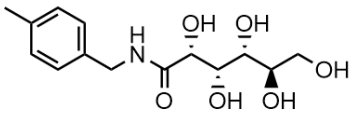

Compound 5 Reaction Scheme:

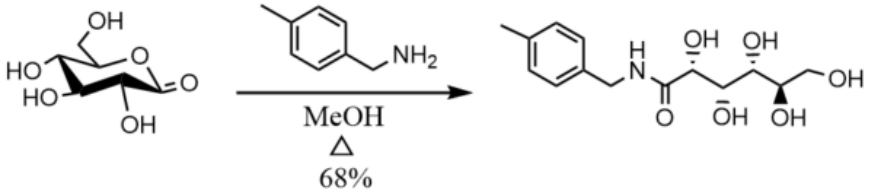

Scheme 6.5. Synthesis of N-4-Methylbenzyl-β-D-gluconamide.

Compound **5** was prepared according to a standard literature procedure.[2] To a solution of D-Gluconic acid-δ-lactone (0.5 g, 2.8 mmol) in MeOH (50 mL) was added 4-methylbenzylamine (0.36 mL, 2.8 mmol). The mixture was stirred under reflux for 24 hours. The solvent was evaporated, and the residue was recrystallized in EtOH to afford **5** as a white powder (0.56 g, 68%). Characterization data is consistent with that previously reported in the literature. ^{1}H NMR (400 MHz; DMSO-d_6): δ 8.09 (t, *J* = 6.2 Hz, 1H), 7.13 (dd, *J* = 14.2, 8.1 Hz, 4H), 5.45 (d, *J* = 5.1 Hz, 1H), 4.56-4.47 (m, 2H), 4.44 (d, *J* = 7.2 Hz, 1H), 4.35 (t, *J* = 5.6 Hz, 1H), 4.23 (d, *J* = 6.2 Hz, 2H), 4.03 (t, *J* = 3.6 Hz, 1H), 3.94-3.90 (m, 1H), 3.59-3.52 (m, 1H), 3.47 (br, 2H), 3.39-3.33 (m, 1H), 2.26 (s, 3H). ^{13}C NMR (400 MHz, DMSO-d_6): δ 172.9, 136.9, 136.0, 129.1, 127.6, 74.2, 72.9, 71.9, 70.6, 63.8, 42.0, 21.1.

Compound 5 NMR Spectra:

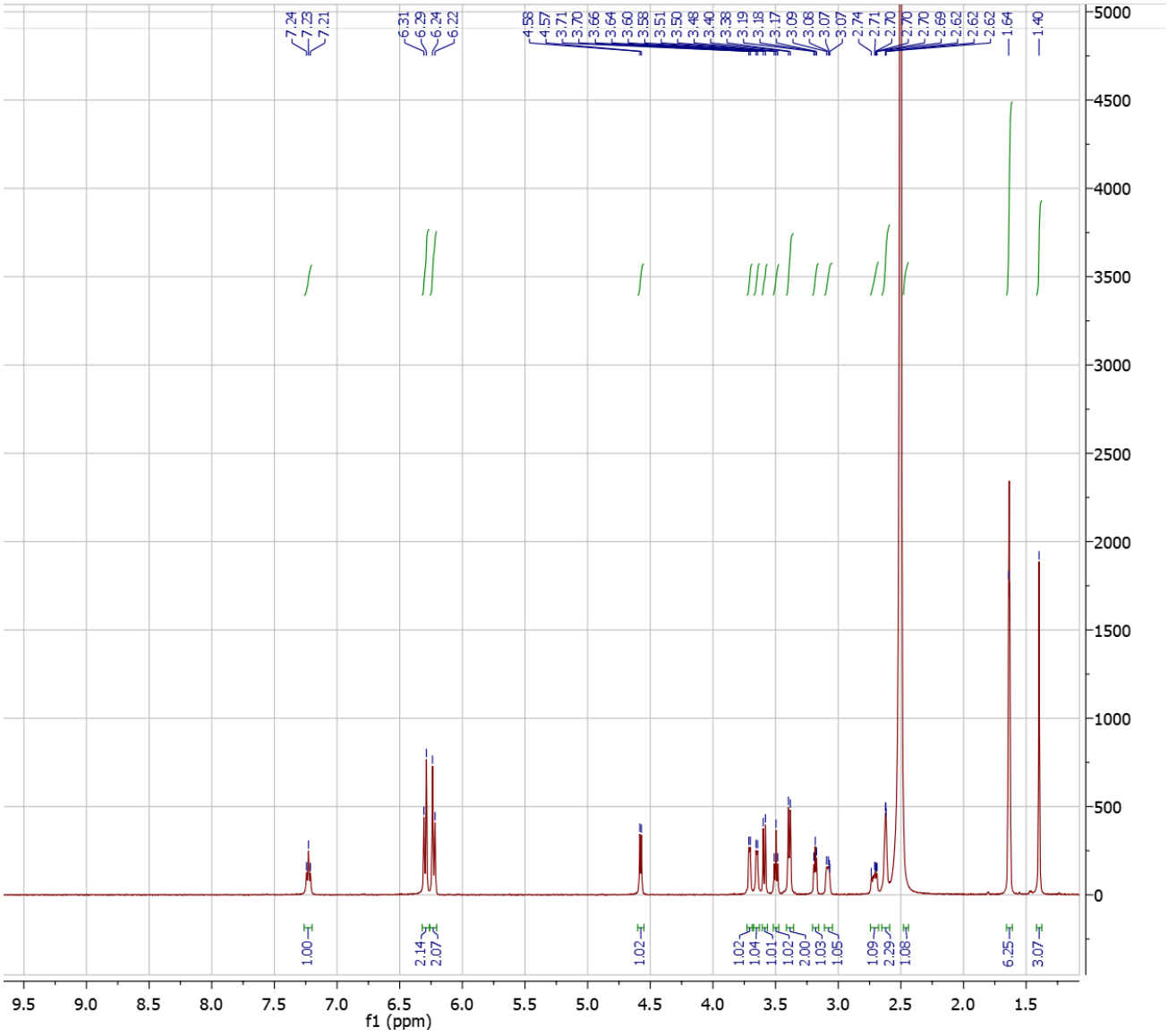

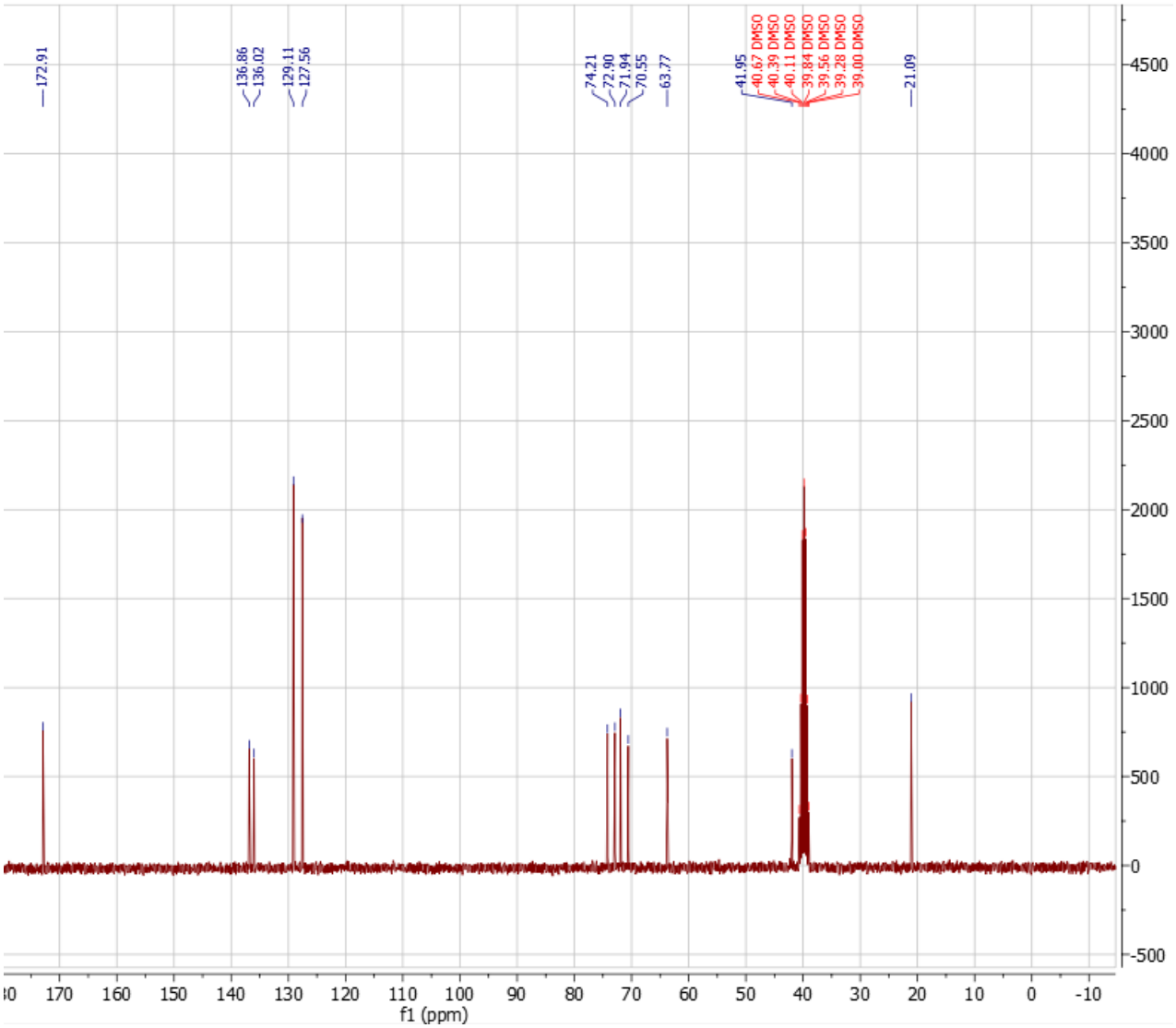
172.91
136.86
136.02
129.11
127.56
74.21
72.90
71.94
70.55
63.77
41.95
40.67 DMSO
40.39 DMSO
40.11 DMSO
39.84 DMSO
39.56 DMSO
39.28 DMSO
39.00 DMSO
21.09
4500
4000
3500
3000
2500
2000
1500
1000
500
0
-500
170
160
150
140
130
120
110
100
90
80
70
60
50
40
30
20
10
0
-10
f1 (ppm)

N-2,6-Difluorobenzyl-β-D-gluconamide (6)

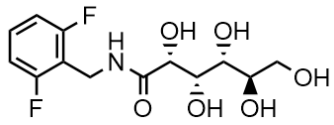

Compound 6 Reaction Scheme:

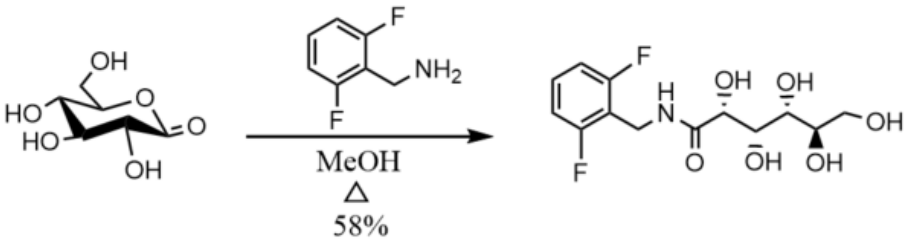

Scheme 6.6. Synthesis of N-2,6-Difluorobenzyl-β-D-gluconamide.

Compound **6** was prepared according to a standard literature procedure.[2] To a solution of D-Gluconic acid-δ-lactone (0.5 g, 2.8 mmol) in MeOH (37.5 mL) was added 2,6-difluoroaniline (0.3 mL, 2.8 mmol). The mixture was stirred under reflux for 24 hours. The solvent was evaporated, and the residue was recrystallized in EtOH to afford **6** as a white powder (0.52 g, 58%). Characterization data is consistent with that previously reported in the literature. ^{1}H NMR (400 MHz; DMSO-d_6): δ 7.82 (t, *J* = 5.5 Hz, 1H), 7.31-7.38 (m, 1H), 7.04 (t, *J* = 8.2 Hz, 1H), 5.32 (d, *J* = 5.1 Hz, 1H), 4.50 (d, *J* = 5.2 Hz, 1H), 4.44-4.24 (m, 5H), 3.96 (t, *J* = 3.7 Hz, 1H), 3.87-3.84 (m, 1H), 3.55-3.50 (m, 1H), 3.41 (br, 1H). ^{13}C NMR (400 MHz, DMSO-d_6): δ 172.6, 112.1, 111.8, 74.0, 72.8, 72.0, 70.6, 63.8.

Compound 6 NMR Spectra:

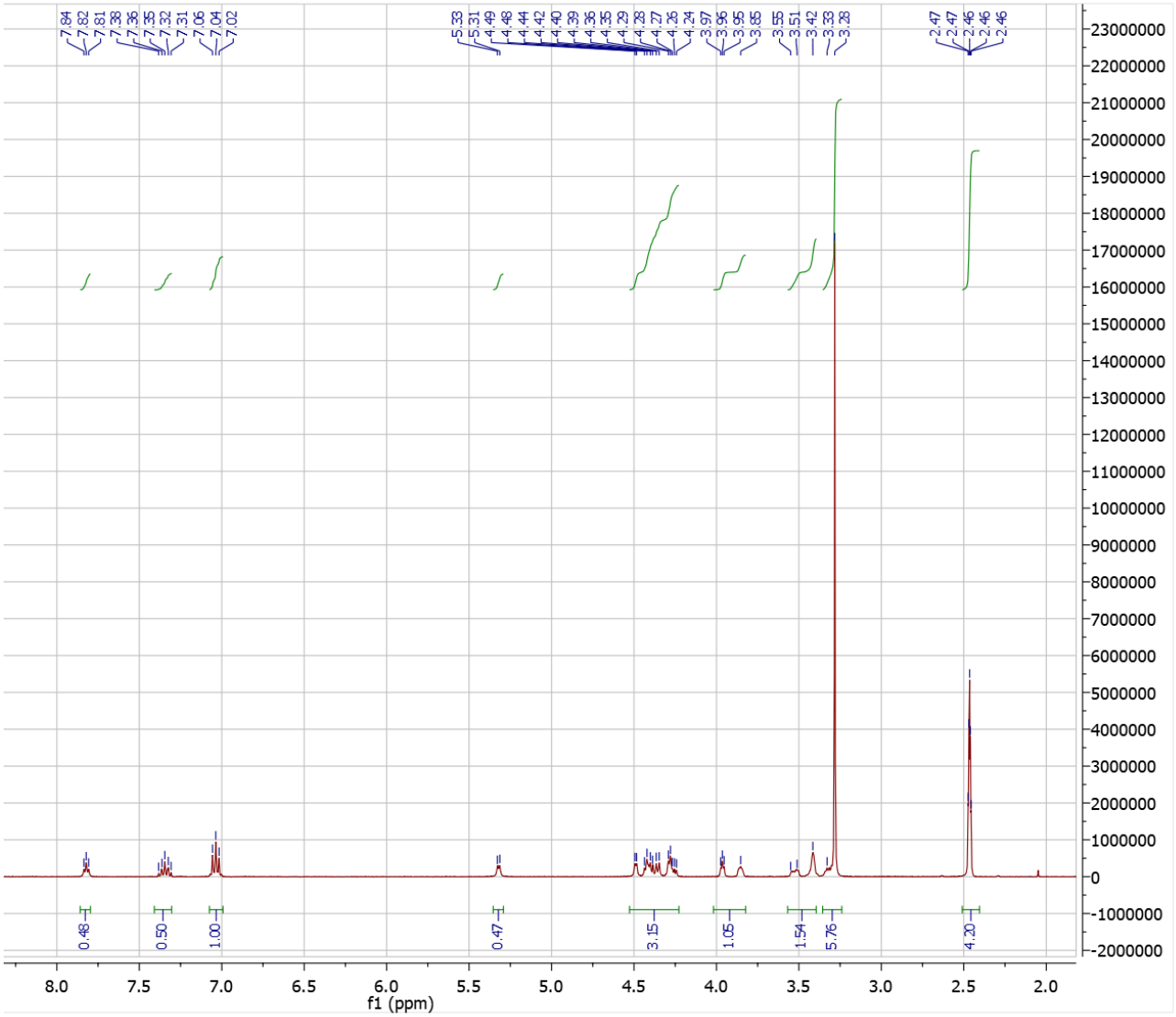

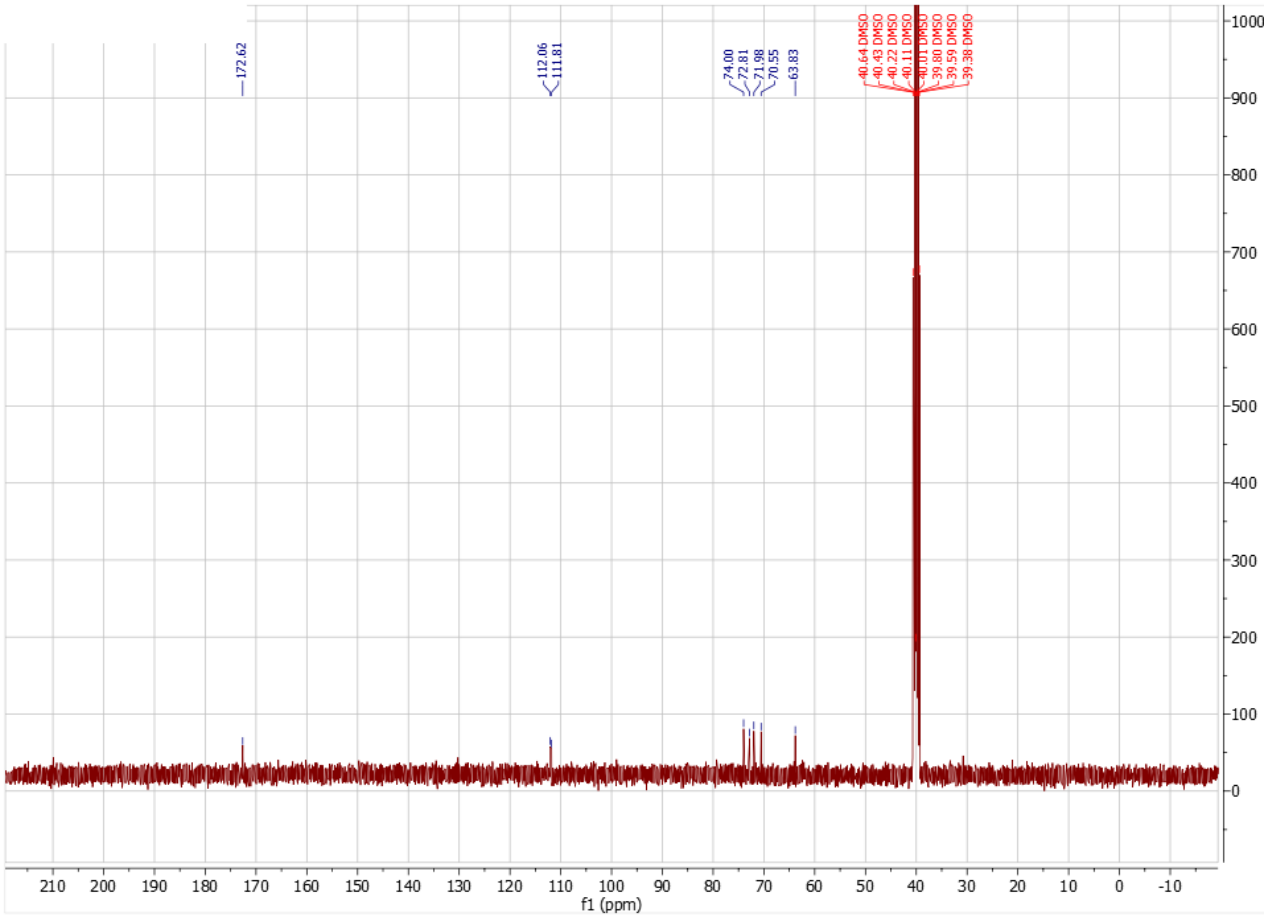
172.62
112.06
111.81
74.00
72.81
71.98
70.55
63.83
40.64 DMSO
40.43 DMSO
40.22 DMSO
40.11 DMSO
40.01 DMSO
39.80 DMSO
39.59 DMSO
39.38 DMSO
1000
900
800
700
600
500
400
300
200
100
0
210 200 190 180 170 160 150 140 130 120 110 100 90 80 70 60 50 40 30 20 10 0 -10
f1 (ppm)

N-4-Chlorobenzyl-β-D-gluconamide (7)

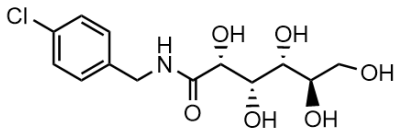

Compound 7 Reaction Scheme:

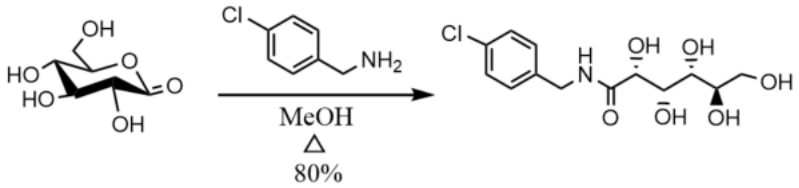

Scheme 6.7. Synthesis of N-4-Chlorobenzyl-β-D-gluconamide.

To a solution of D-Gluconic acid-δ-lactone (0.2 g, 1.12 mmol) in MeOH (10 mL) was added 4-chlorobenzylamine (0.14 mL, 1.12 mmol). The mixture was stirred under reflux for 24 hours. The solvent was evaporated, and the residue was recrystallized in EtOH to afford **7** as a white powder (0.29 g, 80%). ^{1}H NMR (400 MHz, DMSO-d_6): δ 8.22 (t, *J* = 6.5 Hz, 1H), 7.32-7.25 (m, 4H), 5.46 (d, *J* = 5.0 Hz, 1H), 4.56-4.44 (m, 3H), 4.34-4.20 (m, 3H), 4.02 (t, *J* = 4.1 Hz, 1H), 3.93-3.89 (m, 1H), 3.56-3.52 (m, 1H), 3.45 (br, 2H), 3.35-3.32 (m, 1H). ^{13}C (400 MHz, DMSO-d_6): δ 173.2, 139.2, 131.5, 129.4, 128.5, 74.3, 72.9, 72.0, 70.6, 63.8, 41.6. HRMS (ESI+): m/z calcd. for $C_{13}H_{18}ClNO_6$ [M+Na]+ 342.1; found, 342.1.

Compound 7 NMR Spectra:

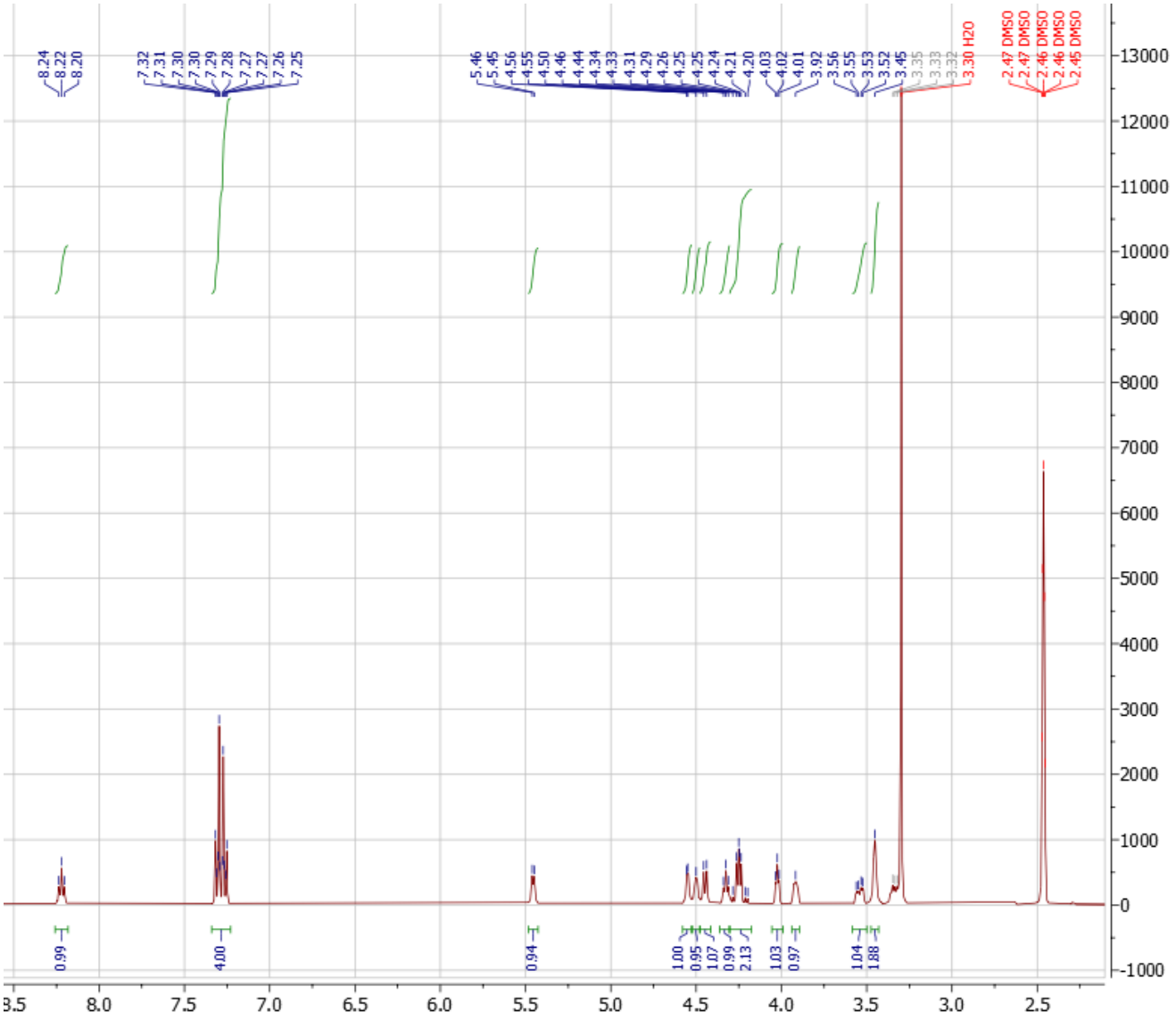

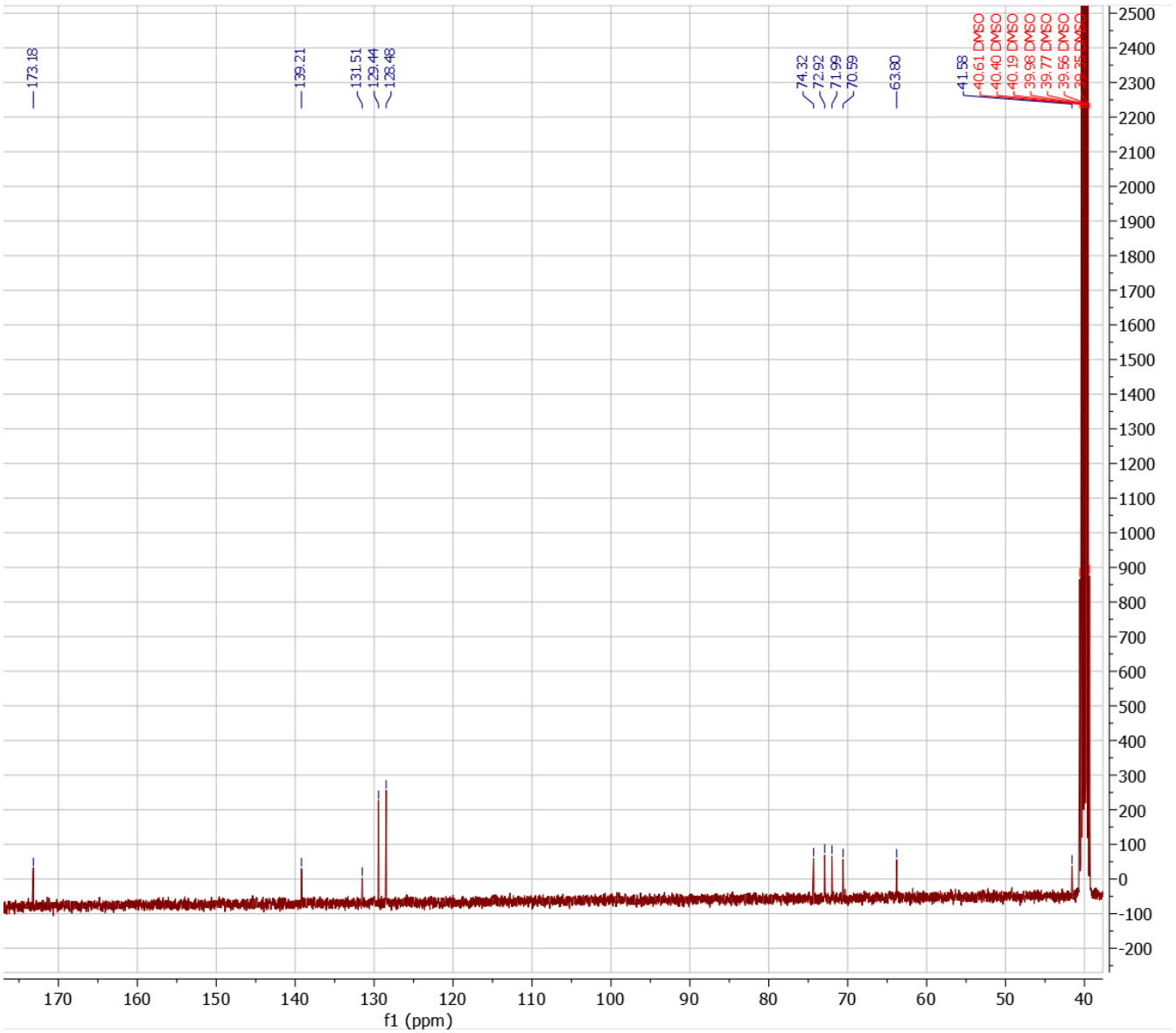
173.18
139.21
131.51
129.44
128.48
74.32
72.92
71.99
70.59
63.80
41.58
40.61 DMSO
40.40 DMSO
40.19 DMSO
39.98 DMSO
39.77 DMSO
39.56 DMSO
39.35 DMSO
f1 (ppm)

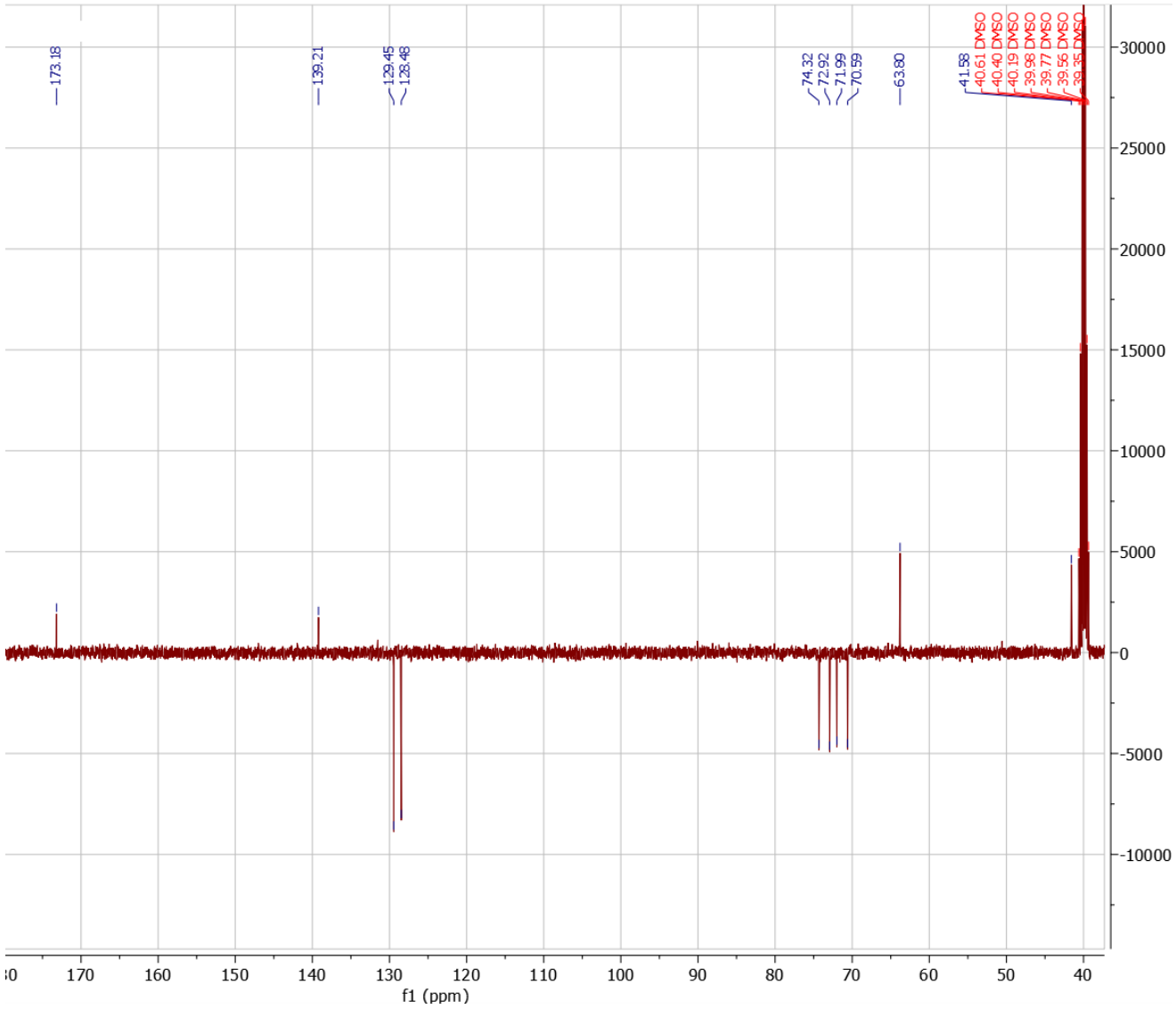
173.18
139.21
129.45
128.48
74.32
72.92
71.99
70.59
63.80
41.58
40.61 DMSO
40.40 DMSO
40.19 DMSO
39.98 DMSO
39.77 DMSO
39.56 DMSO
39.35 DMSO
30000
25000
20000
15000
10000
5000
0
-5000
-10000
170
160
150
140
130
120
110
100
90
80
70
60
50
40
f1 (ppm)

N-4-Methoxybenzyl-β-D-gluconamide (8)

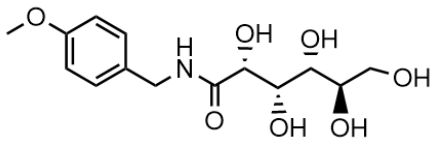

Compound 8 Reaction Scheme:

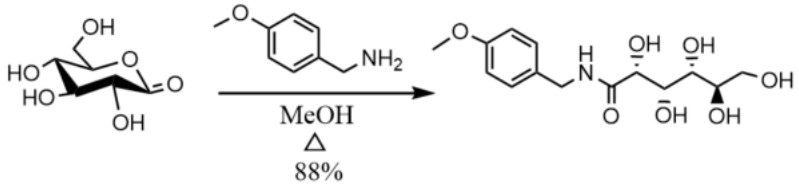

Scheme 6.8. Synthesis of N-4-Methoxybenzyl-β-D-gluconamide.

Compound **8** was prepared according to a standard literature procedure.[2] To a solution of D-Gluconic acid-δ-lactone (0.2 g, 1.12 mmol) in MeOH (15 mL) was added 4-methoxybenzylamine (0.15 mL, 1.12 mmol). The mixture was stirred under reflux for 24 hours. The solvent was evaporated, and the residue was recrystallized in EtOH to afford **8** as a white powder (0.32 g, 88%). Characterization data is consistent with that previously reported in the literature. ^{1}H NMR (400 MHz, DMSO-d_6): δ 8.03 (t, *J* = 6.1 Hz, 1H), 7.18-7.15 (m, 2H), 6.83-6.79 (m, 2H), 5.40 (d, *J* = 5.1 Hz, 1H), 4.54-4.53 (m, 1H), 4.49-4.47 (m, 1H), 4.41 (d, *J* = 7.3 Hz, 1H), 4.32 (t, *J* = 5.7 Hz, 1H), 4.20 (d, *J* = 6.3 Hz, 2H), 4.00 (t, *J* = 4.2 Hz, 1H), 3.92-3.89 (m, 1H), 3.68 (s, 3H), 3.60-3.51 (m, 1H), 3.45 (br, 2H), 3.36-3.33 (m, 1H). ^{13}C NMR (400 MHz, DMSO-d_6): δ 172.9, 158.6, 132.0, 129.0, 114.0, 74.3, 72.9, 72.0, 70.6, 63.8, 55.5, 41.7.

Compound 8 NMR Spectra:

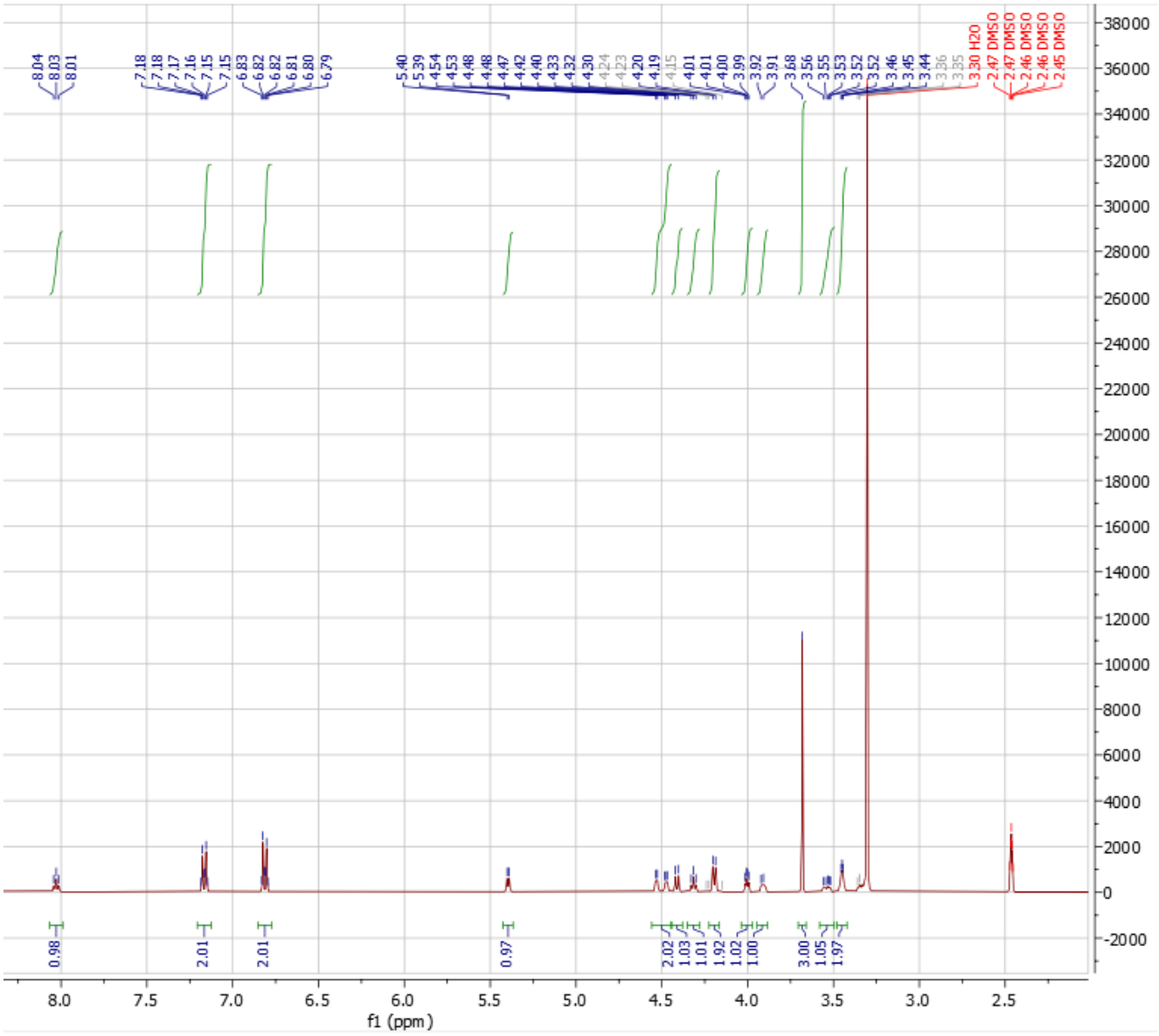

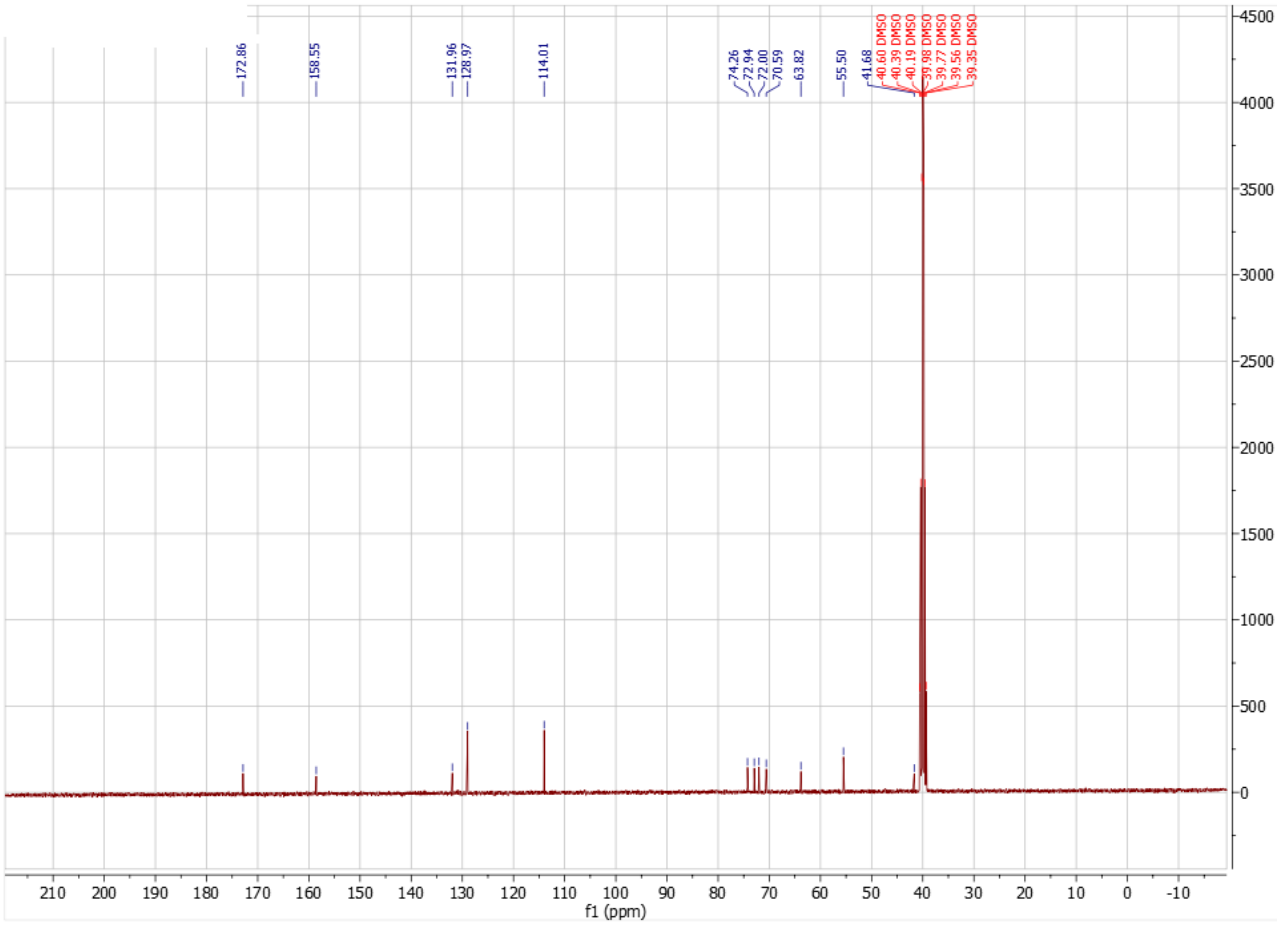
172.86
158.55
131.96
128.97
114.01
74.26
72.94
72.00
70.59
63.82
55.50
41.68
40.60 DMSO
40.39 DMSO
40.19 DMSO
39.98 DMSO
39.77 DMSO
39.56 DMSO
39.35 DMSO
4500
4000
3500
3000
2500
2000
1500
1000
500
0
210 200 190 180 170 160 150 140 130 120 110 100 90 80 70 60 50 40 30 20 10 0 -10
f1 (ppm)

N-4-Bromophenyl-2,3,4,6-tetra-O-acetyl-β-D-glucopyranoside (9a)

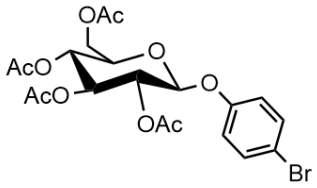

Compound **9a** was prepared according to a standard literature procedure.[1] A solution of 1,2,3,4,6-penta-O-acetyl-β-D-glucopyranose (0.5 g, 1.28 mmol), 4-bromophenol (0.27 g, 1.54 mmol) with boron trifluoride diethyl etherate (24.1 µL, 0.2 mmol). Column chromatography (7:3 hexanes/ethyl acetate) afforded **9a** as a white powder (0.42 g, 85%). Characterization data is consistent with that previously reported in the literature. ^{1}H NMR (400 MHz, DMSO-d_6): δ 7.49-7.47 (m, 2H), 6.94-6.92 (m, 2H), 5.92 (d, *J* = 8.4 Hz, 1H), 5.53 (d, *J* = 8.0 Hz, 1H), 5.42-5.34 (m, 2H), 5.04-4.86 (m, 3H), 4.22-3.94 (m, 5H), 2.03-1.91 (m, 9H). ^{13}C NMR (400 MHz, DMSO-d_6): δ 169.5, 156.1, 132.9, 119.2, 97.6, 72.3, 71.1, 68.5, 20.9, 20.9, 20.8, 20.7.

Compound 9a NMR Spectra:

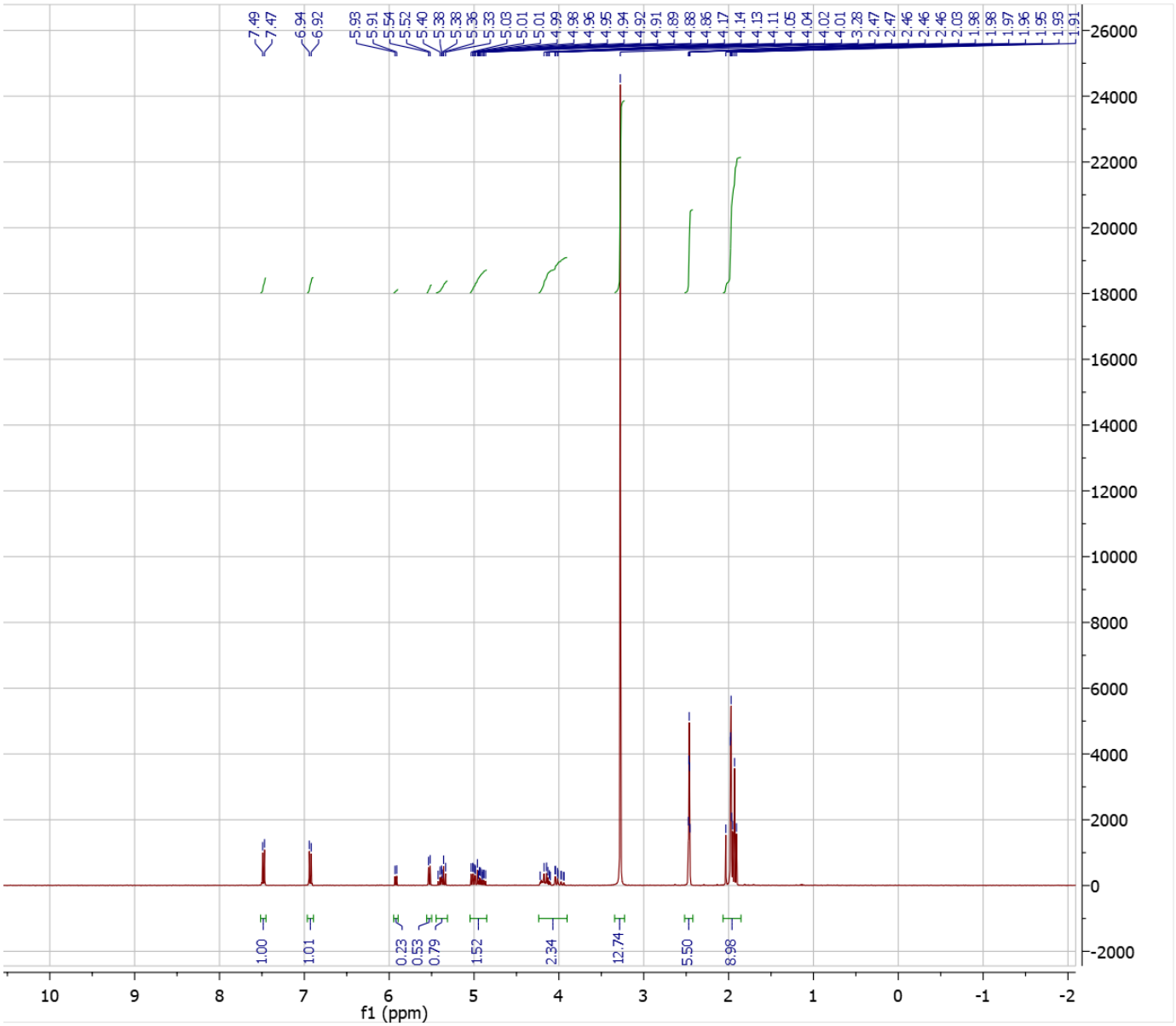

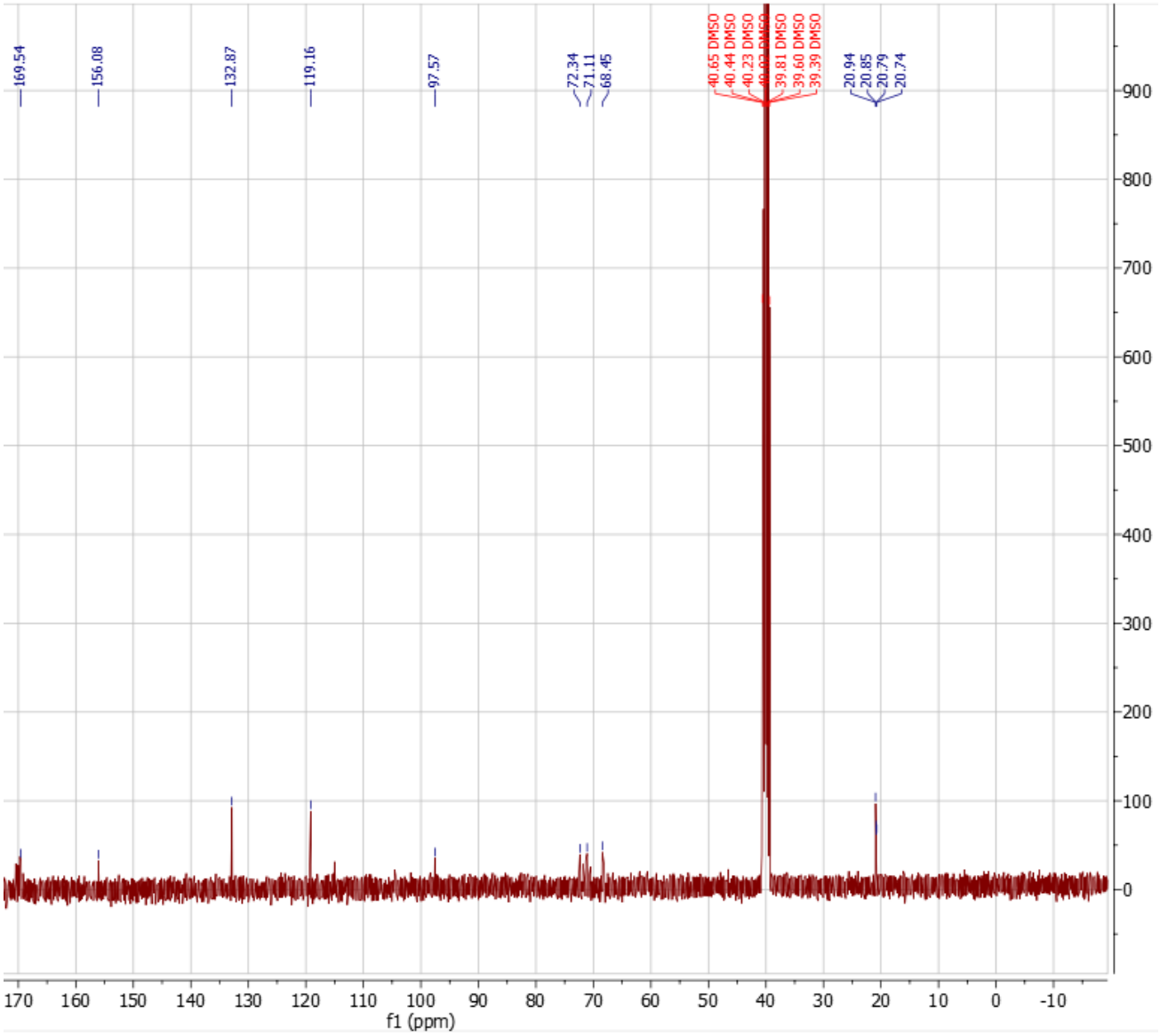
169.54
156.08
132.87
119.16
97.57
72.34
71.11
68.45
40.65 DMSO
40.44 DMSO
40.23 DMSO
39.81 DMSO
39.60 DMSO
39.39 DMSO
20.94
20.85
20.79
20.74
900
800
700
600
500
400
300
200
100
0
170 160 150 140 130 120 110 100 90 80 70 60 50 40 30 20 10 0 -10
f1 (ppm)

N-4-Bromophenyl-β-D-glucopyranoside (9)

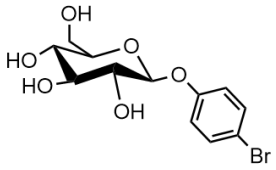

Compound 9(a) Reaction Scheme:

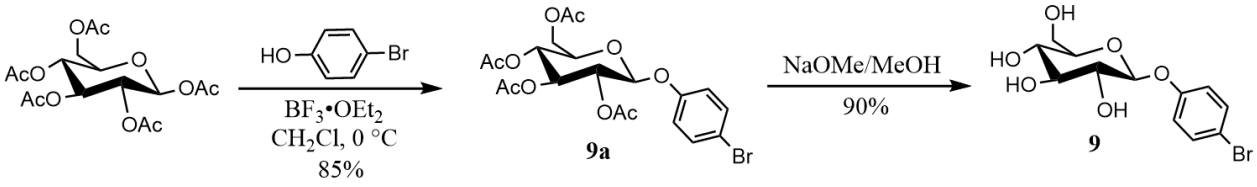

Scheme 6.9. Synthesis of N-4-Bromophenyl-β-D-glucopyranoside.

Compound **9** was prepared according to a standard literature procedure.[1] Compound **9a** (0.42 g, 0.84 mmol) was dissolved in a solution of sodium methoxide in methanol (10.5 mL) and stirred for one hour at room temperature. The solution was then neutralized with Amberlite® IR-120 (H^+) ion-exchange resin and filtered. The filtrate was concentrated, and the product was lyophilized to yield **9** as a white powder (0.25 g, 90%). Characterization data is consistent with that previously reported in the literature. ^{1}H NMR (400 MHz, DMSO-d_6): δ 7.44-7.40 (m, 1H), 6.97-6.93 (m, 1H), 5.31, (d, *J* = 5.0 Hz, 1H), 5.04 (dd, *J* = 13.5, 5.0 Hz, 1H), 4.81 (d, *J* = 7.5 Hz, 1H), 4.54 (t, *J* = 5.8 Hz, 1H), 3.66-3.61 (m, 1H), 3.44-3.38 (m, 1H), 3.28-3.08 (m, 3H). ^{13}C NMR (400 MHz, DMSO-d_6): δ 157.1, 132.5, 119.0, 113.7, 100.8, 77.5, 77.0, 73.6, 70.1, 61.1.

Compound 9 NMR Spectra:

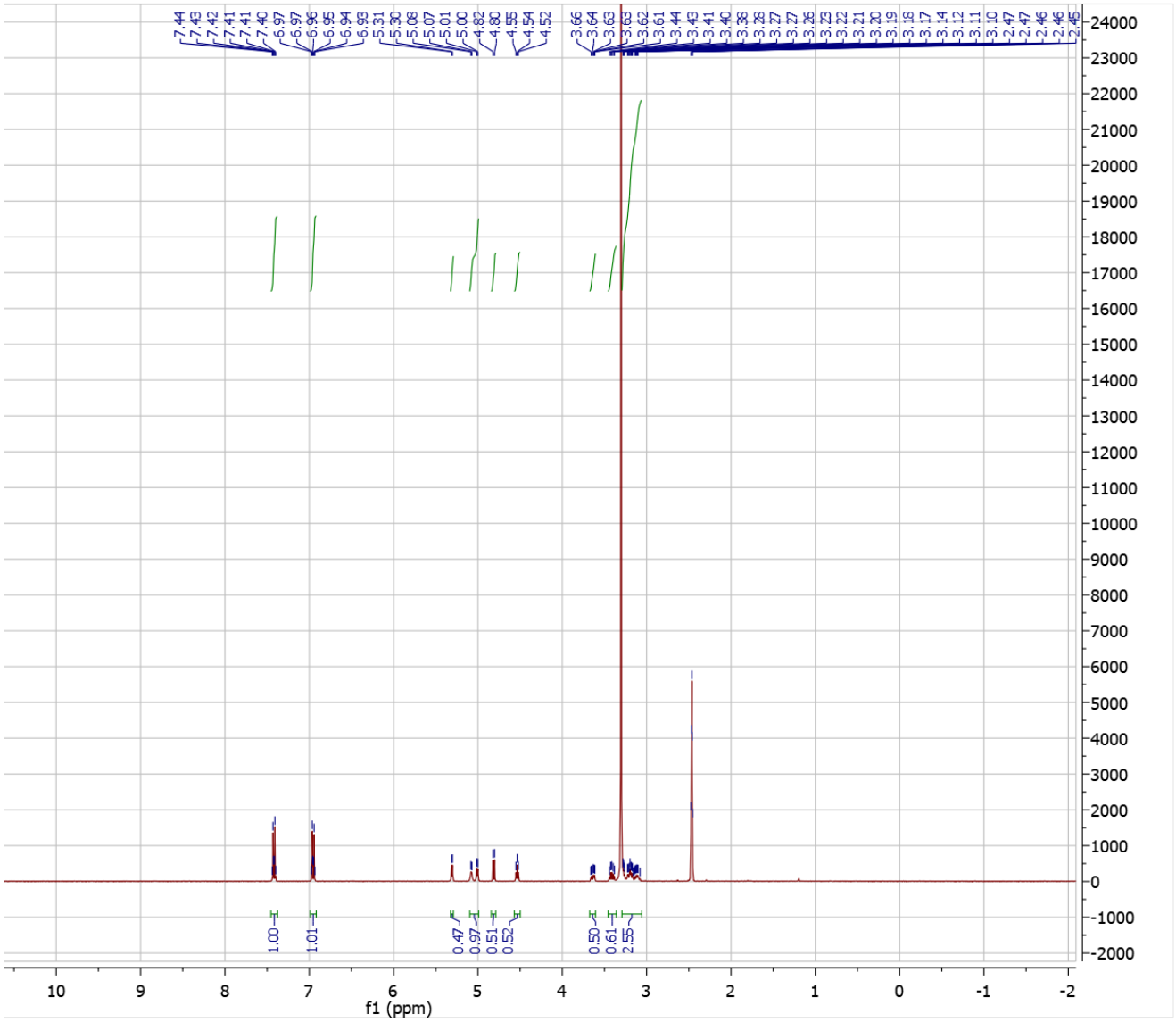

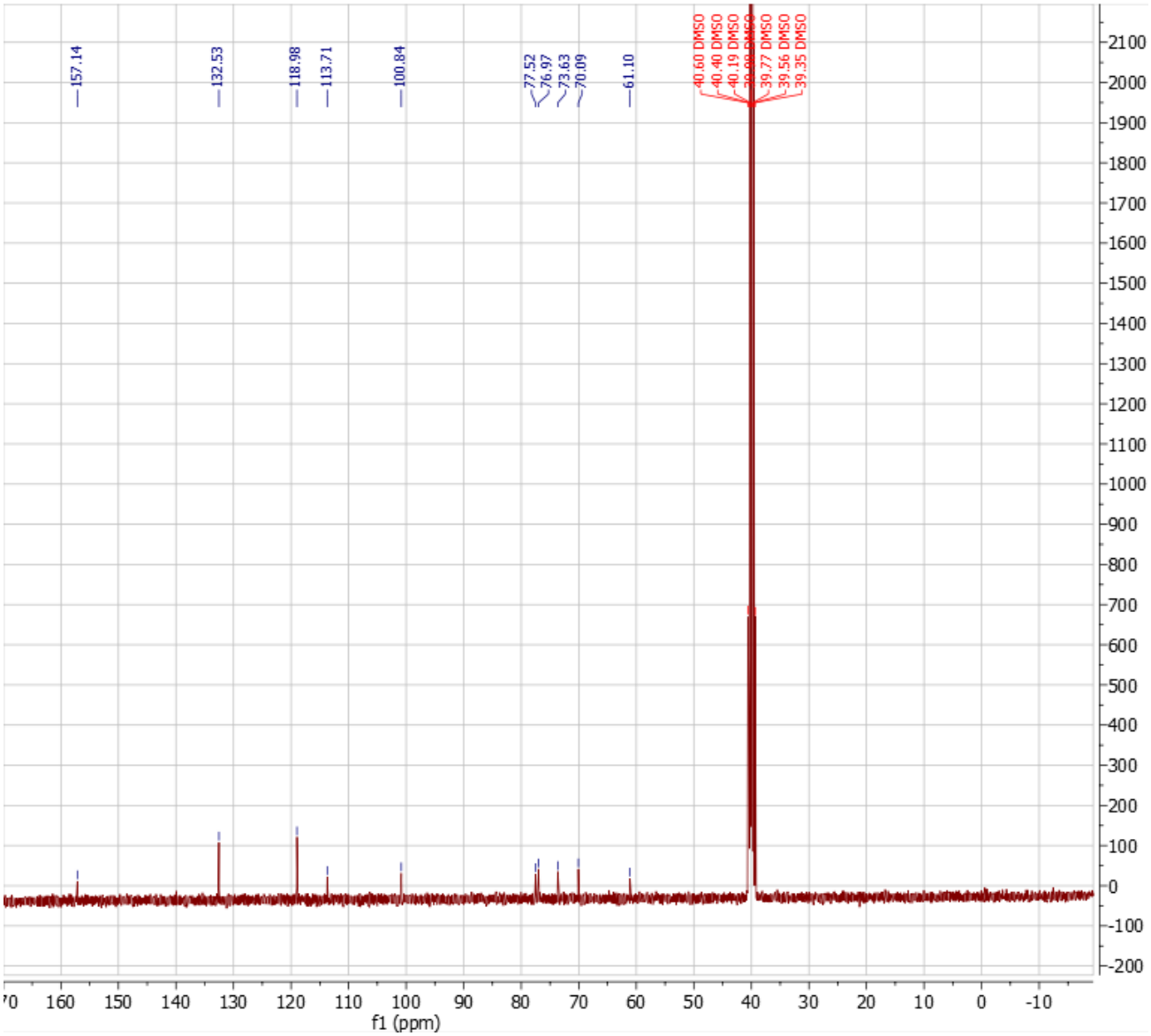
157.14
132.53
118.98
113.71
100.84
77.52
76.97
73.63
70.09
61.10
40.60 DMSO
40.40 DMSO
40.19 DMSO
39.98 DMSO
39.77 DMSO
39.56 DMSO
39.35 DMSO
f1 (ppm)

Ice Recrystallization Inhibition Assay [Modified Splat cooling Assay]:

Ice recrystallization inhibition of compounds was assessed at various concentrations in a phosphate-buffered saline (PBS) solution. A 10 µL droplet of the sample solution was released from a micropipette at a height of approximately 2 meters onto a pre-cooled aluminum block (-80 °C). The droplet was immediately frozen upon impact on the block and the resulting ice wafer (approximately 20 µm thick and 1 cm wide) was then transferred to a pre-cooled glass cover slip and annealed at -6.4 °C on a Cryostage for 5 minutes. Cryostage temperature was maintained with a programmable Peltier unit (S3 Series 800 temperature controller, Alpha Omega Instruments). After this time, the Cryostage was placed under a microscope and the middle of the ice wafer was photographed using a Nikon Camera 20x objective lens.

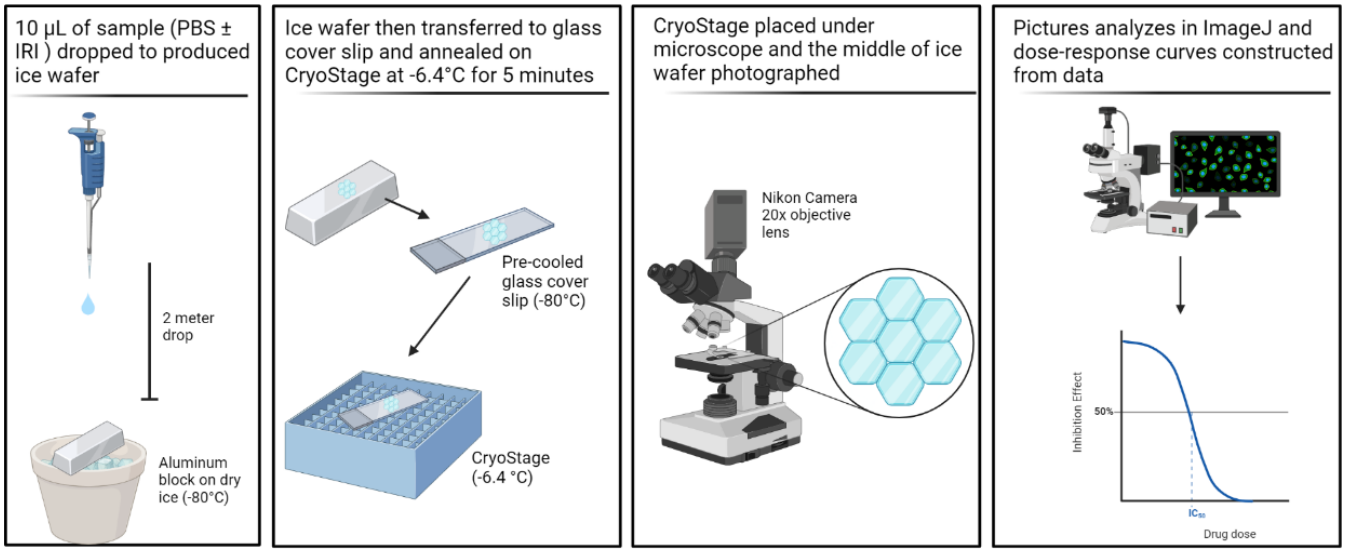

Figure 2.4. Experimental Procedure of Modified Splat Cooling Assay.

Dose-response Curves:

Images of ice crystals in the absence of inhibitor (i.e., PBS only) were analyzed in triplicate. In addition, all compounds were assessed in triplicate at a minimum of 5 different

concentrations. The area of each individual ice crystal within the field of view was analyzed using ImageJ and corrected for the appropriate magnification factor and objective lens utilized in the modified splat cooling assay. The ice crystal areas were "binned" according to their size using an Excel spreadsheet, with the smallest bin occupying ice crystal areas of 0.001 mm^2 and each sequential bin increasing by increments of 0.001 mm^2. From the rate of depletion of ice crystals occupying bin 1, the initial rates of ice crystal growth were calculated using the following equation:

$$\upsilon_t = \frac{1 - A_t^{rel}}{t}$$

where υ_t is the initial rate at 5 minutes, A_t^{rel} is the relative area of bin 1 at 5 minutes, and t is time. From the initial rates of ice crystal growth, dose-response curves were constructed whereby the normalized rate of ice crystal growth (i.e., initial rate normalized to that of PBS) was plotted against the log concentration. From the dose-response curves, IC_{50} values were calculated, that is the concentration at which ice recrystallization inhibitors have achieved half of their maximum inhibitory capability.

6.2 Experimental Protocols for Cell Based Assays

HepG2 Cell Culture:

HepG2 (human liver hepatocellular carcinoma cells, ATCC HB-8065) were cultured in Eagle's minimum essential media (MEM) supplemented with 10% FBS (fetal bovine serum), 1% non-essential amino acids, 1% penicillin-streptomycin, and 1 mM sodium pyruvate in T75 cm^2 Corning® flasks. Cells were incubated in a 37 °C incubator supplied with 5% CO_2.

Culture media was changed every second day until 80% confluent. Once confluent, the cells were removed from the flasks using 5 mL Accutase solution for use in experiments. Passages 9-12 were used in this study.

Alamar Blue (Resazurin) Assay:

HepG2 cells were plated in 96-well plates (~40,000 cells/well) and incubated overnight at 37 °C with 5% CO_2 to allow cells to adhere. Cells were then treated with 100 µL of MEM supplemented with various concentrations of test compounds. Cells were treated with MEM without supplement as a negative control and supplemented with 1% Triton-X as a positive control. Cells were then incubated at 37 °C with 5% CO_2 overnight. Following incubation, 10 µL of resazurin solution (125 µg/mL) in DPBS (Dulbecco's phosphate buffered saline) was added to each well and the plates were incubated at 37 °C with 5% CO_2 for 4 hours. The fluorescence of each well was measured using a fluorescence plate reader with an excitation at 530 nm (emission at 590 nm). Each experiment was repeated at least two times in 7 consecutive wells for each condition. Cell viability was calculated as a percentage of the control.

Cryopreservation of Fibroblast Cell suspension:

This experiment as mentioned in chapter 4 was carried out by the Laval group as outline in the statement of contribution. Fibroblasts (Fb13) in falcon tubes are trypsinated using LOEX protocol. Cells were treated with 1 mL of their respective IRI, 1.5% BSA, and 10% DMSO solution which was prepared the day of freezing. The cell suspension was centrifuged and added to cryovials (~600,000 cells/mL). Cryovials were incubated for 40 minutes at ambient temperature before placing cryovials in CoolCell and transferred to -80 °C freezer for 4

hours. Cryovials were quickly transferred to liquid nitrogen and incubated for 24 hours. Vials are thawed in a 37 °C water bath and a 30 µL of a 1:1 Trypan Blue - cell suspension mixture is then added to a hemocytometer for cell count. The cells were resuspended to 40,000 cells/mL using warm culture medium. 1 mL of cell suspension was plated in 6-well plates, each condition was repeated in 5 consecutive wells. Cells were treated with DME - 10% FBS (Seradigm 203B10) as a negative non-frozen control, treated with 1.5% BSA - 10% DMSO as a positive control, and lethal controls were heat at 60 ºC for 20 minutes. Well plates were then incubated for 96 hours changing cell media at 48 hours. Wells were trypsinated using LOEX protocol and cells were counted using a Coulter (Vi-CELL BLU Cell Analyzer, Beckman Coulter). Passages 5-10 were used in this study.

Cryopreservation of Tissue Products:

This experiment as mentioned in chapter 4 was carried out by the Laval group as outline in the statement of contribution. Tissues were placed in sanded cryosettes (Simport M-956O). Tissues were treated with 1 mL of their respective IRI, 1.5% BSA, and 10% DMSO solution which was prepared the day of freezing. Cryosettes were incubated at room temperature for 40 minutes before being placed in a rate controlled-freezer (Dura-Stop MP lyophilizator). To measure temperature a thermocouple was placed in a perforated cap cryosette as to touch the solution, but not the bottom of the container. The freezing run was performed as follows: Set point temperature of apparatus to 20 °C, hold 5 minutes, cool set point by 1 °C/min until -70 °C. Cryosettes are then transferred to -80 °C freezer for 2 hours before thawing in a 37 °C water bath for 5 minutes. Tissues are then drop wise washed with DME with 10% FBS (Seradigm 203B10) before transferring to a new culture plate. Culture medium is added to each well then, the tissues are incubated for 24 hours. Cells were treated with DME - 10%

FBS as a negative control and supplemented with 1.5% BSA - 10% DMSO as a positive control. Passages 5-10 were used in this study.

SYTOX Green Assay:

This experiment as mentioned in chapter 4 was carried out by the Laval group as outline in the statement of contribution. Following incubation, tissues are washed with phosphate-free buffer 3 times. Negative control tissues were then treated with 4.2% formaldehyde for 20 minutes and acetone permeabilization for 15 minutes at -20 °C. 10 µL of SYTOX Green solution in HBS was added to each well and the plates were incubated at room temperature for 30 minutes. The staining solution was then removed, and the cells were washed 3 times with HBS. The fluorescence of each well was measured using a fluorescence laser scanner (Typhoon™).

AlamarBlue Assay:

This experiment as mentioned in chapter 4 was carried out by the Laval group as outline in the statement of contribution. Tissues were transferred to new 12-well plates and rinsed twice with phenol-free medium without added glutamine (DMEc). DMEc was used as a negative control and DME with phenol was used to check for pH change. 75 µL of AlamarBlue™ was added to each well and the plates were incubated at room temperature for 30 minutes. Plates were centrifuged and the staining solution was then removed. The fluorescence of each well was measured using a fluorescence plate reader (Varioskan™) with an excitation at 560 nm (emission at 590 nm).

6.3 Experimental Protocols for RT-qPCR Analysis

Protein Stabilization Assay [Lyophilization & RT-qPCR]:

This experiment was carried out in collaboration with Berezovski Research Group as outline in the statement of contribution. Cryo-solutions were prepared by dissolving IRIs in dH_2O at their respective concentrations. dH_2O treated without template was used as a negative control and samples treated with trehalose at 0.5% and 10% (weight/volume) was used as a positive control. 1.2 µL (qPCR Chip) or 20 µL (qPCR 96-well plate and tubes) at n = 3 of each sample was added to the respective qPCR receptacle based on experiment. Lyophilization of samples was then performed in a Labconco FreeZone lyophilizer. Master mix was prepared according to CDC guidelines pertaining Promega GoTaq Probe 1-Step RT-qPCR System (A6121, Promega). ssRNA standard (EURM019, Sigma-Aldrich) and primer/probe mix (10006713, IDTDNA) were added to the master mix. The freeze-dried mixes were reconstituted to their original volume with master mix, then underwent a second lyophilization. RNA template in dH_20 (10^6 copies/µL) was added before the RT-qPCR experiment. qPCR was performed as follows: 50 °C for 3 minutes, 95 °C for 30 seconds, and 40 cycles of qPCR with 3 seconds hold at 95 °C and 30 seconds hold at 50 °C. Each condition was replicated in 3 consecutive wells. Cq value (Threshold cycle number) from each replicate was averaged and normalized to the 10% (wt/vol) trehalose control to calculate a percent mean threshold cycle value.

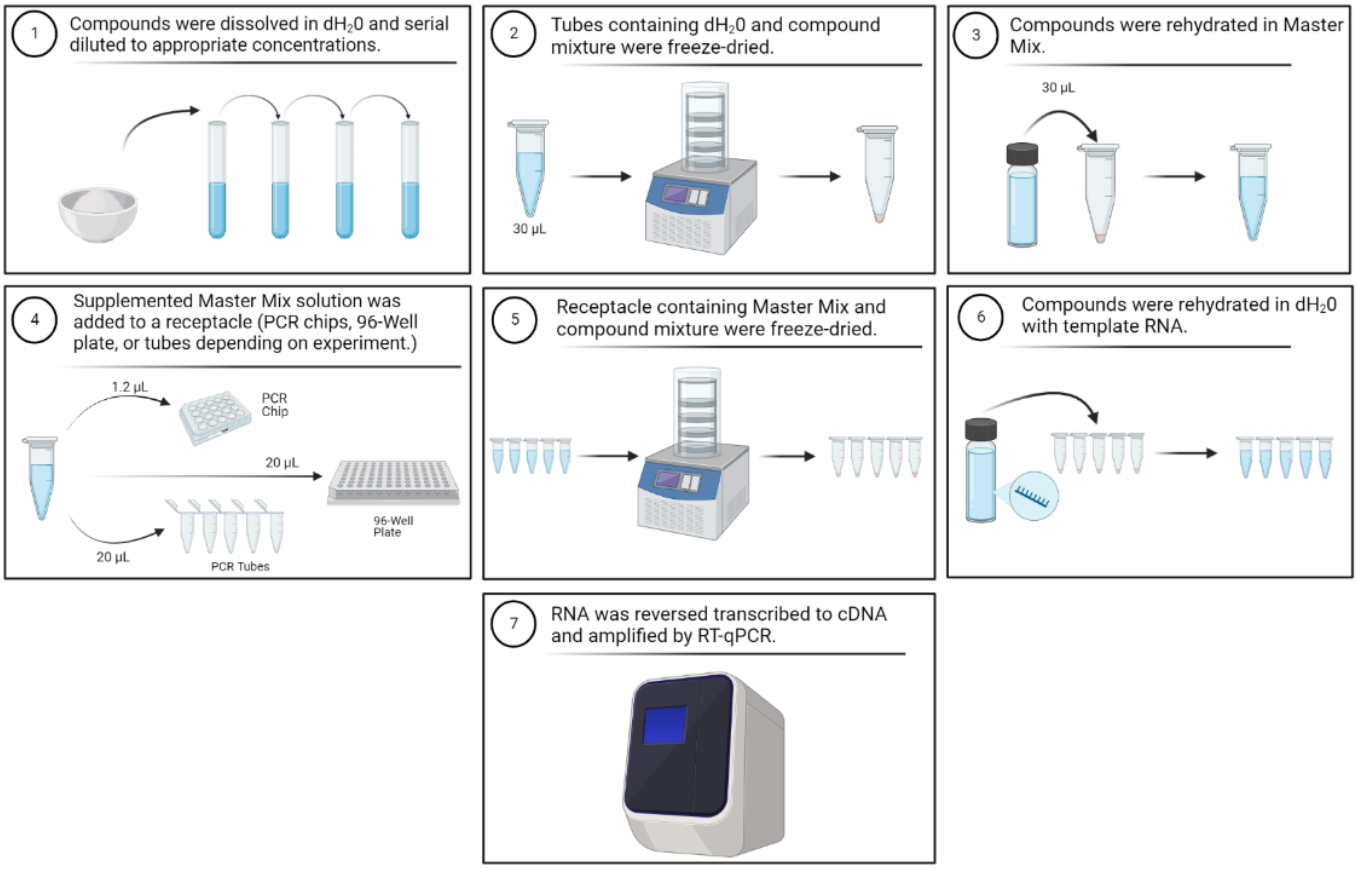

Figure 3.5. RT-qPCR Experimental Design Infographic. *Compounds refer to NOGlc (1), pBrPhGlc (9), 4-MBA (5), and 2,6-DFB (6).*

6.4 References

1 Capicciotti, C. *The Rational Design of Potent Ice Recrystallization Inhibitors for Use as Novel Cryoprotectants* Doctorate in Philosophy degree in Chemistry thesis, University of Ottawa, (2014).

2 Briard, J. G. *The Rational Design and Use of Novel Small-Molecule Ice Recrystallization Inhibitors for the Cryopreservation of Hematopoietic Stem Cells and Red Blood Cells* Department of Chemistry and Biomolecular Sciences thesis, University of Ottawa, (2016).

3 Poisson, J. S. *Synthesis and In Vitro Applications of Ice Recrystallization Inhibitors* Doctorate in Philosophy degree in Chemistry thesis, University of Ottawa, (2019).